Investigating the importance of the Zika virus 3′ untranslated region to viral fitness

Skye Storrie

Clare College

21/12/21

This dissertation is submitted for the degree of Doctor of Philosophy

Declaration

This dissertation is the result of my own work and includes nothing which is the outcome of work done in collaboration except as declared in the Preface and specified in the text.

It is not substantially the same as any that I have submitted, or, is being concurrently submitted for a degree or diploma or other qualification at the University of Cambridge or any other University or similar institution except as declared in the Preface and specified in the text. I further state that no substantial part of my dissertation has already been submitted, or, is being concurrently submitted for any such degree, diploma or other qualification at the University of Cambridge or any other University or similar institution except as declared in the Preface and specified in the text.

It does not exceed the prescribed word limit for the relevant Degree Committee.

Abstract

The RNA binding protein Musashi 1 (MSI1) has been shown to bind to the Zika virus (ZIKV) 3′ untranslated region (3′UTR) and enhance viral replication. MSI1 is present in high levels in neural progenitor cells of the foetal brain, and previous work proposed that MSI1 could drive the pathogenesis caused by ZIKV, and therefore, could be linked to the cases of congenital microcephaly observed during the 2015/2016 epidemic. The work presented here utilises reverse genetics to investigate the mechanism of MSI1 enhancement of ZIKV replication by introducing putative MSI1 binding site mutations into the 3′UTR. Using U251 cells ± MSI1, it was shown that one of the site mutations (Site D) induced a MSI1 dependent reduction in viral replication, indicating that this site may be particularly important for MSI1 binding to the ZIKV 3′UTR. Following viral characterisation in Vero cells, several of the site mutants displayed varying levels of viral attenuation, in one case so severe it was not possible to rescue virus. Passage experiments revealed the importance of one site mutation (Site B), whereby the partial reversion of one of the two mutated nucleotides was observed, indicating the importance of a single nucleotide in the 3′UTR to the overall fitness of the virus. The structure of the flavivirus 3′UTR is well conserved, highlighting its importance to the viral life-cycle. To structurally map the 3′UTR of the different site mutants, a novel structural cassette was designed and employed, allowing, for the first time, in vitro selective 2′-hydroxyl acylation analysed by primer extension mapping of the full 3′UTR structure. This was used to study the contribution of specific nucleotides to the 3′UTR structure, revealing a disruption in RNA structure in the Site B mutant, and thus sfRNA production. Additionally, sfRNA production was found to be restored following the single nucleotide reversion. Further investigations linked the hampered sfRNA production to reduced virion production in IFN competent A549 cells, which was not observed in IFN deficient Vero cells, reaffirming the link between sfRNA production and immune evasion. Overall, this thesis highlights the importance of the ZIKV 3′UTR to viral fitness and provides useful tools for future investigations.

Acknowledgements

I would like to thank my supervisor Dr Trevor Sweeney for his guidance and support throughout my PhD. I am glad to have had a supervisor who is enthusiastic about research but also knows how to have a laugh.

I would also like to thank members of the Sweeney lab past and present. I would like to thank Ted for introducing me to working with ZIKV and for his upbeat attitude to everything. Tom, the words "'just keep swimming"' have gotten me through some difficult times. Renata, thanks to you I will never say the word biscuits normally ever again, and I will miss our tea breaks. Xin, we went through this journey together and your sense of humour never fails to amaze me. Taissa, you arrived just as I was leaving, but thank you for your support and advice towards the end of my PhD. I wish you would have started sooner.

Level 5 Virology is undoubtedly a special place to work, and I would like to thank everyone for making it such a fun and friendly place. I have really enjoyed all the pub trips and tea room chats. I would also like to thank Hazel for introducing me to the world of SHAPE which got things moving along at a time where I really needed something to work.

Thanks to the Wellcome Trust and the Infection, Immmunity and Inflammation program at Cambridge for making this PhD possible.

This journey has not been without its challenges. I would like to thank my family and friends for their continued belief that I could do this. Last but not least, I would like to thank Calum for supporting me no matter what. You are an amazing person and I will always be grateful to you.

Contents

List of Figures

List of Tables

Nomenclature

Acronyms / Abbreviations

Ae.aegypti	*Aedes aegypti*
Ae.albopictus	*Aedes albopictus*
BSA	Bovine serum albumin
C	Capsid protein
CDK	Cyclin dependent kinase
CH25H	Cholesterol 25-hydroxylase
cHP	Short hairpin in the capsid coding region
CPE	Cytopathic effects
CS	Cyclisation sequence
CS2	Conserved sequence 2
DAR	Downstream of AUG region
DB	Dumbbell
DENV	Dengue virus
DMEM	Dulbecco's Modified Eagle Medium
DMSO	Dimethyl sulfoxide
DONGV	Donggand virus
dsRNA	Double stranded RNA
E	Envelope protein
eIF2	Eukaryotic initiation factor 2
eIF4E	Eukaryotic initiation factor 4E
ER	Endoplasmic reticulum
GLD2	Poly(A) polymerase germ line development defective-2
IFN	Interferon
IRES	Internal ribosome entry site

IRF3	Interferon regulatory factor 3
ISFs	Insect-specific flaviviruses
JAK	Janus tyrosine kinase
JEV	Japanese encephalitis virus
kb	Kilobases
M	Membrane protein
MBFs	Mosquito-borne flaviviruses
MCPH1	Microcephalin
miRNAs	microRNAs
MSI	Musashi
MSI1	Musashi 1
MSI2	Musashi 2
mTOR	Akt-mammalian target of rapamycin
MVE	Murray Valley encephalitis virus
Nanoluc	Nanoluciferase
NKVs	No known vector flaviviruses
NMIA	N-methylisatoic acid anhydride
NPCs	Neural progenitor cells
NS	Non-structural
NSCs	Neural stem cells
P	Passage
PABP	Poly(A)-binding protein
PBS	Phosphate-buffered saline
PK	Pseudoknot
poly(I:C)	Polyinosinic:polycytidylic acid
prM	Membrane protein precursor
RCS2	Repeat conserved sequence 2
RdRP	RNA dependent RNA polymerase
RNAi	RNA interference
RRMs	RNA recognition motifs

RT	Reverse transcription
RT-qPCR	Quantitative reverse transcription PCR
sfRNAs	Subgenomic flaviviral RNAs
sgRNA	Small subgenomic RNA
SHAPE	Selective 2′-hydroxyl acylation analysed by primer extension
siRNA	Small interfering RNA
SL	Stem loop
SLA	Stem loop A
SLB	Stem loop B
SSIII	SuperScript III
STAT	Signal transducers and activators of transcription
TBEV	Tick-borne encephalitis virus
TBFs	Tick-borne flaviviruses
TGN	Trans golgi network
UTR	Untranslated region
WNV	West Nile virus
WT	Wild-type
xrRNAs	Xrn1 resistant RNAs
YFV	Yellow fever virus
ZIKV	Zika virus

Chapter 1

Introduction

1.1 Flavivirus features and classification

The *Flaviviridae* family encompasses four different genera; *Flavivirus*, *Pestivirus*, *Hepacivirus*, and *Pegivirus*. Viruses of the *Pestivirus* genus infect pigs as well as wild and domestic ruminants, leading to enteric, haemorrhagic or wasting diseases. Members of this genus include classical swine fever virus, and bovine viral diarrhea virus, which both cause large economic losses to the farming industry. Within the *Hepacivirus* genus, Hepatitis C virus is an important human pathogen which can cause severe liver disease, whereas members of the *Pegivirus* genus also infect mammals, but have not been linked to disease [1]. Zika virus (ZIKV) is a member of the *Flavivirus* genus which includes over 53 species of arthropod-borne viruses that mainly infect mammals and birds [1, 2].

Flaviviruses display clear differences in the utilisation of different host species for transmission and replication. Flaviviruses can therefore be categorised based on their vector species into mosquito-borne flaviviruses (MBFs), tick-borne flaviviruses (TBFs), insect-specific flaviviruses (ISFs), or flaviviruses with no known vector (NKVs) [1, 3, 4]. MBFs and TBFs can replicate in both arthropods and vertebrates, the most common transmission cycle for flaviviruses. Comparatively, NFKs have only been isolated from vertebrates such as mice and bats, and ISFs are restricted to replication in insects. Other notable human pathogens found within the MBFs and TBFs include West Nile virus (WNV), yellow fever virus (YFV), dengue virus (DENV), Japanese encephalitis virus (JEV) and tick-borne encephalitis virus (TBEV) [2, 5]. Flaviviruses can cause severe human disease, including encephalitis as is seen for WNV and JEV, and haemorrhagic diseases as is seen following severe DENV and YFV infections [6].

Flaviviruses are no strangers to outbreaks, having caused many in the past 70 years,

and the geographical range of flaviviruses has only grown wider, highlighting the potential for future epidemics [7]. For example, DENV is endemic in areas inhabited by over a quarter of the world's population, with an estimated 400 million cases of infection each year [8]. In 2010 local transmission of DENV was detected in Croatia and France, and in 2012 an outbreak causing over 2000 cases occurred in the Madeira islands of Portugal [9]. Similar to ZIKV, WNV was initially linked to small outbreaks causing febrile illness, circulating throughout Asia, Africa, the middle East, and Australia. However, in the 1990s cases in Eastern Europe were linked to more severe neurological disease, and in 1999 the introduction of WNV into New York lead to a large scale outbreak and the continued circulation of WNV throughout the United States of America [7]. In 2016 there were outbreaks of YFV in densely populated urban areas within the Democratic republic of the Congo and Angola which has trade links to China, again highlighting the potential for global spread [10]. Despite the existence of licensed vaccines for YFV, DENV, JEV and TBEV, these viruses continue to pose a threat to public health [7]. Thus, flaviviruses are an important group of human pathogens and further studies are required to better understand the spread and continued threat to human health posed by these viruses.

1.2 The Flavivirus genome

1.2.1 Genome organisation

Flaviviruses have a common genome organisation consisting of a positive sense RNA genome of approximately 11 kilobases (kb) in length, encoding one large polyprotein flanked by highly structured 5′ and 3′ untranslated regions (UTRs) (Figure 1.1). For ZIKV, ribosome profiling data has also identified a single upstream open reading frame (uORF) in African isolates which is split into two uORFs in the the Asian strain PE243, although their function is still unknown [11]. Following translation, the polyprotein is cleaved to generate viral proteins as shown in Figure 1.1. The roles of the structural and non-structural proteins are depicted in Table 1.1. ZIKV RNA is capped by the methyltransferase and guanylyltransferase activity of the viral protein NS5, producing RNA that mimics the host RNA, however, unlike host RNA, viral RNA does not have a poly(A) tail. Instead, at the 3′ end of the RNA, there is a highly structured 3′UTR, which in DENV has been shown to bind poly(A)-binding

protein (PABP) and enhance viral translation [12].

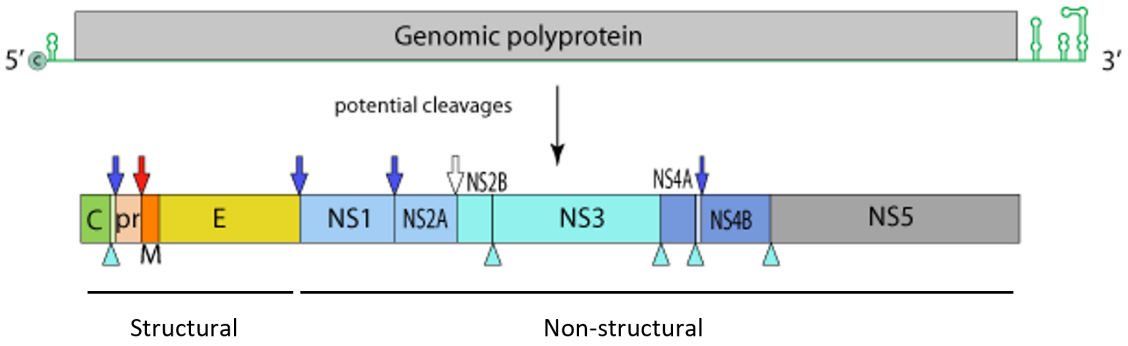

Figure 1.1: The flavivirus genome. Shown is the genome organisation of the ZIKV polyprotein encoding the structural and non-structural proteins. The protease cleavage sites are indicated by arrows coloured to indicate cleavage by different proteases, namely the signal peptidase (dark blue), golgi protease (red) and NS3 (light blue). The 5′ and 3′ UTR structures flanking the coding region are also depicted. Adapted from [13](https://viralzone.expasy.org. Zika virus.).

Table 1.1: Functions of Flavivirus proteins [14].

Viral protein	**Functions**
Structural	
Capsid (C)	Encapsidation of viral genomic RNA.
Envelope (E)	Binds host cell receptors, mediates membrane fusion and entry of virion into host cell.
Membrane protein precursor (prM)	E protein chaperone, protects fusion peptide.
Membrane protein (M)	Component of outer membrane.
Non-structural	
NS1	Role in viral replication and immune evasion.
NS2A	Virion assembly, immune evasion by antagonising IFN α/β response.
NS2B	Co-factor of NS3 for proteolytic cleavage of viral genome.
NS3	Serine protease cleaving viral polyprotein, RNA helicase for viral replication.
NS4A	Role in viral replication. Immune evasion by inhibiting Akt-mammalian target of rapamycin (mTOR) signalling along with NS4B.
NS4B	Role in viral replication. Immune evasion by inhibiting mTOR signalling along with NS4A. Inhibits IFN signalling and promotes remodelling of the ER membrane to form membrane vesicles which are the sites of viral replication.
NS5	Viral RNA dependent RNA polymerase, caps viral genome and inhibits IFN signalling.

1.2.2 The flavivirus UTRs

Both the 5′ and 3′ UTRs of flaviviruses are highly structured, playing important roles in the viral life cycle. The 5′UTR of ZIKV, like other flaviviruses, is highly structured, comprising stem loop A (SLA), followed by stem loop B (SLB). Downstream from SLB there is a short hairpin in the capsid coding region (cHP) [15]. SLA is important for viral replication, binding the RNA dependent RNA polymerase (RdRP), NS5, and directs the formation of the 5′ cap structure [16, 17]. SLB is also important for viral replication, containing a 5′ cyclisation sequence (CS) which interacts with the 3′CS inducing genome circularisation, whereby an RNA ′panhandle′ structure is formed that acts as a template for RNA replication by NS5 (Figure 1.2) [18, 19, 20, 21, 16, 22, 23]. Previous work has shown that this change in ZIKV genome structural conformation acts as the switch between translation and replication, with formation of a circular conformation of the genome inhibiting translation initiation and promoting replication [24].

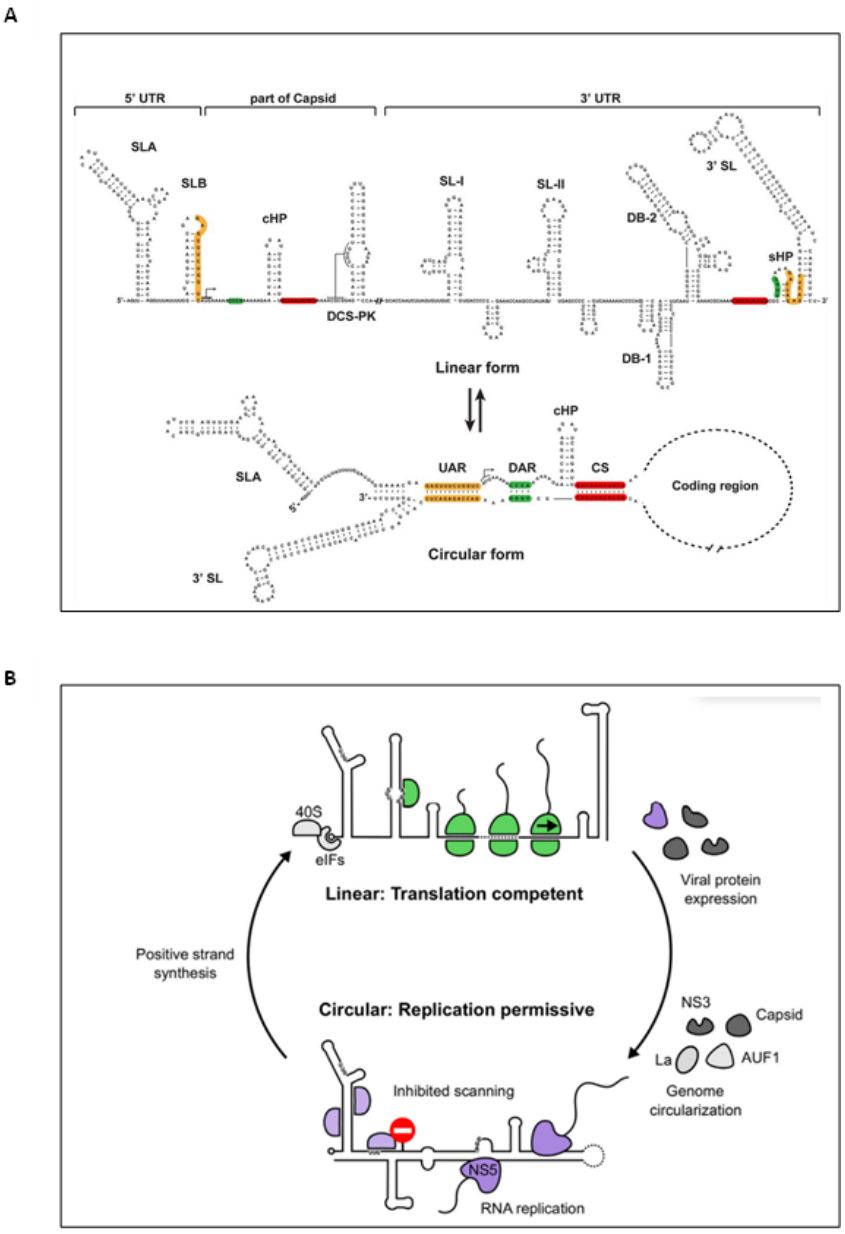

Figure 1.2: Linear and Circular conformations of the ZIKV genome. (A) Shown are the RNA structural elements present in the 5′ and 3′ UTRs of the ZIKV genome as well as the part of the capsid involved in circulirisation (cHP and DCS-PK). Following long range RNA interactions between the upstream of AUG region (UAG), downstream of AUG region (DAR) and cyclisation sequences (CS) in the 5′ and 3′ UTRs, the genome circularises. Taken from [25]. (B) Only the RNA structural elements in the 5′ and 3′UTRs involved in circulirsation are shown. Eukaryotic initiation factors (eIFs) bind to the cap structure of the 5′UTR, promoting recruitment of the 40S small ribosomal subunit to the linear RNA genome. Unwinding of the secondary structures by the helicase eIF4A allows translation initiation to take place, as depicted by the green 48S complex at the start codon (AUG). The change in RNA conformation from linear to circular is promoted by viral and host factors. This inhibits translation by impeding ribosome scanning, instead, promoting replication of the viral genome by the viral RdRP NS5 shown in purple. Taken from [24].

The ZIKV 3′UTR is approximately 428 nucleotides long and highly structured. Flavivirus 3′UTRs not only contain RNA elements that are important for circularisation, but also contain RNA elements that bind many different host and viral proteins, promoting both viral replication and translation [26, 27, 28, 29]. The important role of the RNA structural elements within the 3′UTR is further highlighted by their conservation between different members of the *Flavivirus* genus [30, 31]. The general architecture of the flavivirus 3′UTR contains duplicated stem loop (SL) structures and dumbbell (DB) structures, followed by a small hairpin structure preceding a highly conserved 3′SL structure [32, 33, 31, 30] (Figure 1.3A). The ZIKV 3′UTR follows this structural organisation, although only has one DB structure and one pseudo-DB structure [30] (Figure 1.3B). In particular, the 3′SL and small hairpin preceding the 3′SL are highly conserved amongst flaviviruses [31]. Indeed, mutations within the penta-nucleotide sequence 5′-CACAG-3′ at the top of the 3′SL have been shown to disrupt flavivirus replication, further highlighting the importance of this structural element to the flavivirus life cycle [34, 35, 36, 37].

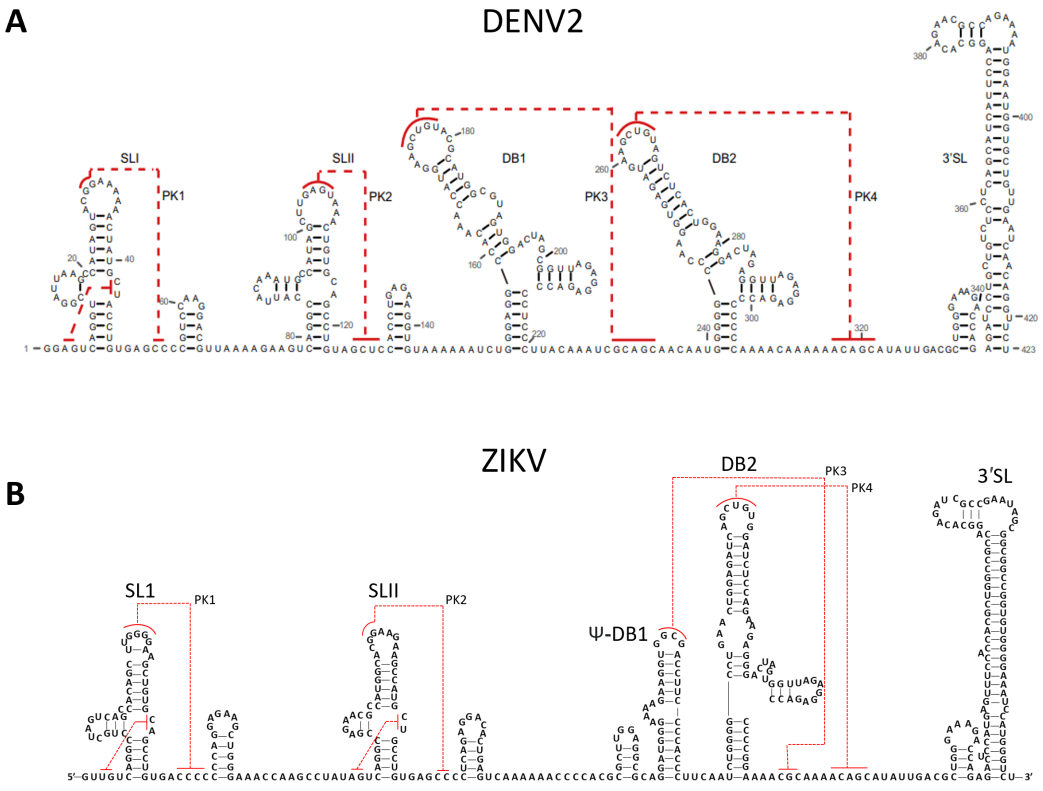

Figure 1.3: Structure of the flavivirus 3′UTR. Shown is the structural architecture of (A) the DENV 3′UTR (Adapted from [30]) and (B) the ZIKV 3′UTR. SL structures, DB structures and the 3′SL are indicated. Pseudoknot interactions are shown as red lines.

Computational analysis has also predicted the formation of multiple pseudoknot (PK) structures within the flavivirus 3′UTR at the SL and DB structures (Figure 1.3) [38, 39]. The crystal structure of the first SL of ZIKV (SL1) and the second SL of Murray Valley encephalitis virus (MVE) (SLIV) have been solved, confirming PK formation at these sites [40, 41]. Additionally, a second internal PK forms through interactions between nucleotides at the base of the stem loop and bases located within the stem loop structure. Both the PK structures support the formation of a P1-P2-P3 three-way junction, with the P1 and P3 helices forming a ring through which the 5′ end of the RNA passes through, positioned by nucleotides in the junction (U4-A24-U42 in ZIKV SLI). The interaction of A37 and U51 closes the loop, securing the 5′ end through the loop. The ring structure is 14 nucleotides, and this size is well conserved amongst other flaviviruses, highlighting the importance of this structural arrangement to the flavivirus life cycle (Figure 1.4) [40, 41].

Recently, x-ray crystallography and structural modelling of the 3′ flavivirus DB structure of Donggang virus (DONGV) also confirmed the formation of a PK at this site, which is supported by the formation of a four-way junction [42]. It is thought that PK structures stabilise RNA secondary structure and are also involved in frameshifting, replication, and translation [43, 44]. Furthermore, formation of these complex RNA structures is important for the production of subgenomic flaviviral RNAs (sfRNAs), which are important for viral fitness and will be discussed further [45].

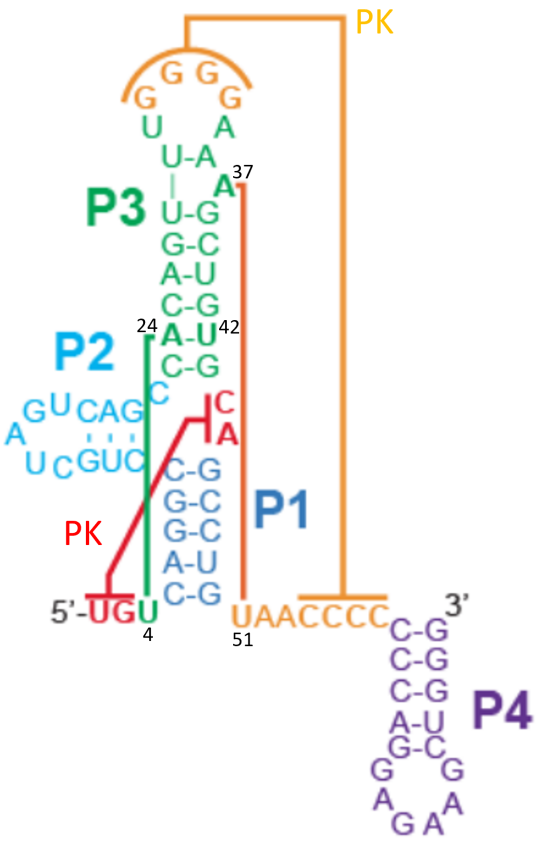

Figure 1.4: Structure of ZIKV xrRNA1. Shown is the crystal structure of xrRNA1 within the ZIKV 3′ UTR. Stems are labelled P1, P2, P3 and P4. RNA-RNA interactions are highlighted by colour coding. The interactions of bases leading to the formation of the internal PK are coloured in red, and the interactions of bases forming the second PK are coloured in light orange. The interaction between U4, A24 and U42 is also shown in green, supporting positioning of the 5′ end of the RNA through the ring formed through the A37-U51 interaction shown in dark orange, thus, threading the RNA through itself to form a knot. The helices P1, P2, and P3 which form the three-way junction are highlighted in light purple, blue, and green respectively.

1.3 Flavivirus life cycle

1.3.1 Viral entry

The interaction of flaviviruses with host receptors is primarily mediated by the viral envelope (E) protein. There have been several different host cell molecules identified as potential receptors for flavivirus entry. This includes $\alpha_v\beta_3$ integrins, C-

type lectin receptors and phosphatidylserine receptors, namely TIM (T-cell immunoglobulin and mucin domain), and TAM receptors (TYRO3, AXL) [46, 47, 48, 49]. For ZIKV, the receptor tyrosine kinase AXL has been identified as a candidate receptor, although different studies have produced conflicting results depending on the cell type utilised. In astrocytes, brain glial cells, endothelial cells, skin cells and Sertoli cells, AXL is important for efficient ZIKV infection, however, AXL is not required for infection of human neural progenitor cells (NPCs) or cerebral organoids [50, 51, 52, 53, 54]. A lack of dependency on AXL has also been seen in interferon (IFN) deficient mouse models [55]. The pattern of glycosylation of flavivirus surface proteins can lead to the utilisation of different host receptors and thus differential tropism [56].

Following binding of the viral envelope to the host cell receptor, the virus enters the cell via clathrin-mediated endocytosis and is transported to a Rab5 positive endosome [57, 58]. Fusion of viral and host membranes occurs following maturation of the endosome to a Rab7 late endosome, and the accompanied acidic pH leads to conformational changes in E protein arrangement. This exposes the fusion peptide on the virions surface leading to the formation of a fusion pore, and the subsequent release of viral genomic RNA in complex with the capsid (C) protein into the cytoplasm so that viral translation and replication can take place [57, 59, 60].

1.3.2 Translation

Flaviviruses require the host cell translation machinery to translate their viral genome into one large polyprotein. As previously mentioned, flavivirus RNA has a cap 1 structure, whereby there is an N7-methylguanosine (m^7G, cap 0) in addition to a 2′-O methylation of the cap proximal nucleotide producing RNA that looks like host RNA (cap 1) (Figure 1.5) [61]. Utilising DENV and WNV replicons, it was shown that mutations which disrupt 2′-O methylation led to viral attenuation, whereas mutations that abolished both mutations were lethal [62, 63]. This can be explained by the reduction in affinity for the eukaryotic initiation factor 4E (eIF4E) observed for a guanosine cap lacking N7-methylation [64]. As eIF4E is essential for cap dependent translation initiation, this subsequently hampers viral translation [65]. Unlike the cap 0 structure, the presence of a cap 1 structure is not essential for flavivirus replication, but is required for evading detection by host cytoplasmic pattern recognition receptors and for immune evasion of the interferon-induced proteins with tetratricopeptide repeats [66, 67].

Several studies, however, have indicated that flaviviruses may also be able to carry out cap-independent translation under certain conditions. For both ZIKV and DENV, polysome profiling demonstrated strong host translation inhibition whilst maintaining the production of viral proteins. Although the mechanism of translation inhibition was not determined, it was found that repression was independent of well-known translation inhibition mechanisms, namely phosphorylation of eukaryotic initiation factor 2 (eIF2) or sequestration of eIF4E [68]. Furthermore, the treatment of cells with cap-dependent translation inhibitors, including eIF4E siRNAs, did not affect DENV, despite hampering cellular translation. Interestingly, eIF4E depletion was shown to partially rescue the titre of virus produced from DENV RNA lacking an m^7G cap structure to 20-30% of wild-type (WT) DENV [69]. This indicates that under conditions where host translational is inhibited, flaviviruses can utilise cap independent mechanisms to maintain viral translation. The use of reporter constructs demonstrated that this was not dependent on the recruitment of translation initiation factors to the RNA in a $5'$ independent manner via an internal ribosome entry site (IRES), but instead, was reliant on interactions between the $5'$ and $3'$ UTRs [69]. However, more recent work indicated that the $5'$UTR of both DENV and ZIKV when utilised in reporter constructs contained IRES activity in baby hamster kidney (BHK) cells [70]. Indeed, utilising an IRES is advantageous, as it allows the virus to continue translating viral proteins even when the host suppresses cap-dependent translation in an attempt to control viral infection. This also allows viruses to target host cell translation without affecting viral protein production [71]. Furthermore, other genera within the *Flaviviridae* family, namely *Hepacivirus*, *Pestivirus* and *Pegivirus*, have been shown to utilise IRES elements for translation of the viral genome [72]. Although it seems plausible that flaviviruses could utilise cap-independent translation, the relevance of this during flavivirus infection still requires further investigation.

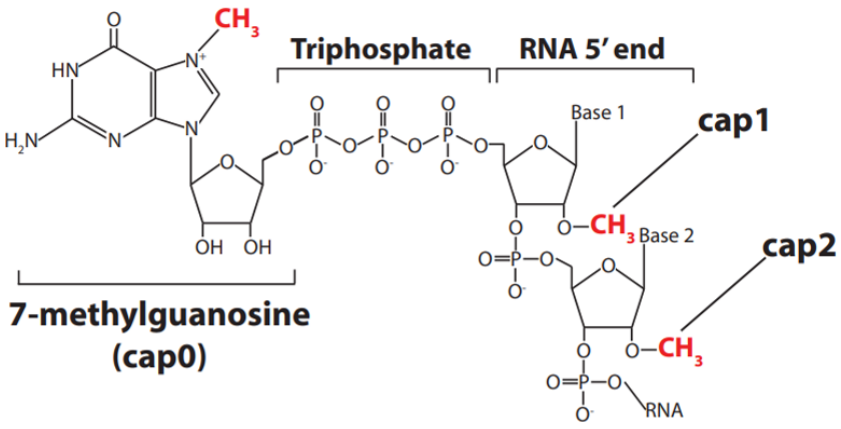

Figure 1.5: Cap structures. Shown are the methylation events producing cap 0, cap 1 and cap 2 structures. Taken from [73].

1.3.3 Replication

Replication of the flavivirus genome occurs within replication complexes derived from the endoplasmic reticulum (ER) (Figure 1.6) [74]. As previously discussed, genome circularisation and the resulting pan-handle structure that is generated provides a template for binding of the RNA dependent RNA polymerase NS5 to SLA in the 5′UTR. This generates a double stranded RNA (dsRNA) intermediate consisting of the positive and negative sense RNA [24, 18, 19, 20, 75]. The viral protein NS3 harbours helicase activity, unwinding the dsRNA so that the newly formed viral genome is released and subsequent rounds of positive strand synthesis can occur [65].

The newly formed viral RNA is then capped and methylated through the combined activity of the viral proteins NS3 and NS5. Following removal of the 5′ triphosphate by the triphosphatase activity of NS3, the guanylyltransferase domain of NS5 adds guanosine monophosphate producing a GpppA cap. The methyltransferase domain of NS5 then methylates the cap at N-7 and 2′-O to produce a cap 1 structure [76, 77, 78].

1.3.4 Virion assembly and egress

Assembly of the virus genome with the C, prM and E proteins occurs at the membrane of the endoplasmic reticulum (Figure 1.6). Immature particles are formed by budding from the ER membrane which are transported to the Golgi and trans-Golgi

network (TGN) [79, 80]. Transport to the TGN, and subsequent drop in pH, leads to structural rearrangements of the prM-E protein, allowing cleavage by host furin and maturation of the virion [81]. In the final step, the matured virions are released from the cell via exocytosis (Figure 1.6) [60].

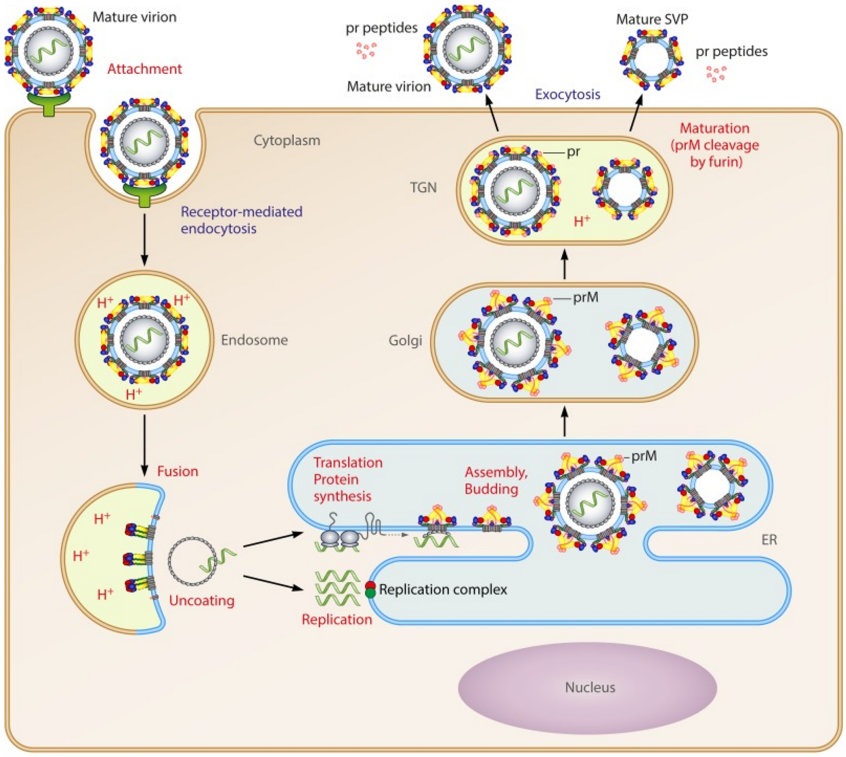

Figure 1.6: Flavivirus life cycle. Following viral attachment to the host cell, the virion enters the cell via clathrin-mediated endocytosis. The low pH environment of the endosome triggers the fusion of the viral and host membranes and the release of viral RNA into the cytoplasm. Translation of viral proteins occurs in the endoplasmic reticulum, and replication of the viral genome in replication complexes associated with the ER membrane. Following assembly, the virions are transported through the Golgi and trans-Golgi networks where glycans on the spiky immature virion are trimmed, and a drop in pH triggers structural rearrangements allowing cleavage of prM by host furin to produce mature virions. The mature virions exit the cell via exocytosis. Figure taken from [82].

The mature ZIKV virion exhibits an icosahedral structure consisting of a viral membrane containing 180 copies of E and M proteins. The E protein forms dimers that arrange into trimeric conformations to form rafts, with each virion consisting of 30 rafts [83, 84]. The structure of the nucleocapsid containing the C protein and genomic RNA is not well understood. Although, recent work utilising cryo electron microscopy obtained subnanometer resolution of the structure of the capsid proteins

within the virion by utilising an antibody that binds across the E and prM proteins. This stabilised the immature Zika particles and displayed that three capsid dimers interact to form a triangular capsid complex that bridges the negatively charged viral RNA and the negatively charged lipid membrane. Each virion contains 120 copies of capsid protein, making up a total of 60 capsid dimers [85].

1.4 Transmission and epidemic potential of ZIKV

1.4.1 ZIKV outbreaks

ZIKV transmission is mainly linked to mosquitoes of the *Aedes* genus, although transmission can also occur vertically from mother to foetus, and cases of sexual transmission have also been reported (Figure 1.7) [86, 87]. ZIKV was first isolated in 1947 from a Rhesus macaque in the Zika forest in Uganda. Following this, a few sporadic cases of infection were reported in Asia and Africa. It wasn't until 2007 that there were reports of an outbreak on the Yap island in Micronesia, which subsequently spread to French Polynesia and by 2015 was reported in Brazil, spreading throughout the Americas and the Caribbeans (Figure 1.8). In 2016 after potential links were established between ZIKV infection and congenital microcephaly, the World Health Organization declared ZIKV a public health emergency [87].

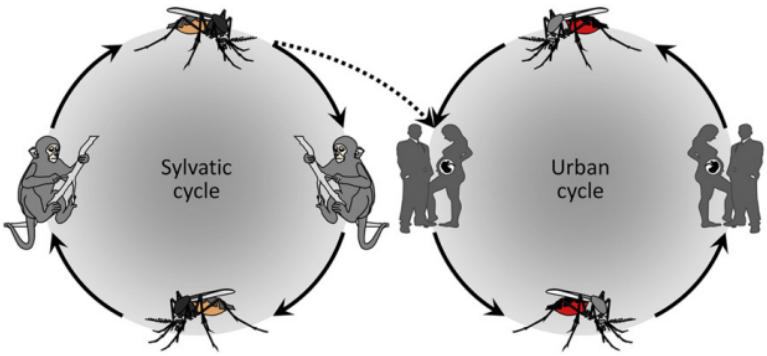

Figure 1.7: Transmission of ZIKV by mosquitoes. The sylvatic cycle transmits ZIKV between arboreal mosquitoes and non-human primates in forests. In the urban cycle, ZIKV is transmitted between urban mosquitoes and humans. It is presumed that arboreal mosquitoes can also transmit ZIKV between non-human primates and humans. Taken from [86].

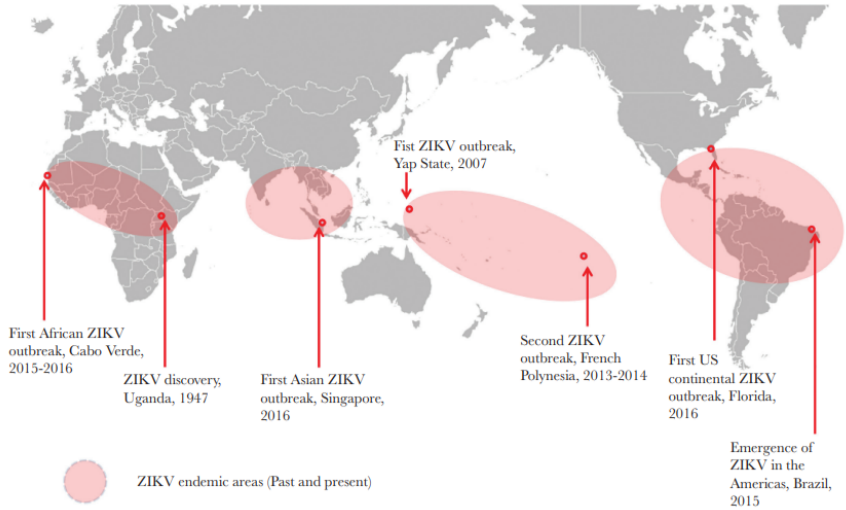

Figure 1.8: ZIKV Endemic areas. Shown are the geographical locations where ZIKV circulates and the dates of reported ZIKV outbreaks. Taken from [87].

Phylogenetic analysis identified two main lineages of ZIKV, namely African and Asian, and the strain that caused the epidemic in the Americas is of the Asian lineage, often denoted as the American strain [88]. Different strains of the Asian lineage, which are not epidemic strains, but are circulating throughout Asia, have also been linked to adverse pregnancy outcomes and caused a recent outbreak in India in 2018. This highlights the epidemic potential and continued threat posed by endemic strains [89, 90, 91, 92]. Interestingly, despite *in vitro* experiments and *in vivo* animal models demonstrating increased transmissibility and a more aggressive pathology for recently circulating African strains, human outbreaks and associated cases of newborn microcephaly have only been linked to Asian strains [93, 94, 95, 96, 97, 98, 99, 100, 101, 102, 103, 92, 104]. This may be explained by a lack of surveillance and reporting of ZIKV infections in Africa, herd immunity in African populations, reduced vector capacity of African mosquitoes, as well as a more aggressive pathology leading to foetal death [102]. Work utilising recently circulating African strains has further highlighted the epidemic potential of these viruses, displaying higher transmissibility and pathogenicity than viruses of the Asian lineage [102].

It is important to highlight that because many cases of infection are asymptomatic, and there is a crossover of symptoms with other viral infections, surveillance and detection of the global circulation of ZIKV remains difficult [92]. It is, therefore, possible that ZIKV infection is much more widespread globally than current figures reflect.

1.4.2 Worldwide spread of ZIKV

The wide geographic distribution of the main vectors for urban transmission cycles of ZIKV, namely *Aedes aegypti* (*Ae.aegypti*) and *Aedes albopictus* (*Ae. albopictus*), highlights the potential for worldwide ZIKV spread [105, 106]. Although both species have been linked to ZIKV outbreaks, infections carried out with an Asian strain of ZIKV led to low levels of viral dissemination indicating low vector competency [107]. However, both mosquito species bite mainly during the daytime, providing ample opportunity for infection of human hosts. In particular, *Ae. aegypti* displays a high vectorial capacity for ZIKV transmission due to human blood being its main food source, crossover with human habitats, and the fact that it bites several humans during one gonotrophic cycle [108, 105]. *Ae. aegypti* mosquitoes are found in both tropical and subtropical climates, while *Ae. albopictus* mosquitoes are more widespread, with habitats found also in cooler temperate regions [86, 105, 106]. The increased global spread of *Ae. albopictus* has been attributed to international trade, particularly of used tyres, and an ability to adapt easily to new environments [108, 106]. Furthermore, *Ae. albopictus* has been displaying signs of adaption to cooler temperatures, and this, along with climate change, will likely widen its already broad distribution and thus potential to spread ZIKV worldwide [106].

Controlling these vector populations and hence spread of ZIKV remains difficult due to insecticide resistance and toxicity to other non-target species [109]. The release of sterile male mosquitoes is more environmentally friendly, however, this requires their continual release, in addition to them competing with wild mosquito populations. Other methods include the release of males carrying a dominant lethal gene, which when inherited by offspring will kill females and be passed onto future generations by male offspring [109]. Additionally, the use of an endosymbiotic bacteria of arthropods, namely *Wolbachia*, has been shown to effectively inhibit ZIKV replication, and the release of infected mosquitoes allows the spread of this bacteria throughout wild mosquito populations [110, 111]. Despite this, major obstacles to the implementation of these methods still exist, including hesitancy by local communities and ensuring that non-target insect species are not inadvertently harmed. It is also important to highlight the potential for adverse effects to the ecosystem caused by manipulating mosquito populations [109]. Due to the absence of a vaccine, vector control remains the major strategy for ZIKV transmission control.

Worldwide transmission of ZIKV has been further perpetuated by international travel, with sporadic cases of infection detected globally in Australia, the United

States of America, and several European countries. This combined with the increased distribution of vector species, provides the potential for ZIKV to enter immunologically naive populations and spread rapidly, potentially causing further epidemics or even a pandemic [86].

1.5 ZIKV disease

1.5.1 Disease manifestations

The majority of ZIKV infections are thought to be asymptomatic or cause mild illness. Common symptoms include fever, headache, rash, conjunctivitis, muscle aches and joint pain [86]. ZIKV infection can also cause more serious pathology, whereby infection in pregnant women has been associated with stillbirth, foetal death, premature birth, and congenital Zika syndrome. Congenital Zika syndrome is characterised by neurological symptoms, including microcephaly, brain calcifications, eye abnormalities, and issues with brain development [112]. Infection of adults has also been linked to Guillain-Barre syndrome, whereby nerve damage leads to paralysis [86].

1.5.2 Neurotropism

Many flaviviruses have been identified as neurotropic, including WNV, JEV, and TBEV. This can induce neuropathology such as paralysis, encephalitis, and cognitive impairment [7]. DENV infection has also been linked to neuropathology, following the observation that infected patients display neurological symptoms, and DENV was identified in brain tissue following fatal DENV infection [113].

It was not until the 2015/2016 epidemic that a link between ZIKV infection and neural tropism was first established, following the rising cases of microcephaly in neonates during this epidemic (Figure 1.9), as well as cases of Guillain-Barre syndrome in adults [114]. ZIKV was detected in the brain tissue of a foetus displaying microcephaly following maternal infection [115]. This led to further investigations, establishing neural tropism of ZIKV through infections of human neurospheres, human brain organoids, and mouse models [116, 117, 118, 119, 120]. Indeed, infection of pregnant mice with an Asian strain clinical isolate of ZIKV from Brazil led

to foetal infection, with pups displaying hampered growth, reduced cell number, and cortical layer thickness, reminiscent of the microcephaly phenotype observed in human neonates [116]. This neuropathology was also observed with other Asian strains of ZIKV following the direct injection of virus into embryonic mouse brains [120, 121]. Further links between ZIKV infection and microcephaly were established through the infection of neural progenitor cells and brain organoids [116, 118, 119]. In particular, human brain organoids are useful for modelling ZIKV induced microcephaly in human cells, producing pathology that mimics the reduction in cortical layer thickness observed in microcephalic foetuses [117, 118, 115].

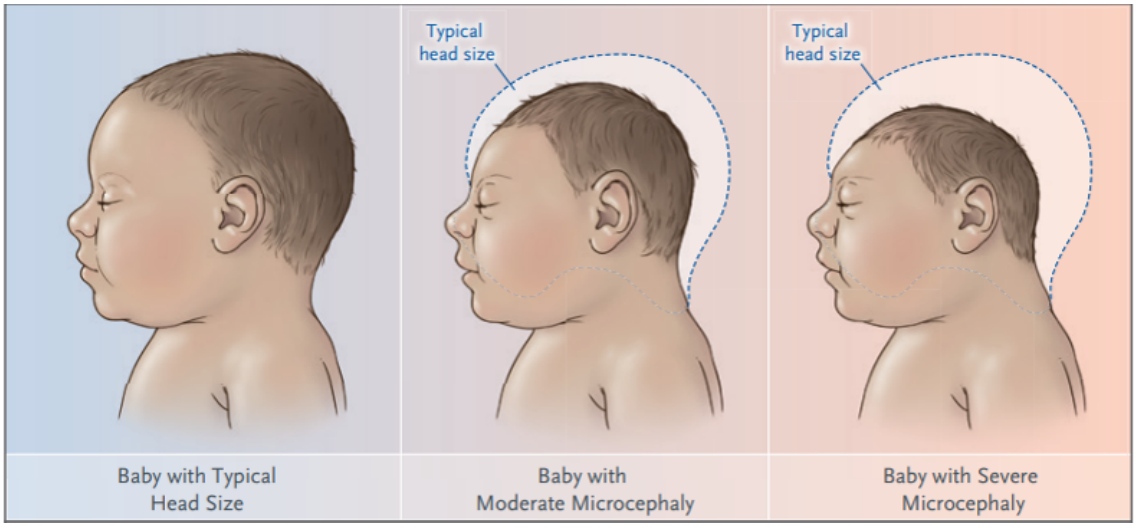

Figure 1.9: ZIKV induced microcephaly. Depicted is the reduced head size observed for infants infected with ZIKV compared to a typical newborn. Taken from [108].

This neuropathology was not only observed for Asian strains of ZIKV, but also African strains, despite no clinical cases of microcephaly associated with African strains of virus [117, 122, 104]. Interestingly, several studies have shown increased neuropathology caused by African strains compared to Asian strains of ZIKV, with increased replication rates and death in neural cells [93, 94, 95, 96]. This has also been observed in mouse models, with more severe neuropathology and higher mortality rates observed following infection with African strains compared to Asian strains [97, 98, 99, 100, 101, 102]. However, experiments in non-human primates have provided conflicting results, with ZIKV strains of the Asian lineage demonstrating higher infectivity than the African strains [123, 124]. This enhanced infectivity of the Asian lineage was also observed in human neurospheres, alongside increased pathology when compared to a strain of the African lineage [116]. It has been suggested that the conflicting results in pathogenicity observed for different ZIKV

strains may reflect the lack of availability of newer African strains, as well as the repeat passaging of strains leading to host adaption [125]. Indeed, utilising a primate adapted African ZIKV isolate and comparing it to a human adapted Asian isolate, demonstrated that the African strain infected chimpanzee organoids, whereas the Asian strain did not [116]. Furthermore, conducting infections with low passage African strains has been shown to recapitulate the increased pathology observed previously when compared to Asian strains, with higher mortality rates in mice and increased death of NPCs, as well as enhanced infectivity [102, 95]. The differences in virulence observed for different passages of ZIKV may be explained by differences in glycosylation motifs. The presence of an N154 glycosylation motif has been observed in recently circulating Asian strains of ZIKV but is absent in many African strains [126, 127]. It has been proposed that the extensive passaging of the historical African strain MR766 in mouse brains has led to the loss of the N154 glycosylation motif [128]. This is further supported by work sequencing MR766 with different passage histories, displaying the loss of potential glycosylation sites in some strains [129]. Furthermore a loss of N154 glycosylation in Asian and African lineage strains has been shown to lead to viral attenuation in mice, potentially due to hampered attachment and infection of lectin-expressing leukocytes [130]. Cumulatively this highlights the importance of utilising currently circulating strains of ZIKV, as well as appropriate models for infection to obtain useful insights into the virulence and pathology of ZIKV.

1.6 SfRNA generation

The term sfRNA was first coined following the observation that members of the *Flavivirus* genus within the *Flaviviridae* family produced small subgenomic RNA (sgRNA) derived from the 3′UTR. These small sgRNAs were not observed in representative viruses from the *Pestivirus* and *Hepacivirus* genera within the *Flaviviridae* family [38]. It is widely thought that the host enzyme Xrn1 is responsible for the production of sfRNAs [45]. Normally, Xrn1 is involved in RNA turnover, degrading decapped 5′ monophosphate RNA [131]. Similarly, Xrn1 is thought to degrade viral RNA in a 5′-3′ direction, but stalls at highly structured regions within the flavivirus 3′UTR, termed Xrn1 resistant RNAs (xrRNAs), leading to the production of sfRNAs [45]. The link between Xrn1 and sfRNA production has been further established by work demonstrating that silencing of Xrn1 lead to a 90% reduction in sfRNA production by YFV in human derived SW13 cells. Additionally, incubation of Xrn1

with a YFV reporter RNA produced sfRNA [132]. Following the isolation of RNA from WNV infected cells and treatment with Xrn1, it was shown that sfRNA is resistant to Xrn1 degradation, supporting that sfRNA is generated by Xrn1 stalling [38].

Indeed, the size of sfRNA1, 2, and 3, produced following infection with WNV, DENV, and ZIKV, corresponds to stalling at the SL structures and the first DB structure within the 3′UTR [133, 38, 134, 40, 135]. Thus, it seems likely that SLI, SLII, DB1, and DB2 correspond to xrRNA1, xrRNA2, xrRNA3, and xrRNA4 respectively (Figure 1.10) [135]. This is further supported by work demonstrating that the mutation of a single nucleotide within ZIKV SLI and MVE SLIV, disrupted the formation of the three-way junction and was enough to abolish Xrn1 resistance [40, 41]. Additionally, in both WNV and ZIKV, disruption of complex folding at xrRNA1 and xrRNA2 abolished the production of sfRNA1 and sfRNA2 respectively [41, 136, 40]. Further evidence for the role of RNA structure in sfRNA generation came from the finding that the introduction of mutations to restore the PK1 structure also restored sfRNA1 formation in WNV [133]. However, when mutations were introduced to disrupt PK2 formation at SLIV, abolishing sfRNA production, restoration of nucleotide complementarity did not rescue sfRNA2 production. In this case, it was concluded that sfRNA2 production was reliant on nucleotide specificity and not an intact PK2 structure. However, the authors did not use structural mapping to confirm the restoration of PK2 structure, and sequence interactions were restored by introducing a classical Watson-Crick base pair (CGC with GCG) when the original interaction contained a non-Watson-Crick base pair (GCG with UGC) [133]. The consensus is that sfRNA production occurs through Xrn1 stalling at these highly structured regions within the 3′UTR.

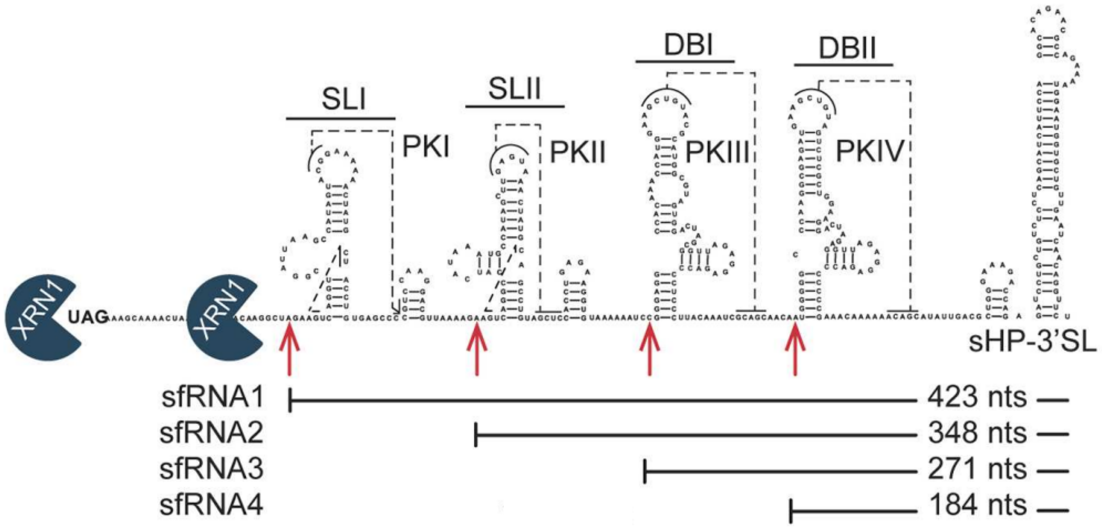

Figure 1.10: sfRNA is generated by Xrn1 stalling at RNA structures in the 3′UTR. Shown is the secondary structure of the DENV 3′UTR. Stalling of 5′-3′ degradation by the host enzyme Xrn1 at SL and DB structures within the 3'UTR produces sfRNAs of different sizes. Taken from [135].

However, several studies have questioned the role of Xrn1 in the production of all sfRNA species. Although Xrn1 was successfully halted by DENV-2 SL1 and SLII, this was not observed for DB1, DB2 or the 3′SL. It was suggested that perhaps interaction of these structures with another protein is also required to confer resistance [134]. Furthermore, for ZIKV, knockdown of Xrn1 reduced sfRNA2 production but had no effect on sfRNA1 production [40]. Recent work demonstrated that sfRNA3 in ZIKV is likely not formed through Xrn1 resistance at the DB structure, as probing of the ZIKV sfRNA demonstrated that sfRNA3 did not contain the 3′SL structure [42]. Therefore, although Xrn1 may be involved in the production of some sfRNA species, it is likely that other cellular enzymes or proteins are also involved. For ZIKV, it has been suggested that the production of sfRNA3 is through trimming by another nuclease from the 3′ end and is therefore not reliant on Xrn1 [42]. Other host exoribonucleases may also be involved. Indeed, WNV xrRNA2 displayed resistance to 5′-3′ exoribonuclease degradation by bacterial RNase J1 and yeast Dxo1. This was shown to be dependent on structural integrity, as the mutation of a single nucleotide to disrupt xrRNA folding abrogated resistance to degradation [137]. Cumulatively this shows that RNA structural elements within the 3′UTR play a key role in sfRNA generation, and that further investigations are required to elucidate the production of different sfRNA species.

1.7 Role of sfRNA in the flaviviral life cycle

The production of sfRNAs is important for viral pathogenicity, replication, and transmission for many different flaviviruses [38, 138, 135, 139]. The importance of sfRNAs to flaviviruses is highlighted by the finding that sfRNAs are produced by flaviviruses regardless of vector species and have been observed for MBFVs, TBFVs, ISFs and NKVs [38, 140, 137]. Consequently, there have been many studies investigating the potential roles of flaviviral sfRNAs in promoting viral infection. These studies have linked sfRNA production to deregulation of mRNA turnover, evasion of host immune responses, and regulation of apoptosis [45].

1.7.1 sfRNAs deregulate host mRNA turnover

A potential role for sfRNAs is the deregulation of host mRNA turnover through binding of the host enzyme Xrn1. If Xrn1 is sequestered by viral sfRNAs, it is unable to perform its key role in the degradation of uncapped monophosphate RNAs [45, 131, 141]. Indeed, when an sfRNA defective WNV mutant was compared to WT WNV, there was an increase in uncapped mRNAs and generally enhanced stability of host mRNAs, indicating impairment of the host mRNA decay pathway [141]. This could lead to an insufficient host immune response to viral infection due to the deregulated expression of antiviral proteins and cytokines which are normally turned over rapidly [141].

1.7.2 sfRNAs inhibit siRNAs and miRNAs

The production of sfRNAs could also hamper host immune signalling through the suppression of small interfering RNA (siRNA) in invertebrates and microRNAs (miRNAs) in both vertebrates and invertebrates [45]. SiRNAs are 21 nucleotides in size and derived from the cleavage of viral double stranded RNA intermediates and directly target viral RNA. Comparatively, miRNAs are encoded by the host and elicit anti-viral effects through the post transcriptional regulation of genes encoding antiviral proteins, as well as proteins utilised for viral replication [142, 45]. Consequently, flaviviruses have developed strategies to overcome the anti-viral effects of both siRNAs and miRNAs. DENV and WNV sfRNA has been shown to suppress siRNA and miRNA induced RNA interference (RNAi) pathways, inhibiting

the silencing of a firefly luciferase reporter RNA in both mammalian and insect cells [143]. In mosquitoes, a 3-fold drop in efficiency in RNAi silencing was observed following infection with an sfRNA deficient WNV mutant compared to WT WNV [144]. Similarly, utilising an sfRNA1 deficient ZIKV mutant, it was shown that there was an increased number of viral siRNAs when normalised to viral titres, indicating an increased RNAi response [145]. Even sfRNAs derived from the more divergent tick-borne flaviviruses have been shown to hamper RNAi knockdown of a reporter gene in tick cells, although the effects were modest [140]. Mechanistically, it has been proposed that sfRNAs inhibit RNAi by sequestering components of the siRNA machinery [146]. Indeed, WNV sfRNA has been shown to co-precipitate with components of the RNAi machinery, namely Argonaute 2 and Dicer, and sfRNAs can act as substrates for Dicer producing smaller RNAs [144, 146, 143]. Flaviviruses have also been shown to utilise miRNAs to promote viral replication. For DENV-2, upregulation of the miRNA miR-146a, leads to a reduction in IFN-β signalling, which enhanced DENV replication [147].

Despite the findings that sfRNAs inhibits RNAi in vertebrate and invertebrate hosts, it is unclear how vital a role sfRNA driven RNAi suppression plays in viral fitness. Following ZIKV infection of mosquitoes, there was still a substantial number of siRNAs produced [145]. Additionally, in WNV, disruption of sfRNA1 production was shown to have no effect on siRNA production in mosquitoes when compared to WT WNV, however, this mutant still produced sfRNAs in the form of sfRNA2 instead [146]. Although disruption of both sfRNA1 and sfRNA2 in WNV led to hampered viral growth in mosquito cells and a reduction in infection rates of mosquitoes, the link between reduced fitness and RNAi was not investigated [146]. Disruption of sfRNA1 or sfRNA2 in ZIKV appeared to have little effect on viral fitness in relation to RNAi. The titres obtained for these mutants and WT virus were not significantly different, regardless of whether infection was carried out in RNAi deficient or RNAi competent mosquito cells lines [148].

1.7.3 sfRNAs inhibit the IFN response

During flavivirus infection, the type I IFN response drives anti-viral immunity in vertebrates by triggering the expression of hundreds of antiviral genes. This occurs through the activation of IFN regulatory factors which induce type I IFNs. Type I IFNs subsequently bind the IFN receptor and trigger the Janus tyrosine kinase (JAK) and signal transducers and activators of transcription (STAT) signalling cas-

cade. This induces the expression of IFN stimulated genes, producing an anti-viral state within the cell [67, 149]. Subsequently, flaviviruses have developed strategies to overcome IFN signalling, including the production of sfRNA [67].

Utilising an sfRNA deficient WNV mutant, it was shown that a lack of sfRNA production led to a reduction in viral growth and pathogenicity in cell culture and mice [38]. Further work then linked the production of sfRNAs to the type 1 IFN response. Replicative defects of an sfRNA deficient WNV mutant compared to WT WNV were only displayed in cells that could mount a type I IFN response [150]. Importantly, the replicative defect of the sfRNA defective WNV mutant could be re-established in these cells through IFN-α treatment. Furthermore, a partial rescue of sfRNA deficient WNV was observed in mice that were type I IFN deficient, with reduced survival rates when compared to IFN competent mice [150]. For DENV, increased production of sfRNA by an epidemic strain, compared to the lower levels of sfRNA produced by a pre-epidemic strain, was linked to the ability to overcome the host IFN response. Replication of the epidemic strain was not enhanced following knockdown of the upstream IFN-β regulator, interferon regulatory factor 3 (IRF3), unlike the pre-epidemic strain which replicated much more efficiently than in WT cells [151]. Furthermore, the transfection of DENV sfRNA or ZIKV sfRNA into polyinosinic:polycytidylic acid (poly I:C) treated cells led to lower levels of expression of IFN-β [151, 139]. Similarly, transfection of sfRNAs alongside JEV infection reduced phosphorylation of IRF3 and its subsequent nuclear localisation, coinciding with an observed reduction in IFN-β promoter activity of 57% in A549 cells [138]. DENV-2 sfRNA has also been shown to interact with proteins involved in mediating the IFN response, namely G3BP1, G3BP2, and CAPRIN1. It was suggested that by sequestering these proteins that DENV sfRNA inhibits IFN stimulated gene translation, and therefore, the antiviral response. However, binding of these proteins was not demonstrated for DENV-3 or WNV [152]. The interaction of DENV sfRNA with TRIM 25 was also shown to hamper the IFN response through inhibition of ubiquitination of the pattern recognition receptor RIG-I [151]. Furthermore, ZIKV sfRNA was also shown to inhibit the induction of RIG-I induced IFN-β production, although, unlike DENV, could also inhibit MDA-5 signalling [139]. This highlights that different flaviviruses likely exploit different mechanisms for sfRNA directed repression of IFN signalling.

1.7.4 Role of sfRNAs in cytopathicity and pathogenesis

The production of sfRNA is also important for viral cytopathicity and pathogenesis, as sfRNA1 deficient WNV and DENV mutants produced defective plaques in both Vero and BHK-21 cells which are IFN deficient [38, 153]. Additionally, infection of mice with a WNV sfRNA1 deficient mutant led to no encephalitis and 0% mortality compared to the 100% mortality observed following WT infection. This was despite the detection of similar viral loads in the brain. It was suggested that the enhanced pathogenicity observed following WT WNV could be explained by linking sfRNA production to the induction of cell death [38]. Controlled cell death, or apoptosis, is often utilised by host cells to control viral infection. However, apoptosis may also act to perpetuate viral spread. Indeed, several ZIKV proteins have been shown to induce apoptosis, including C, M, PrM, E and NS4B [154]. An increasing amount of research has linked sfRNA production to the regulation of apoptosis. An sfRNA deficient DENV2 mutant did not display major replicative defects, but did lead to a massive reduction in apoptosis in BHK-21 cells which could be partially restored by transfection of sfRNA [153]. Other studies have shown a down-regulation of apoptosis following flavivirus infection. In ZIKV, the production of sfRNAs has been linked to inhibiting apoptosis in mosquitoes, as infection with sfRNA defective ZIKV mutants led to an increase in apoptosis compared to WT ZIKV. Differences in the expression profiles of genes involved in cell death was also observed between WT ZIKV and sfRNA deficient mutants. Of particular interest was the observation that an sfRNA deficient ZIKV mutant induced expression of the pro-apoptotic enzyme caspase-7, whereas WT ZIKV did not [148]. Furthermore, transfection of sfRNA alongside JEV infection of A549 cells reduced IFN-β induced apoptosis by 23%. This combined with the observation that sfRNA:genome copies were higher in persistently infected cells compared to acutely infected cells, led the authors to suggest that sfRNAs inhibit apoptosis and that this allows viral persistence [138]. Although the data is somewhat conflicting, perhaps there is a balance between the inhibition of apoptosis to allow viral replication to take place and the induction of apoptosis to promote viral spread.

1.8 sfRNA and the host switch

There are clear differences in sfRNA patterns for DENV following infection of mammalian vs mosquito cells, indicating that sfRNAs play a role in host switching.

During mammalian cell infection, DENV mainly produces sfRNA1 [135]. Following adaption to a mosquito host, disruption of DENV xrRNA2 due to the accumulation of mutations/deletions in SLII, leads to the accumulation of smaller sfRNAs, namely sfRNA3 and sfRNA4 [135, 31]. Mutations disrupting xrRNA2 also lead to a reduction in sfRNA1 production which can be rescued by restoration of the SLII structure. Accumulation of sfRNA1 was shown to be important for viral replication in mammalian cells, whereas sfRNA3 accumulation was associated with a reduction in viral fitness. Furthermore, this reduction in viral fitness was linked to the induction of a stronger type I IFN response, indicating that mutations that allow adaption to mosquitoes leads to a stronger antiviral response in human cells [135]. This fits a model whereby the tertiary structure of xrRNAs is modulated through mutation of secondary structures within the 3′UTR, controlling the pattern of sfRNA production, and allowing viral replication to occur in different hosts [32]. The presence of structural duplications allows a rapid switch between different host environments to take place without adversely affecting viral fitness [135, 32].

Similar to DENV, WNV produces mainly sfRNA1 following infection of mammalian cells and a small amount of sfRNA2. Interestingly, unlike DENV, additional sfRNA species are observed in mammalian cells, including an sfRNA of intermediate size between sfRNA1 and sfRNA2 which is lost in mosquito cells. Disruption of xrRNA2 leads to the production of a smaller sfRNA species, likely sfRNA3, as has been seen during DENV adaption to mosquitoes [134, 135, 31]. However, this does not appear to play a role in WNV adaption to different hosts, as the overall pattern of sfRNAs is similar between mosquito and mammalian cells, with sfRNA1 predominantly produced, with a small amount of sfRNA2 [134, 146]. Utilising an sfRNA1 deficient WNV mutant, it was shown that viral titres were lower in the body and saliva of mosquitoes, indicating that the production of sfRNA1 was crucial for infection and transmission in mosquitoes. Correspondingly, this was only observed when mosquitoes were infected via blood feeding and not through injection, indicating that the viral defects observed were due to an inability to cross the midgut barrier [146]. This mutant displayed similar levels of replication in both mosquito cells and Vero cells compared to WT WNV, and induced similar levels of death in Vero cells. This indicated that a lack of sfRNA1 did not cause replicative defects or effect cytopathicity. However, the authors did not look at plaque morphology and previous work has shown a smaller plaque phenotype for sfRNA1 deficient WNV mutants [146, 38]. The production of sfRNA1 by WNV also appears to be important in mammals, as an sfRNA1 deficient mutant was shown to be much less pathogenic than WT WNV in a mouse model [38].

In ZIKV, like WNV, a similar sfRNA pattern is observed in both mammalian and mosquito cells. In this case mainly sfRNA1 and sfRNA2 are produced [40, 136, 135]. In mosquitoes, however, an increase in ZIKV sfRNA3 is also observed [148, 136]. For ZIKV, it is not sfRNA1 that is important for efficient transmission and infection in mosquitoes, as has been demonstrated for WNV and DENV2, but the production of sfRNA2 [148]. Similar to WNV sfRNA1, ZIKV sfRNA2 was deemed important for crossing the midgut barrier, as if the sfRNA2 deficient virus was administered by blood meal it reverted to WT, but if infection was carried out via injection the mutation was maintained [148]. As seen for both DENV and WNV, sfRNA1 production is likely important for ZIKV replication in mammalian cells. Disruption of sfRNA1 production reduced ZIKV replication in Huh-7 human cells and in the placenta and brain of an infected mouse [155, 136]. Although the attenuation observed appeared to be tissue specific, as the sfRNA1 deficient mutant replicated to similar levels as WT ZIKV in the mouse spleen [155].

The differences in sfRNA patterns displayed between DENV and ZIKV can be explained by the finding that the ZIKV SLI structure is more related to DENV SLII in terms of structure and sequence, and ZIKV SLII is more similar to DENV SLI, indicating an inversion of the SL structures [136]. Interestingly, disruption of the xrRNA1 structure of ZIKV following mutation did not significantly affect viral replication compared to WT in mosquito cells. However, the deletion of SLI increased replication in mosquito cells. It was therefore suggested that it was not changes in the sfRNA pattern of ZIKV allowing the host switch to mosquitoes, but instead deletion of inhibitory sequences within SLI [136]. Thus, despite the conservation of secondary structures within the 3′UTR of WNV, ZIKV and DENV, these flaviviruses seem to have adapted different mechanisms of host switching.

Table 1.2: Summary of sfRNA production and function in a mammalian vs mosquito host. Shown is the pattern of sfRNAs produced for ZIKV, DENV and WNV in a mammalian vs mosquito host. A summary of the main functions of flaviviral sfRNAs in different host environments is also shown.

	Mammalian host	**Mosquito host**
sfRNA pattern		
ZIKV	sfRNA1	sfRNA2
DENV	sfRNA1	sfRNA3
WNV	sfRNA1	sfRNA1
sfRNA functions		
	Deregulates host mRNA turnover (immune evasion)	Inhibits siRNAs (immune evasion)
	Inhibit miRNAs (immune evasion)	Inhibits miRNAs (immune evasion)
	Inhibits IFN response (immune evasion)	Inhibits apoptosis (immune evasion)
	Promotes apoptosis and thus viral spread	Promotes viral dissemination

1.9 Musashi 1

1.9.1 MSI1 background and function

Named after Miyamoto Musashi, the knockout of the Musashi (MSI) gene leads to a double-bristle phenotype of sensilla in Drosophila, reminiscent of the double sword fighting technique perfected by this Japanese samurai [156]. The Musashi family of proteins are found in both vertebrates and invertebrates (Table 1.3) [157]. Unlike drosophila which only have one MSI gene, mammals encode both Musashi 1 (MSI1) and Musashi 2 (MSI2), which are highly conserved, sharing 75% amino acid identity (Figure 1.11) [158]. Both are RNA binding proteins with two RNA recognition motifs (RRMs). RRM1 is found at the N terminal part of the protein where the sequence is highly conserved between different species and is primarily responsible for binding to RNA targets. The main role of RRM2 is to enhance the binding of MSI to the RNA along with RRM1 [159, 160, 161].

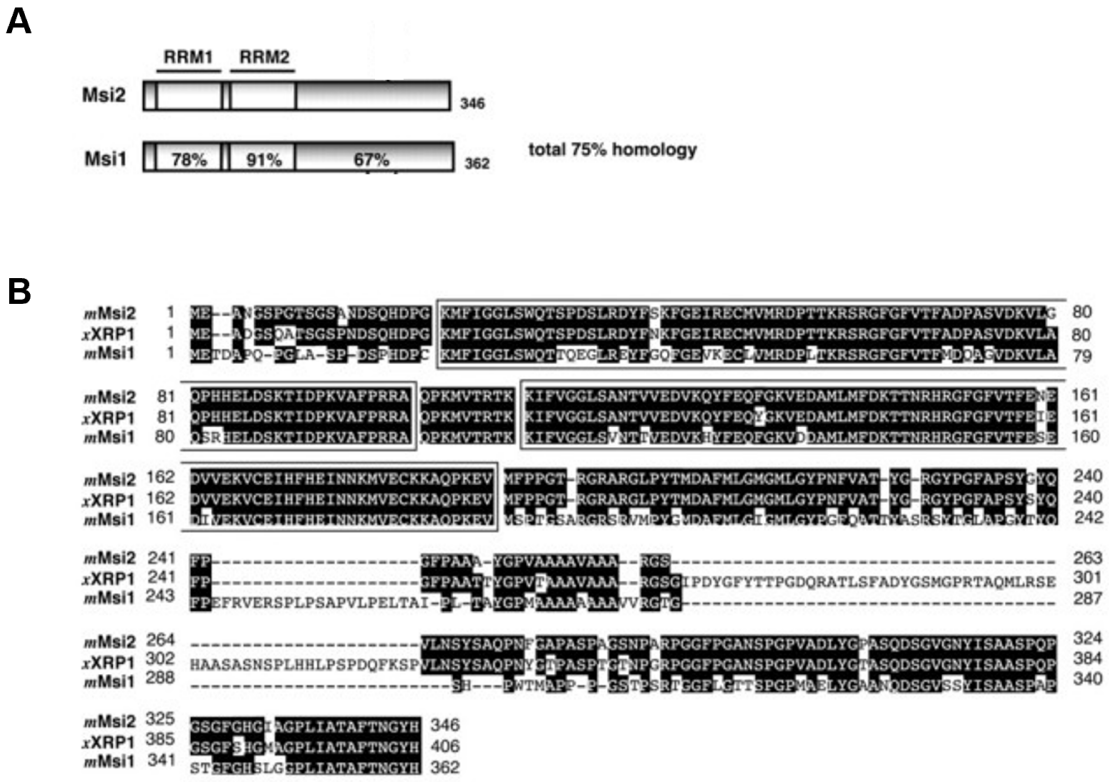

Figure 1.11: MSI12 and MSI2 display high sequence homology. (A) Sequence homology at the amino acid level between mouse MSI1 and MSI2 in the RNA recognition motifs (RRM) and the C terminal region are shown. (B) Alignment of amino acid sequences of mouse MSI2 with its homologs Xenopus RNA-binding protein (XRP1) and mouse MSI1. The RRMs are surrounded by boxes and any gaps in the alignment are indicated by the dashed lines. Taken from [158].

Table 1.3: Musashi proteins in invertebrates and vertebrates (taken from Okano et al, 2002).

Species	*musashi* gene family	GenBank code
Drosophila melanogaster	*musashi*	X79339
Caenorhabditis elegans	*MSI-1*	AB036738
Halocynthia roretzi	*MUSASHI*	AB030275
Xenopous laevis	*nrp1*	M34894, 5
	xrp1	L02953
Mouse	*musashi1*	D49654
	musashi2	AB056102, 3
Human	*musashi1*	AB012851

Musashi proteins mainly localise to the cytoplasm but both RRMs contain nuclear localisation signals [158, 162]. It is therefore postulated that the binding of RNA to the Musashi proteins blocks transport to the nucleus [163]. Reflecting their primary localisation in the cytoplasm, MSI1 and 2 are both translational regulators. Large scale screens have identified many different target genes that are both upregulated and downregulated by MSI1 and MSI2 [164, 165, 166]. Genome wide RNA binding protein immunoprecipitation-microarray analysis of MSI1 bound mRNA identified genes involved in cell proliferation, differentiation and growth, and genes involved in protein modification [166]. In mammals, MSI1 is expressed in neural stem cells (NSCs), where, along with MSI2, it plays a role in the maintenance and proliferation of these cells [167, 168]. In NSCs, MSI1 is known to bind to and inhibit translation of mammalian *numb*, which encodes an antagonist of Notch [169, 170]. As Notch signalling has been shown to promote the undifferentiated state of mammalian neural stem cells, this leads to stem cell maintenance [157]. Similarly, MSI1 has been shown to inhibit the cyclin dependent kinase inhibitor, $p21^{WAF-1}$ promoting cell proliferation, and thus, progenitor cell maintenance [171]. MSI2 has been found to regulate genes involved in oncogenesis and is also important for haemopoietic stem cell maintenance and stem cell fate [164, 165]. The Musashi proteins have gained a lot of attention due to their links to oncogenesis with high expression levels found in tumours, particularly in cases of poor disease outcomes [172, 173, 174, 166].

Mechanistically, the repression of target transcripts is thought to occur via MSI1 binding to PABP at the same site as the eukaryotic initiation factor 4G (eIF4G). This disrupts the PABP-eIF4G interaction, a key step required in canonical translation initiation, and therefore, inhibits translation of bound mRNA [163, 175]. To upregulate target transcripts, MSI1 binds to the poly(A) polymerase germ line development defective-2 (GLD2), which polyadenylates, and thus, stabilises mRNA promoting translation [176]. As the binding site of GLD2 and PABP on MSI1 overlap, it is plausible that the switch between translational repression and activation may be controlled by whether PABP or GLD2 binds [177].

1.9.2 ZIKV and MSI1

Links between the host protein MSI1 and ZIKV were first established following the finding that MSI1 could directly bind to the 3′UTR of ZIKV. MSI1 binding led to a modest enhancement in the translation of a ZIKV reporter RNA, but a significant enhancement in ZIKV replication. It was proposed that due to the high expression

levels of MSI1 observed in NSCs and not in mature neurons, that MSI1 expression could promote the susceptibility of these cells to ZIKV infection [178]. Animal studies depleting MSI1 have also shown that a lack of MSI1 induces microcephaly in zebrafish, and that mice lacking MSI1 display altered brain morphology, including thinning of the cerebral cortex [168, 179]. Cumulatively, this indicates that MSI1 could be linked to the ZIKV induced neuropathology observed in the foetal brain.

Further work investigating the potential role of MSI1 in neuropathology identified a mutation of Alanine to Valine at position 184 in RRM2 of MSI1 in siblings born with reduced cerebral cortex size. The phenotype observed was reminiscent of the microcephaly observed in new-born infants with congenital Zika syndrome [178]. Interestingly, introducing this mutation into MSI1 hampered its binding to target RNAs, and disrupted the MSI1 driven enhancement of ZIKV replication observed in the presence of wild type MSI1. Thus, it was proposed that the microcephaly phenotype observed in infected neonates could be explained by the binding of MSI1 to the ZIKV 3′UTR, sequestering MSI1 from its target transcripts and leading to the deregulated expression of proteins required for normal NSC function [178].

Perhaps sequestration of MSI1 by the ZIKV 3′UTR is also responsible for the pathology observed in other tissues, including the ocular pathology observed in adult humans and infants following ZIKV infection, and the testicular damage and infertility observed in ZIKV infected IFN deficient mice [180, 181, 182]. Indeed, MSI1 expression has been observed in retinal and testicular tissues which are vulnerable to ZIKV infection [182, 183, 184, 185, 186]. Additionally, knockout of MSI1 in mice retinal pigment epithelium coincided with pathology reminiscent of retinal disease [185]. Similarly, MSI1 knockdown disrupted spermatogenesis and the blood-testis barrier structure [186]. Future work utilising knockout/knockdown of MSI1 in different cell types alongside ZIKV infection will further elucidate the role of MSI1 in ZIKV replication and the pathology induced in different tissues.

To further understanding of the interaction of MSI1 with the ZIKV 3′UTR, the identification of MSI1 binding sites is required. Previous work identified the binding motif of MSI1 as (G/A)U_nAGU (n = 1 to 3) [169]. Later work used this binding motif sequence and tested each nucleotide for contribution to MSI1 binding, finding that UAG was the core motif required. This was further confirmed using individual nucleotide resolution cross-linking and immunoprecipitation experiments [159, 187]. Using *in silico* analysis and structural modelling, three putative MSI1 sites were mapped onto the ZIKV 3′UTR RNA. All sites were found to be present at bulge

regions in stem loops and therefore deemed to be energetically favourable for MSI1 binding [178]. Indeed, the cumulative mutation of Sites 1, 2 and 3 led to the inhibition of MSI1 binding, indicating that one or all of these sites contributed to MSI1 binding, although further investigation of the contribution of individual sites is required (Figure 1.12) [178]. Furthermore, additional putative MSI1 binding sites were later identified, and thus also require testing (Figure 1.12) [188]. As MSI1 promotes ZIKV replication, it seems likely that site mutations in the ZIKV genome that disrupt MSI1 binding will harm viral fitness, however, the effects of these site mutations on ZIKV replication have not yet been tested.

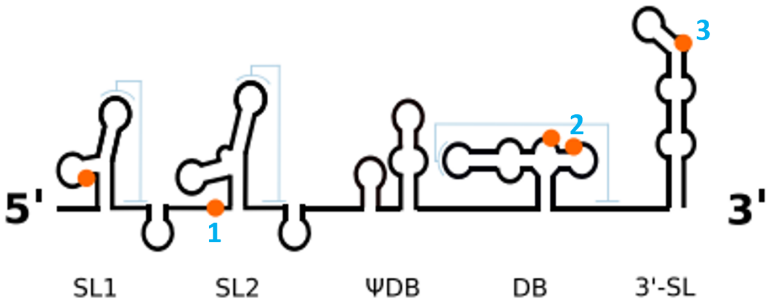

Figure 1.12: Putative MSI1 binding sites. Shown are the candidate sites for MSI1 binding to the ZIKV 3′UTR depicted as orange circles. PK interactions are shown in light blue. Modified from [188].

1.10 Aims of this study

Despite the epidemic of 2015/2016 leading to increased research and a better understanding of ZIKV infection, there are still no effective antivirals for treatment of ZIKV or a licensed vaccine. The RNA binding protein MSI1 has previously been shown to bind directly to the ZIKV 3′UTR, enhancing ZIKV replication. This may lead to the enhanced pathology observed in ZIKV infected NPCs, providing a potential link between MSI1 and congenital microcephaly. Furthermore, several sites within the ZIKV 3′UTR have been identified as putative MSI1 binding sites, but have yet to be studied. Investigating the mechanism of this interaction will provide insights into viral replication, and the potential of ZIKV to cause more aggressive pathology in cells expressing this protein. Furthermore, any mutations that cause defects in viral fitness and enhance our understanding of viral-host interactions provides the potential for the design of an effective and safe vaccine, as well as novel drugs treatments to prevent future epidemics.

This study aims to further understand MSI1 enhancement of ZIKV replication by assessing the impact of these site mutations on ZIKV fitness, and in doing so investigate the importance of the ZIKV 3′UTR to viral fitness.

Objectives:

- Utilise reverse genetics to mutate individual putative MSI1 binding sites in the ZIKV 3′UTR
- Investigate the fitness of the ZIKV MSI1 binding site mutants in the presence and absence of MSI1
- Determine if mutation disrupts MSI1 binding, or if the site mutations induce other changes which are disruptive to viral fitness

Chapter 2

Materials and methods

2.1 Plasmids and molecular cloning techniques

2.1.1 MSI1 plasmids

pCDNA plasmids encoding WT MSI1 (MSI1 WT), MSI1 containing a point mutation of Alanine to Valine at position 184 (MSI1 AV) or empty vector (EV) were kindly gifted from Fanni Gergely [178].

2.1.2 FL ZIKV plasmids

The full length open reading frame from ZIKV BeH819015 flanked by the 5′UTR and 3′UTR of ZIKV PE243 (KX197192.1; FL WT) was encoded in a CopyControl pCC1 BAC vector (Epicentre). The same plasmid backbone containing a nanoluciferase (nanoluc) reporter inserted between duplicated Capsid proteins and flanked by a 2A peptide sequence (FL WT nano) was also constructed. Both plasmids were a kind gift from Andres Merits [189]. A synthetic gene fragment (Integrated DNA Technologies, IDT) encoding a T7 promoter was inserted between EcoRI and NheI sites by Thomas Sanford. This replaced the original SP6 promoter in these plasmid constructs. Full length ZIKV constructs were generated by nested polymerase chain reaction (PCR), introducing site mutations into the 3′UTR of the FL WT nano plasmid (carried out by Ted Fajardo). BstBI and PmeI sites were utilised to replace the WT 3′UTR sequence with the mutant sequences. Full length ZIKV constructs with a nanoluc reporter will henceforth be referred to as FL ZIKV nano. Mutants in the FL WT backbone were generated by PCR amplification of the 3′UTR using FL ZIKV nano plasmids as templates and ligations carried out using FseI and BstBI sites (see section 2.1.3). Additional mutations were introduced in FL WT by nested

PCR (see section 2.1.3). Full length ZIKV constructs without a nanoluc reporter will be referred to as FL ZIKV. Sequencing of the ZIKV genome in FL ZIKV constructs was carried out using the primers shown in Table 2.1.

Table 2.1: Sequencing primers for the ZIKV genome. Shown are the forward (F) and reverse (R) sequencing primers used for sequencing the full ZIKV genome in order from the 5′UTR to the 3′UTR. Nucleotide positions of primer binding sites in the FL WT plasmid are shown in brackets.

Sequencing primer	**Sequence**
1F	GGATGTGCTGCAAGGCGATTAAGTTGG (230-256)
2F	AGTTGTTGATCTGTGTGAATCAG (329-351)
3F	GAAGCCTAGGACTTGATTGTG (1856-1876)
4R	CAAATCTGAAAAGTCAAGGCCTGTCCTCGG (1879-1908)
5R	CATCTCAGCCTCCAGAGCTC (2117-2136)
6F	GGAATGTCCTGGTTCTCAC (2680-2698)
7R	GGTACTTGTACCTGTCCCTC (2901-2920)
8F	GAGATCAACCACTGCAAGC (3711-3729)
9R	GGTCATTCTCTTCTTCAGCCC (3940-3960)
10F	GCAGGTGACATCACATGGG (4717-4735)
11F	GACTTGCATCCTGGAGCTGG (5518-5537)
12R	GGCTGTAGTAGACGTGAAG (5714-5719)
13F	GCATAGGCAGGAATCCCAAC (6317-6336)
14R	GGTCTTCCTTTGCTCCGTCC (6515-6534)
15F	CTAATGGGAAGGAGAGAGG (7228-7306)
16R	CCTATCATTAGCAGCGGGACTCC (7516-7538)
17F	CCGCTTGAACCAGATGTCGG (8037-8056)
18R	GGTTCTTCATGACCAGGG (8316-8333)
19R	CGTTCAAGAATCCAAGGGCTTCGAACTCTAGAAATC (9443-9478)
20F	GCTCCCACCACTTCAACAAGC (10127-10147)
21R	GCTTGTTGAAGTGGTGGGAGC (10127-10147)
22F	GGATCTCTCATAGGGCACAGACCG (10543-10566)
M13R	CAGGAAACAGCTATGAC (11180-11196)

2.1.3 PCRs for generation of FL ZIKV mutants

Generation of Site mutants A, B, D, E and A+B+D+E in the FL WT backbone was carried out utilising PCR primers PCR1 F and PCR2 R (Table 2.2). 60 ng of FL ZIKV nano constructs containing the different site mutations were used as

templates. PCR reaction conditions were as follows; 1X Buffer for KOD Hot start DNA Polymerase, 1 mM MgSO4, 0.2 mM of each dNTP, 0.3 μM forward and reverse primers, 0.02 U/uL KOD Hot Start DNA polymerase (Novagen). Cycling conditions were 95°C for 2 minutes followed by 25X (95°C for 30 seconds, 60°C for 30 seconds, 70°C for 97 seconds) and a final extension of 70°C for 5 minutes.

Generation of the Site C, Site C+D and Site A+B+C+D+E mutant inserts was carried out by nested PCR prior to ligation into the FL WT backbone. All primers utilised are shown in Table 2.2. The FL WT plasmid was used as a template for generation of the Site C mutant insert, using the primers PCR1 F which binds upstream of the BstBI site in the 3′UTR, and the Site C PCR1 R primer which introduces the Site C mutation to produce PCR product 1. The second PCR product was generated using the primers Site C PCR2 F to introduce the Site C mutation and PCR2 R which binds downstream of the FseI site in the 3′UTR. For generation of the Site C+D and Site A+B+C+D+E mutant inserts, FL ZIKV constructs containing the Site D mutation or Site A+B+D+E mutations respectively were used as templates. Amplification was carried out using the PCR1 F primer, alongside the Site C+D PCR1 R primer which includes both the Site C and Site D mutations to generate PCR product 1. PCR product 2 was generated using the primers Site C+D PCR2 F encoding the Site C and D mutations and PCR2 R. PCRs were carried out using the same reaction conditions as previously described. For PCR 1, cycling conditions were an initial denaturation at 95°C for 2 minutes, followed by 28X (95°C for 30 seconds, 52°C for 30 seconds, 70°C for 30 seconds), and a final extension of 70°C for 5 minutes. For PCR2, cycling conditions were an initial denaturation at 95°C for 2 minutes, followed by 28X (95°C for 30 seconds, 65°C for 30 seconds, 70°C for 45 seconds) and a final extension of 70°C for 5 minutes. Samples were PCR purified prior to the final PCR reaction. 21.38 fmol each of PCR product 1 and 2 were used in the final PCR reaction using primers PCR1 F and PCR2 R utilising the same conditions as previously described.

Table 2.2: Primers used in nested PCR for generation of Site C, Site C+D and Site A+B+C+D+E mutants. Nucleotide positions of primer binding sites in the FL WT plasmid are shown in brackets. Highlighted in green is Site C and in red Site D of the ZIKV 3′UTR.

Primer name	**Sequence**
PCR1 F	GTGGCTAGGGGCTAGATTTC (9429-9448)
Site C PCR1 R	GGTCTCCTCTAACCAGGAGTCCCTCTTCTGG (10978-11008)
Site C+D PCR1 R	GGTCTCCTGGAACCAGGAGTCCCTCTTCTGG (10978-11008)
Site C PCR2 F	CCAGAAGAGGGACTCCTGGTTAGAGGAGACC (10978-11008)
Site C+D PCR2 F	CCAGAAGAGGGACCCTGGTTCCAGGAGACC (10978-11008)
PCR2 R	GAGGTATCCACAACGCCGG (13230-13248)

2.1.4 Plasmid transformation

Restriction enzymes were used in digests in accordance with the manufacturer's instructions (New England Biolabs (NEB)). For the FL WT construct, an FseI digestion site upstream of the PmeI site was utilised to generate a sticky, instead of a blunt end, to enhance the ligation reaction. Following digestion with FseI and BstBI, the inserts were gel extracted. The FL WT plasmid backbone was dephosphorylated following digestion by incubation with shrimp alkaline phosphatase (NEB) at 37°C for 3 hours, heat inactivated and PCR purified. Ligations were carried out at 16°C for 3 hours and then the temperature raised to 22°C for 4 hours. All ligations were carried out with 90 ng of vector and 112.5 ng of insert to achieve a 1:5 vector to insert ratio using T4 DNA Ligase (NEB).

Transformations of pCDNA plasmids were carried out in homemade DH5-α competent *E.coli* cells and transformations of FL ZIKV plasmids in fresh NEB Turbo competent *E.coli* cells. FL ZIKV plasmids were grown on agar plates containing 17.5 μg/ml chloramphenicol. Generation of plasmids stocks were carried out utilising a Plasmid Midi Kit (Qiagen). To generate sufficient quantities of FL ZIKV plasmids, a single colony was picked and inoculated into 200 mL of 2XTY containing 17.5 μg/ml chloramphenicol with shaking at 37°C overnight. The overnight culture was split in half and ran down two separate columns. Following elution, isopropanol precipitation was carried out, prior to washing with ethanol and resuspension in water. Sequencing was carried out using the primers shown in Table 2.3.

Table 2.3: Primers for sequencing insert cloned between BstBI and FseI sites in FL ZIKV. Shown are the sequencing primers in order from the 5′ end to the 3′ of the cloned insert. Nucleotide positions of primer binding sites in the FL WT plasmid are shown in brackets.

Sequencing primer	**Sequence**
23F	TGCCAGAGTTGTGTGTATAACATG (9337-9360)
24F	CGGAATATGGAGGCTGAGG (9862-9880)
25F	CCTGGTCAATCCATGGAAAG (10382-10401)
26F	GACGCTGGGAAAGACCAG (11035-11052)
27F	CACTTATTCAGGCGTAGCAAC (11456-11476)
28F	CAGGCGGGCAAGAATGTG (11976-11993)
29F	GCTGCTGCTGACGGTGTG (12494-12511)

2.2 RT-qPCR

Total RNA was extracted from ZIKV infected cells as follows. Media was removed and the cells washed 2X with phosphate-buffered saline (PBS). Cells were lysed by the addition of 500 μL of TRI reagent (Sigma) directly to cells in a 24-well plate. After five minutes, samples were pipetted up and down and collected into 1.5 mL tubes prior to the addition of 100 μL chloroform. Samples were centrifuged at 12,000 g for 10 minutes at room temperature and the upper aqueous phase collected. Samples were then precipitated by the addition of 0.7 volumes of isopropanol and 0.1 volumes of 3M NaOAc (pH 4.8) in the presence of 20 ng/μL glycoblue (Invitrogen) and incubated at room temperature for 30 minutes. Following centrifugation at 4°C for 30 minutes, excess salts were removed from the RNA pellet by washing with ice cold 70% EtOH. Following resuspension in water, RNA samples were quantified by Qubit analysis using the Qubit RNA broad range Assay kit (Invitrogen).

RT-qPCR was carried out using the Zika Virus genesig standard kit (Primerdesign) and PrecisionPLUS OneSTep RT-qPCR Master Mix (Primer design). 5 ng of RNA was added to each reaction plus 0.3 μL of primer/probe mix and 5 μL of master mix in a total volume of 10 μL. Standards were also run alongside samples for quantification, and a negative control containing water also included. Reactions were carried out in a 96-well plate format in the Applied Biosystems StepOnePlus Real-Time PCR system. Cycling conditions were as follows: 50°C RT for 30 minutes, followed by 45X (95°C for 5 minutes, 95°C for 15 seconds and 60°C for 1 minute).

2.3 Western blotting

Protein lysates were generated following washing of cells with PBS and the addition of RIPA buffer (150 mM NaCl, 50 mM Tris-HCL pH 7.4, 1% Igepal, 0.5% Sodium deoxycholate, 0.1% SDS) plus 1:100 of protease inhibitor cocktail without EDTA (abcam) for 15 minutes on ice. Following collection into 1.5 ml tubes, protein lysates were spun down at 10,000g for 10 minutes and resolved by SDS-PAGE using a 12.5% polyacrylamide gel [190]. A precision plus dual colour standard was also run alongside the samples (Biorad). Proteins were transferred using a Trans-Blot SD semi-dry blotter (Bio Rad) to a 0.45 μM nitrocellulose membrane. Blocking was carried out in 5% marvel in PBS at room temperature for 1 hour. Primary antibodies were diluted in 5% BSA in PBS containing 0.1% tween and incubation carried out at 4°C overnight. Primary antibodies utilised were rabbit monoclonal antibody raised against MSI1 EP1302 (1:500, ab52865, abcam), rabbit polyclonal Zika virus envelope protein antibody (1:1000, GTX 133314 , GeneTex), mouse monoclonal anti-GAPDH (1:1000, ab8245, abcam) and rat anti-beta tubulin (1:10) grown from a hybridoma kindly provided by Stephen Graham. The secondary antibodies Goat anti-rabbit IgG H&L IRDye 800CW antibody (1:10,000, ab216773, abcam) and Goat anti-rat IgG H&L Alexa Fluor 680 (1:10,000, ab175778, abcam) were used for detection using an Odyssey CLx Imaging System (Li-Cor).

2.4 Cell culture

All cells were maintained in Dulbecco′s Modified Eagle Medium (DMEM, Sigma) supplemented with 2 mM L-glutamine, penicillin (100 SI units/ml), streptomycin (100 μg/ml) and 10% filtered bovine serum, FBS Good (FBS, PAN-Biotech) (complete medium) at 37°C in 5% $C0_2$. U251 cells were also supplemented with 1% non-essential amino acids (Sigma).

2.5 ZIKV generation and infection experiments

2.5.1 FL ZIKV RNA transcription

Following midiprep, FL ZIKV constructs were digested with 3 μL AGEI enzyme and 10 μL Buffer O + Bovine serum albumin (BSA) (Thermofisher Scientific) in a final volume of 100 μL at 37°C overnight. Following heat inactivation at 70°C for 20 minutes, 10 μL of this mixture was added into a 100 μL transcription reaction and incubated at 37°C for 2 hours prior to the addition of 4 μL of DNASE (NEB) for 30 minutes at 37°C. Transcription reaction conditions are shown in Table 2.4. To purify RNA, 100 μL of TRI reagent was added to each sample and 50 μL of chloroform prior to spinning at 12,000 g for 10 minutes and collection of the upper aqueous layer. Samples were then precipitated with isopropanol as previously described in Section 2.2. RNA was resuspended in 50 μL of water and passed down an Illustra MicroSpin-G50 column (GE Healthcare). 60 μg of FL ZIKV RNA was capped using the ScriptCap m^7G Capping System (Cambio) following the manufacturers instructions by incubation with 40 U of capping enzyme for 2 hours at 37°C (CellScript). Capped RNA was further purified by TRI reagent chloroform extraction and isopropanol precipitation, prior to resuspension in water and passing down another Illustra MicroSpin-G50 column.

Table 2.4: Transcription reaction components for FL ZIKV RNA generation.

Reagent	**per reaction (μL)**
1M Hepes (pH 7.5)	10
320 mM MgOAc	10
400 mM DTT	10
20 mM spermidine	10
100 mM ATP	7.5
100 mM CTP	7.5
100 mM GTP	7.5
100 mM UTP	7.5
RNASEOUT	2
T7 pol (50ng/μL)	5
water	13
Total	90

2.5.2 Measuring FL ZIKV nano site mutant fitness

Following transcription of FL ZIKV nano site constructs and capping to generate a cap 0 structure (Section 2.5.1), 1 μg of RNA was transfected into 80% confluent Vero cells in 12-well plates. 1 μg of RNA was diluted in 50 μL of OptiMEM reduced-serum medium (OptiMEM, Life Technologies). A negative control replacing the RNA with water was also included. 3 μL of Lipofectamine 2000 (Thermofisher) was added to 50 μL of OptiMEM reduced-serum medium (OptiMEM, Life Technologies) and incubated for 5 minutes at room temperature. The diluted RNA was then added to the diluted lipofectamine. Following incubation for 20 minutes, cells were washed 2X with PBS, prior to addition of 200 μL of DMEM without FBS, and the water or RNA complexed with lipofectamine. Cells were incubated at 37°C for 1 hour with gentle shaking. 300 uL of DMEM without FBS was then added and the cells incubated for an additional 2 hours. Following incubation, the media was removed and the cells washed 2X with DMEM and 1 ml of complete DMEM without antibiotics added to each well. The cells were then incubated at 37°C until lysis of cells was carried out.

Cells were harvested at the indicated time points by washing 2X with PBS prior to incubation with 100 μL of 1X passive lysis buffer (Promega) for 15 minutes and then stored at -80°C. Samples were diluted 1:5 in PBS and nanoluciferase levels were measured using the GloMax (Promega) following the addition of 50 μL of 50 μM colenterazine to 50 μL of sample.

2.5.3 Virus generation

Reverse genetics was used to produce ZIKV stocks. Capped, *in vitro* transcribed FL ZIKV RNA (1 μg) was electroporated into 3 x 10^6 Vero cells resuspended in 100 μL of OptiMEM. Electroporations were carried out using a NEPA21 electroporator (Nepagene). The conditions displayed in Table 2.5 were ustilised. Cells were recovered in pre-warmed complete DMEM for 5 minutes prior to seeding into T150 flasks. DMEM was supplemented with 20 mM HEPES (Gibco) for viral growth. Media was replaced 16 hours post electroporation, and virus collection started when cytopathic effects were observed. Virus was collected over multiple days into separate tubes for each day and centrifugation carried out at 4°C to remove cell debris prior to aliquoting and storage in the -80°C. Vials containing ZIKV were only freeze thawed once.

Table 2.5: Electroporation conditions.

Poring Pulse						Transfer Pulse					
V	Length (ms)	Interval (ms)	No.	D. Rate (%)	Polarity	V	Length (ms)	Interval (ms)	No.	D. Rate (%)	Polarity
125	5	50	2	10	+	20	50	50	5	40	+/-

2.5.4 Plaque assay

Viral dilutions were carried out in serum free DMEM following a single defrost of viral aliquots. Vero cells were infected at 80% confluency in 6-well plates in serum free DMEM for 1 hour at 37°C, with shaking every 15 minutes. 3X UltraPure Low Melting Point Agarose (Invitrogen) was prepared in sterile distilled water to make a 3% solution, prior to a 1:3 dilution in DMEM containing 2.5% FBS, L-glutamine, penicillin and streptomycin (plaquing medium). Virus was removed and 2 mL of plaquing medium added to each well. Following incubation for 4 days at 37°C in 5% $C0_2$, plaques were fixed with 10 % formal saline (100 mL formalin, 900 mL tap water and 8.5 g NaCl) overnight, and following removal of agarose stained with 0.1% w/v toludine blue and plaques counted.

2.5.5 Virus infections

Virus infection were carried out with day 2 P0 virus unless otherwise indicated. Cells were infected at 80% confluency at the indicated multiplicity of infection (MOI) in serum free DMEM for 1 hour at 37°C with shaking every 15 minutes. Virus was then removed, cells washed with PBS and DMEM containing 2.5% FBS, L-glutamine and antibiotics added to the cells. Cells were then incubated at 37°C in 5% $C0_2$ and samples harvested at the indicated time points.

2.5.6 Passage experiments and ZIKV sequencing

Vero cells were infected in 6-well plates with day 2 P0 virus at MOI 0.1, and 3 days post infection, viral supernatants collected for further blind passages. RNA was extracted from 500 μL of viral supernatants by the addition of 500 μL of TRI reagent and 200 μL of chloroform. Following centrifugation and collection of the upper

aqueous layer, isopropanol precipitation was carried out as described in Section 2.2 and the RNA resuspended in 10 uL of water.

1 μL of the RT primer (10 μM) (AGACCCATGGATTTCCCCACACCGGC (10782-10807) in 7 uL of water was added to 1 μg of RNA diluted in 5 uL of water and incubated at 65°C for 5 minutes and then placed on ice for 2 minutes. Reverse transcription (RT) reactions were carried out in a final volume of 20 μL using the following reactions conditions; 1X first-strand buffer (Invitrogen), 5 mM DTT, 1U/μL RNASE OUT (Invitrogen), 0.5 mM dNTPs (Thermo scientific), and 10U/μL SuperScript III (SSIII) (Invitrogen). Reactions were incubated at 50°C for 1 hour and inactivation carried out at 75°C for 15 minutes, prior to the direct use of 3 μL of this reaction mix for PCR amplification and sequencing with the primers shown in Table 2.6.

The 3′UTR was amplified using primers 3′UTR_F and 3′UTR_R and the PCR reaction conditions described in Section 2.1.3. Cycling conditions were an initial denaturation of 95°C for 2 minutes followed by 40X (95°C for 30 seconds, 60°C for 30 seconds, 70°C for 30 seconds) and a final extension at 70°C for 5 minutes.

The 5′UTR was amplified using primers 5′UTR_F and 5′UTR_R and the PCR reactions conditions described in Section 2.1.3, except 2.25 mM $MgSO_4$ was used. Cycling conditions were an initial denaturation of 95°C for 2 minutes followed by 40X (95°C for 30 seconds, 50°C for 30 seconds, 70°C for 20 seconds) and a final extension at 70°C for 5 minutes.

Sanger sequencing was carried out by the Department of Biochemistry DNA sequencing Facility (University of Cambridge) using primers 3′UTR_F and 3′UTR_R for the 3′UTR and primer 5′UTR_seq for the 5′UTR. Primer sequences are shown in Table 2.6.

Table 2.6: Primers for sequencing 5′ and 3′ UTRs. Numbers in brackets represent nucleotide positions within the ZIKV genome.

3′UTR_F	GGATCTCTCATAGGGCACAGACCG (10215-10238)
3′UTR_R	AGACCCATGGATTTCCCCACACCGGC (10782-10807)
5′UTR_F	AGTTGTTGATCTGTGTGAATCAG (1-23)
5′UTR_R	CCAGCCTCTGTCCACTAACGT (1260-1280)
5′UTR_seqR	CTTGATTGCCGTGAATCT (270-287)

2.5.7 HEK MSI1 overexpression experiments

MSI1 WT, MSI1 AV, or EV plasmids were transfected into 40% confluent HEK 293T cells in 10 cm dishes (Thermo Scientific). 9 μg of plasmid was diluted in 1.5 mL of OptiMEM. 18 μL of Lipofectamine 2000 was diluted in 1.5 mL of OptiMEM and incubated at room temperature for 5 minutes. The diluted DNA and lipofectamine were then mixed together and incubated for 30 minutes prior to addition to each plate containing 7 mL of complete DMEM without antibiotics. Cells were then incubated at 37°C in 5% $C0_2$ for 24 hours and trypsinised prior to re-seeding at a density of 250,000 cells per well of a 24-well plate. Any spare cells were lysed in RIPA buffer plus 1:100 of protease inhibitor cocktail without EDTA for later probing for MSI1 expression, as described in Section 2.3. Six hours after re-seeding, infections were carried out using the standard protocol, except for a 2 hour incubation without shaking was utilised. Cells were then incubated for an additional 48 hours in 2.5% DMEM at 37°C, prior to extraction and purification of the RNA and RT-qPCR as described in Section 2.2.

2.6 Structural mapping of the ZIKV 3′UTR

2.6.1 SHAPE construct generation

Selective 2′-hydroxyl acylation analysed by primer extension (SHAPE) constructs were generated from FL ZIKV plasmids by PCR amplification using the protocol described in Section 2.1.3 and the primers shown in Table 2.7. Cycling conditions were denaturation at 95°C for 2 minutes, followed by 28X (95°C for 30 seconds, 57°C for 30 seconds, 70°C for 30 seconds) and a final extension of 70°C for 5 minutes.

Table 2.7: Primers for amplification of the ZIKV 3′UTR containing a T7 promoter and SHAPE extension cassette. Shown are the sequences for the forward primer encoding the T7 sequence for transcription in red, the 5′SHAPE extension cassette in black and the 5′ end of the 3′UTR in blue. The sequences for the reverse primers are also shown containing the different lengths of extension cassettes. The reverse transcription primer binding site is shown in green, the extension sequence in purple, and the 3′ end of the 3′UTR in blue.

SHAPE F	TAATACGACTCACTATAGGCCTTCGGGCCAA GCACCAATCTTAATGTTGTCAGG
SHAPE R 24 nts	GAACCGGACCGAAGCCCGATTTGGATCCGGCGAACCGGATCT AGACCCATGGATTTCCCCAC
SHAPE R 33 nts	GAACCGGACCGAAGCCCGATTTATAGTAAATGGATCCGGCGAA CCGGATCTAGACCCATGGATTTCCCCAC
SHAPE R 41 nts	GAACCGGACCGAAGCCCGATTAAATAAAATATAGTAAATGGAT CCGGCGAACCGGATCTAGACCCATGGATTTCCCCAC
SHAPE R 50 nts	GAACCGGACCGAAGCCCGATTTAAATAAATAAATAAAATATAG TAAATGGATCCGGCGAACCGGATCTAGACCCATGGATTTCCCCAC

Following PCR, products were gel extracted and 1 μg of purified DNA was then used in a transcription reaction for 2 hours at 37°C (Table 2.8) prior to DNASE treatment for 1 hour. An equal volume of phenol chloroform (pH 4.5) was added, samples centrifuged at 12,000 g for 10 minutes and the upper aqueous layer collected. Samples were then ethanol precipitated by the addition of 2 volumes of ice cold ethanol and 0.1 volumes of 3M NaOAc (pH 4.8) in the presence of 20 ng/μL glycoblue at -80°C for 30 minutes or -20°C overnight. Following incubation, the samples were centrifuged at 12,000 g for 30 minutes at 4°C and washed with ice cold 70% ethanol. The RNA pellet was then resuspended in 50 uL water, passed down an Illustra Microspin G-50 column (GE Healthcare) twice and quantified using the Qubit RNA broad range Assay kit. RNA integrity was assessed by agarose gel electrophoresis.

Table 2.8: Standard transcription reaction components.

Reagent	**per reaction (μL)**
400 mM Hepes (pH 7.5)	10
320 mM MgOAc	10
400 mM DTT	10
20 mM spermidine	10
100 mM GTP	7
100 mM ATP	7
100 mM CTP	7
100 mM UTP	7
DNA	25
RNASE OUT	2
T7 pol (50ng/μL)	5
Total	100

2.6.2 Radioactive RT

Primer labelling reactions were carried out with 10 U of T4 polynucleotide kinase (3′ phosphotase minus, NEB), 0.3 μg primer, 1X PNK incubation buffer, 1 μl of (γ^{32}P) ATP (6000 Ci/mmol; PerkinElmer) in a final volume of 20 μl. Reactions were incubated at 37°C for 20 minutes and heat inactivated at 80°C for 5 minutes. RT primers used were SLI (GAGTCTCTGGTCTTTCCCAGC, 10710-10730), SL2 (CGCCGCTATTCGGCGATCTG, 10762-10781) and the cassette primer (GAACCGGACCGAAGCCCG).

15 ng of ^{32}P-labelled primer was added to 20 pmol of 3′UTR RNA containing the structured extension cassette diluted in 10 μl of 0.5X TE and heated to 95°C for 5 minutes, 35°C for 5 minutes and chilled on ice for 2 minutes. Following primer annealing, RT reactions were carried out with SSIII at 55°C using the reaction conditions described in Section 2.5.6. After 30 minutes, 180 μl of stop solution (0.25% SDS, 12.5 mM EDTA) was added and cDNA purified by the addition of an equal volume of Phenol chloroform (pH 8), spinning at 12,000 g for 10 minutes at room temperature, and collection of the upper aqueous phase. The sample was then ethanol precipitated as described in Section 2.6.1.

Following purification, samples were resuspended in 10 μl of denaturing loading dye

(0.05% bromophenol blue, 0.05% xylene cyanol, 20 mM EDTA, pH 8, and 91% formamide). Samples were then separated in a denaturing 6% polyacrylamide gel containing 7M urea, and detection carried out by autoradiography using overnight exposure of a phosphoscreen and an FLA 7000 Typhoon scanner (GE Healthcare).

2.6.3 Modification

8 pmol of RNA in 20 μL 0.5X Tris EDTA (0.5X TE; 10 mM Tris-HCl (pH 8), 1 mM EDTA (pH 8)) was heated to 95°C for 2 minutes and snap cooled on ice for 2 minutes. Re-folding was carried out in SHAPE refolding buffer (88 mM Hepes, 5.3 mM $MgCl_2$ and 88 mM NaCl) containing 0.5U/μL of RNaseOUT (40U/μL) in a final reaction volume of 500 μL, prior to incubation at 37°C for 30 minutes. RNA was then split into two separate reactions and treated with 10 mM N-methylisatoic acid anhydride (NMIA), or the equivalent volume of Dimethyl sulfoxide (DMSO) at 37°C for 50 minutes. RNA was then purified by ethanol precipitation as previously described in Section 2.6.1 but in the presence of 20 ng/μL glycogen instead of glycoblue. Following centrifugation, the RNA pellet was resuspended in 10 μL of 0.5X TE.

2.6.4 Reverse transcription of modified RNA

For primer annealing, 1 μL of water and 1 μL of 10 μM RT primer 5′ end labelled with VIC (Applied Biosystems) was added to 10 μL of sample diluted in 0.5X TE. Samples were incubated at 65°C for 5 minutes, 35°C for 5 minutes and then placed on ice for 2 minutes.

RT reactions were carried out in a final volume of 20 μL as described in Section 2.5.6, apart from SSIII was not added until the reaction mix had been heated to either 55°C or 52°C for 3 minutes. Following addition of SSIII, the samples were incubated at the indicated temperature for 30 minutes. Following RT, alkaline hydrolysis was carried out by incubation at 95°C for 3 minutes in the presence of 2 μL 2M NaOH and samples cooled on ice for 2 minutes. 2 μL of 2M HCl was then added, and the samples purified by ethanol precipitation as previously described in Section 2.6.1 but in the presence of 20 ng/μL glycogen instead of glycoblue and resuspended in 20 μL of water.

2.6.5 RNA ladder preparation

Sequencing reactions were carried out utilising the same RNA samples that were used in the initial modification reactions. For each reaction, 6 pmol of RNA in 7.5 μL 0.5X TE was heated to 95°C for 2 minutes and snap cooled on ice. Primer annealing was carried out as before, but 1 μL of 10 μM RT primer 5′ end labelled with NED (Applied Biosystems) and 2 μL of water was added to each reaction. The RT reaction was carried out using the same conditions as described in Section 2.5.6, apart from SSIII and 1 mM of ddCTP (Roche) was added after the reaction components had been heated to either 55°C or 52°C for 3 minutes. After addition of SSIII and ddCTP, the samples were incubated for a further 30 minutes. Samples were then ethanol precipitated as previously described in Section 2.6.1 but in the presence of 20 ng/μL glycogen instead of glycoblue, prior to resuspension in 20 μL of water.

2.6.6 Submission of SHAPE experiments and analysis of results

7 μL of each sample plus 2 μL of sequencing reactions were added per well of a 96-well plate and left to dry overnight at room temperature. Separation by capillary electrophoresis was carried out by the Department of Biochemistry DNA sequencing facility at the University of Cambridge. All SHAPE data was analysed utilising QuSHAPE.

2.7 Northern blotting

2.7.1 Sample preparation

Vero cells were infected at 80% confluency in a 6-well plate format with ZIKV at an MOI of 3. Cells were lysed at 48 hours post infection by the addition of 1 mL of TRI reagent per well. Following harvest, 200 μL of chloroform was added and total RNA extracted and isopropanol precipitated as described in Section 2.2. Following resuspension in 10 μL of water, samples were quantified by Qubit analysis using the Qubit RNA broad range Assay kit.

For a size control ZIKV 3′UTR RNA was generated. ZIKV 3′UTR DNA was generated using the F primer (TAATACGACTCACTATAGCACCAATCTTAATGTTGTCAGGCCTG), adding a T7 promoter to the 5′ end of the 3′UTR and the reverse primer (AGACCCATGGATTTCCCCACACCGGC) which anneals to the end of the ZIKV 3′UTR. PCR amplification was carried out as previously described in Section 2.1.3 using 40 ng of FL WT plasmid as a template. Cycling conditions were an initial denaturation of 95°C followed by 28X (95°C for 30 seconds, 60°C for 30 seconds, 70°C for 30 seconds) and a final extension of 70°C for 5 minutes. Following PCR amplification, DNA was ethanol precipitated and purified by gel extraction. Transcription was carried out as described in Section 2.6.1.

2.7.2 Urea-PAGE

2 μg of each sample and 1 ng of 3′UTR RNA were diluted in 5 μL of water and mixed with 5 μL 2X RNA loading dye containing ethidium bromide (50 μg/mL). Samples were then incubated at 95°C for 5 minutes and snap cooled on ice. An 8M Urea 6% Polyacrylamide gel was pre-run in 1X Tris-borate-EDTA (TBE) at 80V for 5 minutes. Samples were then run at 80V for 15 minutes and then 120V for 1 hour 38 minutes, until the Xylene Cyanol dye was almost run off of the gel. The gel was washed in 0.5X TBE prior to visualisation in the transilluminator.

2.7.3 Transfer

Northern blotting was carried out based on the protocol from [40]. The Urea gel was equilibrated by washing in 0.5X TBE buffer 2X for 15 minutes. The nylon membrane (Hybond-XL, Amersham) was equilibrated by washing in water for 5 minutes and 0.5X TBE for 5 minutes. Blotting paper was also soaked in 0.5X TBE buffer. Electrophoretic transfer was carried out using a Trans-Blot Semi-Dry Electrophoretic Transfer cell (BioRad) and the blotting sandwich assembled as follows (bottom up); blotting paper, nylon membrane, gel, blotting paper. Transfer was carried out at a current of 2 mA/1cm2 gel for 60 minutes. After the transfer was finished the membrane was UV cross-linked twice at 1200 X 100μJ/cm2 in a UV stratalinker. The membrane was then rinsed in water and stored in wet saran wrap at 4°C prior to hybridisation.

2.7.4 Preparation and hybridisation of probe

The following steps in the Northern Blot protocol involving the use of ^{32}P were carried out by Trevor Sweeney. The DNA oligonucleotide (5′-TCCTCTAACCACTAGT CCCTCTTCTGGAGATCCAC-3′) complementary to the ZIKV 3′UTR at nucleotides positions 10642-10676 of the ZIKV genome, was labelled with γ^{32}P as previously described in Section 2.6.2. The radiolabelled probe was heated to 100°C for 2 minutes prior to the addition of 10 mL of ULTRAhyb Oligo hybridisation buffer (Ambion) and incubated with the northern blot membrane overnight at 42°C.

2.7.5 Visualisation of Northern Blot

Following probing, northern blots were washed in 2X saline-sodium citrate (SSC) buffer with 0.5% SDS for 10 minutes at 42°C four times. Blots were exposed to a phosphoscreen for 4 days and imaged using an FLA 7000 Typhoon scanner.

Chapter 3

Investigating the effects of putative MSI1 binding site mutations on ZIKV fitness

3.1 Introduction

Several host proteins have been shown to interact with flavivirus 3′UTRs and are important for the viral life cycle. Through a dynamic interplay between the viral RNA and host proteins, flaviviruses manipulate the host cell environment to promote viral replication and translation, and to subvert the host immune response [29].

Previous work identified the host protein MSI1 as directly interacting with the 3′UTR of Asian lineage ZIKV PE243 and African lineage ZIKV MR766 [178]. MSI1 is an RNA-binding protein that is a master translation regulator, with roles in regulating cell proliferation, differentiation, and growth [166]. Neural progenitor cells, as well as other tissues deemed susceptible to ZIKV infection from the retina and testis, express high levels of MSI1, providing a potential link between MSI1 and ZIKV tropism [178, 184, 183, 185, 182, 186] . Furthermore, infection with ZIKV disrupts binding to target transcripts, including the transcript encoding the protein Microcephalin (MCPH1) [178]. Cells that are deficient in MCPH1 display premature chromosome condensation, a phenotype that is also observed when MSI1 is knocked out of human glioblastoma cells [191, 192, 178]. Additionally, patients with autosomal primary microcephaly contain a point mutation in MSI1 (A184V) that disrupts RNA binding and abolishes the MSI1 driven replication enhancement of ZIKV [178]. Cumulatively this indicates that ZIKV binds to MSI1 sequestering it from its target transcripts and that the subsequent dysregulation causes microcephaly. MSI1 has also been shown to stabilise cyclin dependent kinase (CDK) 6, and treatment of cells with CDK inhibitors has been shown to inhibit ZIKV replication, providing a potential explanation for the enhanced replication of ZIKV observed in the presence of MSI1 [193, 194]. This enhanced replication may lead to

increased pathology due to cell death, although previous work has shown that viral replication rates in mice did not necessarily directly correlate with pathogenicity [195, 98].

In addition to direct binding to the 3′UTR, UV cross linking and RNA immunoprecipitation experiments have shown that MSI1 also binds to the PE243 genome following infection, and super-resolution microscopy has shown co-localisation with double stranded viral RNA replication intermediates [178]. This indicates that MSI1 can bind to the FL ZIKV genome as well as sfRNAs. This raises questions around the mechanism of MSI1 regulation and therefore the regulation of ZIKV replication as infection progresses. There is a balance between replication of the viral genome and translation of viral proteins. It is plausible that MSI1 promotes viral replication and is mopped up by the increasing concentration of sfRNAs generated over the course of infection. This may then promote a translation competent form of the genome, tilting the balance from genome replication towards the generation of viral proteins. This highlights the requirement for further work picking apart the mechanism of MSI1 enhancement of ZIKV replication.

MSI1 regulates its target genes by binding to the 3′UTR region of target transcripts, and, therefore, the search for MSI1 binding sites within the ZIKV genome was narrowed down to the 3′UTR [157]. Multiple putative MSI1 binding sites have been identified within the PE243 ZIKV 3′UTR, consisting of a central UAG motif in regions that appear accessible for protein binding [159, 187, 178]. Five potential sites were identified labelled A-E in order of their location in the 3′UTR, from the 5′ to the 3′ end. Sites B, D and E correspond to sites 1, 2 and 3 respectively, previously identified by Chavali *et al*, 2017. Sites A and E were discovered at a later date [188] (Figure 3.1).

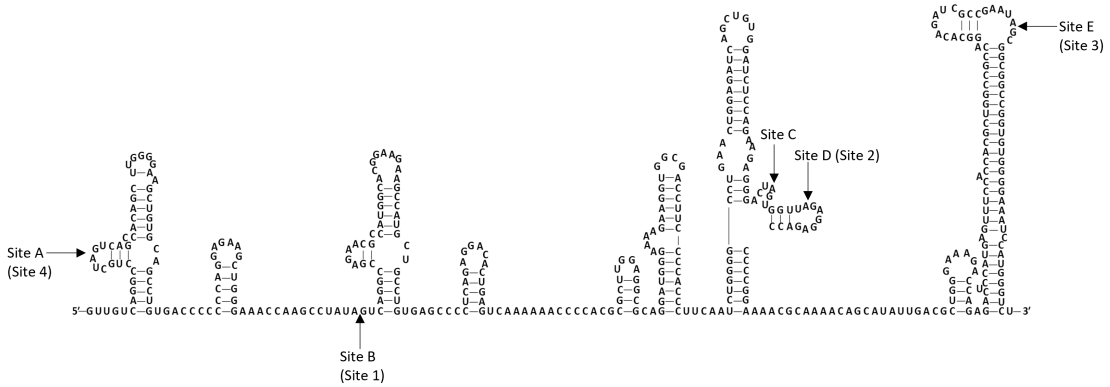

Figure 3.1: Putative MSI1 binding sites in the ZIKV 3′UTR. Binding sites are indicated by arrows. The nomenclature used in this study is shown and nomenclature from Chavali *et al*, 2017 is shown in brackets

The cumulative mutation of Sites B, D and E in the 3′UTR of ZIKV PE243 has been shown to disrupt MSI1 binding, although low levels of binding were still observed. The MR766 strain of ZIKV lacks a putative binding Site E, indicating that this site is not essential for MSI1 binding [178]. The contribution of individual putative MSI1 binding sites within the 3′UTR was not investigated, or the effects of these site mutations when introduced into the full length viral genome on viral fitness. Therefore, additional investigations are required to identify the site and/or sites that are required for MSI1 binding to further elucidate the role of MSI1 in ZIKV replication enhancement. To do this, it was decided that ZIKV mutants carrying mutations of putative MSI1 binding sites would be utilised. This would also provide further insights into the importance of the 3′UTR in ZIKV fitness, and any mutations that attenuate viral fitness provides useful information for vaccine design.

The main aim of this chapter was to determine whether mutation of each of these putative MSI1 binding sites disrupted viral fitness in a MSI1 dependent manner. This required the generation of constructs encoding the full length ZIKV genome (FL ZIKV) containing site mutations in the 3′UTR, and utilisation of reverse genetics to generate mutant viruses. Following virus generation, infection of cells +/- MSI1 would be carried out to test viral fitness and the link between viral replication and MSI1.

3.2 Results

3.2.1 Utilising reverse genetics to study the effects of site mutations in the ZIKV 3′UTR on viral fitness

Previous work in the lab generated ZIKV mutants containing AG to CC mutations at putative MSI1 binding Sites A, B, D, E and A+B+D+E in a FL ZIKV nanoluciferase reporter construct (FL ZIKV nano). These constructs were utilised to investigate whether any of the site mutations had an impact on viral fitness. Following *in vitro* transcription, capped FL ZIKV nano RNA was transfected into Vero cells, the cells lysed, and nanoluciferase (nanoluc) levels measured at different time points post transfection (Figure 3.2). There was a clear fitness defect observed for the Site E and Site A+B+D+E mutants, with nanoluc production reduced by 60 and 70X respectively, relative to WT at 72 hours post transfection. The Site B and D mutants displayed a 6X and 4.5X reduction in nanoluc production compared to WT at 72 hours post transfection, also indicating that these site mutations impaired viral fitness. The Site A mutant showed similar nanoluc levels compared to WT, indicating that this mutation did not impact viral fitness.

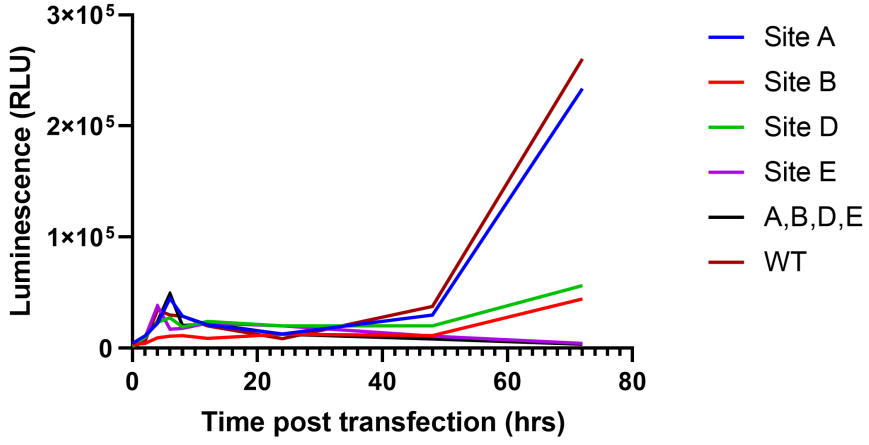

Figure 3.2: Effects of mutating putative MSI1 binding sites on ZIKV fitness. FL ZIKV nanoluc reporter constructs containing the WT 3′UTR or putative MSI1 binding site mutations were transfected into Vero cells. Vero cells were lysed at 0, 2, 4, 6, 8, 12, 24, 48 and 72 hours post transfection and nanoluc levels measured (n=1).

Many studies utilise flavivirus reporter constructs to investigate viral fitness, allowing for more rapid quantification of virus levels [196, 197, 198, 199, 200]. However,

insertion of a reporter gene commonly leads to viral attenuation [201, 198, 202, 197, 203, 204, 205, 206]. This can make viral reporters less useful for studying mutations that affect viral replication or pathogenesis [207]. Indeed, when FL WT nano was compared to FL WT without a nanoluciferase reporter (FL WT), a smaller plaque phenotype was observed and a one-day delay in the development of cytopathic effects (CPE) (Figure 3.3). It was therefore decided that the site mutants would be cloned without the nanoluciferase reporter to ensure that the viruses were as biologically relevant as possible.

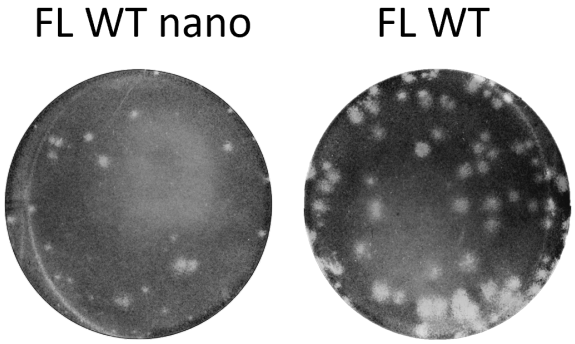

Figure 3.3: Attenuation of WT ZIKV following insertion of a nanoluciferase reporter. Shown is the attenuated plaque morphology for FL WT nano compared to FL WT ZIKV. Viruses were titrated on Vero cells by plaque assay before formal saline fixation and toluidine blue staining at 4 days post infection.

As it became apparent that another site within the 3′UTR may also be a potential MSI1 binding site (Site C), it was decided that this site mutant would also be cloned. It has previously been suggested that the positioning of Site C in the dumbbell (DB) structure alongside Site D could present two binding sites for each of MSI1s two RNA binding domains [188]. To further investigate this a double mutant containing Site C+D was cloned.

Cloning conditions were optimised to enhance the efficiency of cloning with a large plasmid (≈19 kb). For ligations, instead of utilising the PmeI restriction enzyme site, the FseI site was used in combination with the BstBI site to produce double sticky ends. Additionally, instead of a 16°C overnight ligation, ligations were carried out at 16°C for 3 hours and then the temperature raised to 22°C for 4 hours. This was found to greatly enhance ligation efficiency alongside using a high insert to vector ratio of 5:1. It was also found that the use of fresh NEB Turbos is important as their efficiency reduced quickly following storage in the -80°C.

Following the construction of plasmids encoding the full length ZIKV genome (FL

ZIKV) containing the WT 3′UTR or different site mutations, capped FL ZIKV RNA was electroporated into Vero cells, and virus was collected over multiple days following observation of CPE. CPE was determined by looking for the formation of early viral plaques and increased cell death compared to the negative control. From this, it became apparent that Site B, D, C+D, E and (A+B+C+D+E) mutants were less fit than WT, displaying a delay in the appearance of CPE and a smaller plaque phenotype compared to the WT virus (Figure 3.4). In particular, the Site B mutant virus displayed the smallest plaque phenotype, indicating a greater reduction in viral fitness compared to the other site mutants. Comparatively, the Site A mutant displayed a similar plaque phenotype to the WT virus, indicating that this mutation did not affect viral fitness. The virus was collected over three days for all the site mutants, apart from the Site A mutant and the WT virus, where cell death was more rapid, and so virus was collected over two days. In some cases the virus collection was delayed over multiple days due to the slower progression of infection for some of the site mutants. The Site E virus was collected 16, 17, and 18 days post electroporation, following observation of very mild CPE. The Site A+B+C+D+E virus showed no CPE following 20 days of observation. Sequencing confirmed the presence of the site mutations in passage 0 (P0) stocks of virus. On the occasion where virus rescue was possible for the Site E mutant, sequencing identified another mutation in the 3′SL adjacent to the mutated site, which was still carrying the expected mutations (Figure 3.5). Following viral collection, titres were determined by plaque assay for virus collected two days following observation of CPE. These p0 stocks were used for subsequent experiments.

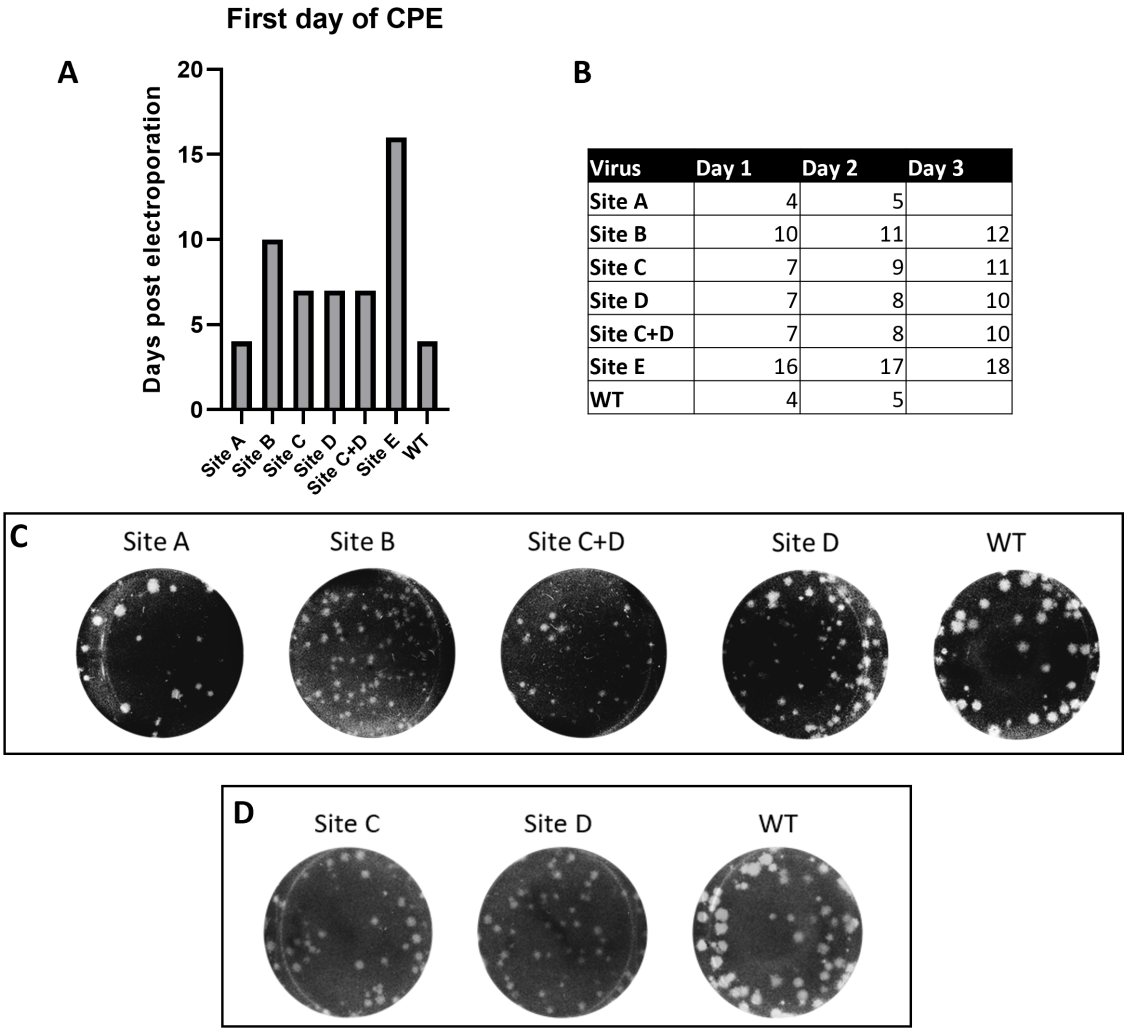

Virus	Day 1	Day 2	Day 3
Site A	4	5	
Site B	10	11	12
Site C	7	9	11
Site D	7	8	10
Site C+D	7	8	10
Site E	16	17	18
WT	4	5	

Figure 3.4: Generation of ZIKV site mutants. (A) WT FL ZIKV RNA and FL ZIKV RNA containing the different site mutations was electroporated into Vero cells. Shown is the time taken to display initial CPE post electroporation, measured as increased cell death compared to the uninfected negative control cells and the formation of clusters of dead cells. (B) Days of viral collection following electroporation of FL ZIKV RNA are shown for the site mutant and WT viruses. The first day of collection was carried out when mild CPE was apparent and then collection carried out on subsequent days until over 70% of cells were dead. (C) Plaque morphology of the indicated site mutants compared to the WT virus. (D) Plaque morphology of the Site C mutant virus generated at a later date, the Site D mutant, and WT virus. All titrations were carried out on Vero cells and fixed and stained at 4 days post infection.

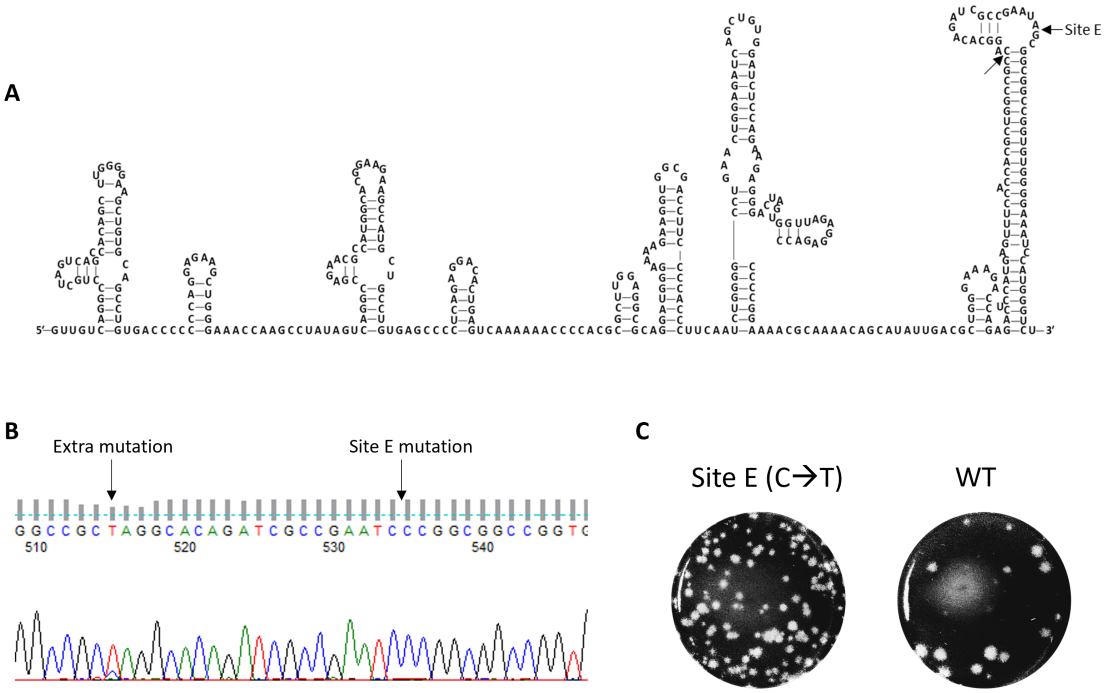

Figure 3.5: An extra mutation in the 3′UTR is present following the attempted rescue of the Site E mutant virus. (A) Shown is the location of Site E and the site of the additional mutation within the 3′UTR structure. (B) Sanger sequencing trace depicting the extra C→T mutation in the 3′UTR located upstream of Site E. (C) Plaque morphology of the Site E mutant containing the additional mutation compared to the WT virus following titration on Vero cells.

To further assess the stability of the site mutations introduced into the 3′UTR, Vero cells were infected with the different site mutants at MOI 0.01, and supernatants were collected three days post infection. The supernatants were blind passaged onto Vero cells up to five times, and the viral RNA extracted and used to generate cDNA for sequencing both the 3′UTR and the 5′UTR. Site A, D, C+D and E mutants maintained the site mutations introduced into the 3′UTR and the WT virus maintained the WT sequence. Interestingly, the Site B mutant partially reverted to the WT sequence, switching from CC at the mutation site to CG. This reversion could be seen as early as passage 2 (P2) and complete reversion was observed by passage 3 (P3) (Figure 3.6).

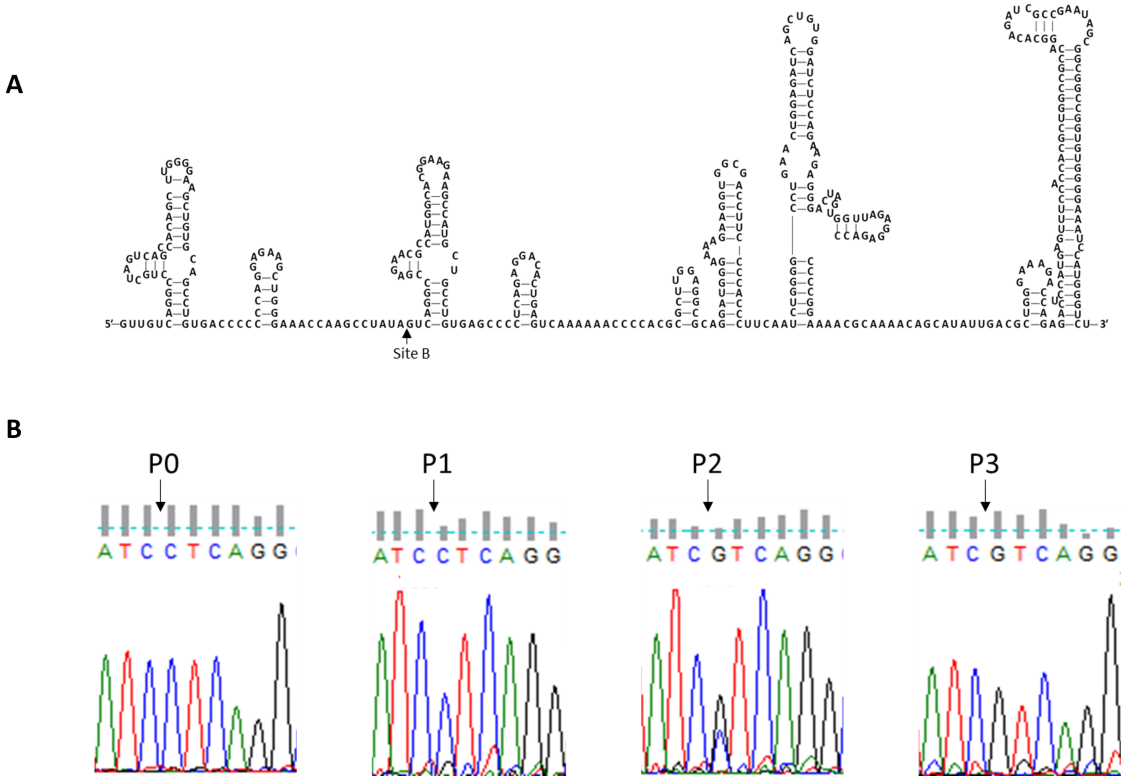

Figure 3.6: Partial reversion of the Site B mutant. (A) Location of the Site B mutation within the 3′UTR structure is depicted. (B) Shown are the sanger sequencing traces for the Site B mutant following passage onto Vero cells.

3.2.2 Selecting a cell line to study MSI1 driven enhancement of ZIKV replication

To investigate viral fitness of the different site mutants, different cells lines were considered for testing. Previous work showed that HEK 293-T cells contained no MSI1, and therefore, could be used for overexpression experiments with MSI1 (MSI1 WT) and MSI1 containing a mutation that should disrupt binding to target transcripts (MSI1 AV) [178]. However, unexpectedly, initial experiments utilising overexpression of MSI1 in HEK 293-T detected MSI1 expression in HEK-293 T cells transfected with empty vector (HEK empty), as well as in non-transfected cells (HEK) (Figure 3.7).

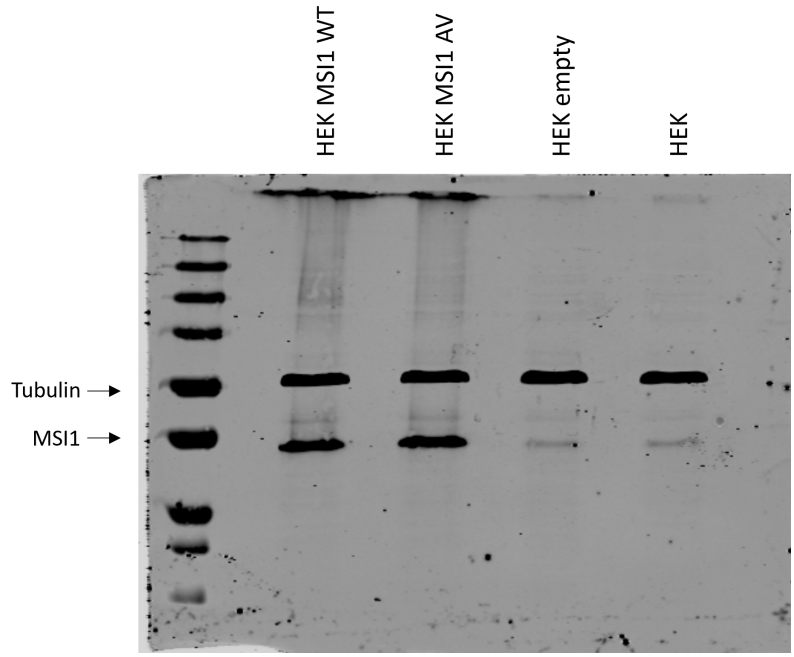

Figure 3.7: Detection of MSI1 in HEK 293 T cells. Transfection of HEK cells with a pCDNA plasmid encoding WT MSI1, MSI1 AV, or empty vector was carried out. 24 hours following transfection, cell lysates were collected and western blotting against MSI1 and tubulin was carried out. Non-transfected HEK cells were also included as a negative control.

It was decided that the effects of MSI1 overexpression in HEK 293T cells would be further investigated to determine if this could boost ZIKV replication as has been previously observed [178]. It was shown that ZIKV displayed a minimal enhancement in replication in HEK 293T cells expressing MSI1 WT compared to cells expressing MSI1 AV or empty vector, however, this was not significant (Figure 3.8). It was, therefore, decided that these cells would not be utilised for future experiments.

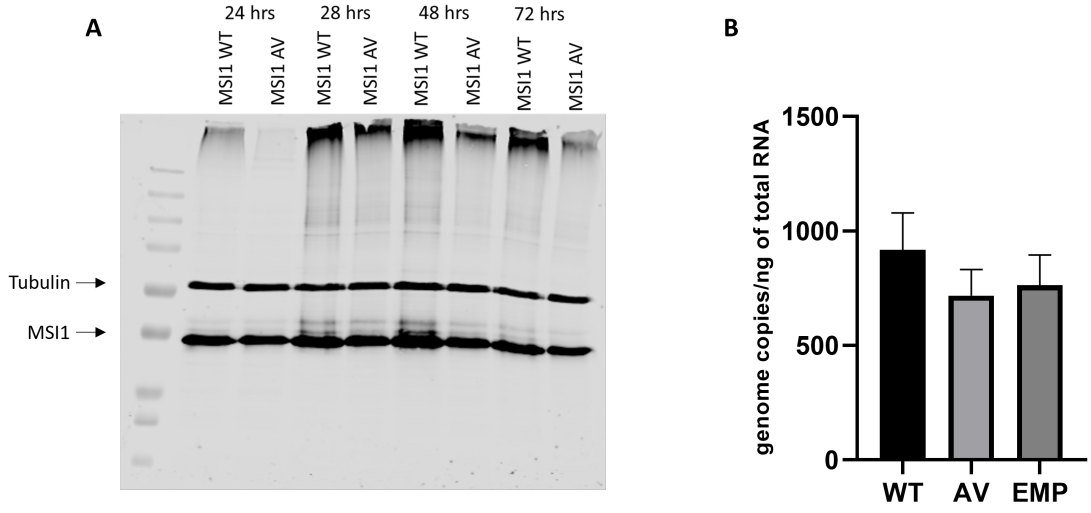

Figure 3.8: Effects of MSI1 overexpression on ZIKV replication. (A) Western blot for MSI1 and the loading control tubulin. Plasmids encoding MSI1 WT or MSI1 AV were transfected into HEK-293 T cells and cells lysed at the indicated times post transfection for western blotting. (B) HEK-293 T cells were transfected with plasmids encoding MSI1 WT, MSI1 AV or empty vector and infected with ZIKV 24 hours later. 48 hours post infection, total RNA was extracted, and RT-qPCR carried out to quantify ZIKV genome copies (n=2).

Previous work carried out by Chavali et al, 2017 generated MSI1 knockout cells using U251 human glioblastoma cells (U251 KO), demonstrating a two-log increase in viral replication at 24 hours post infection in wild-type U251 cells (U251 WT) compared to U251 KO cells. As ZIKV has been shown to infect brain tissue, and these cells have been shown to contain MSI1, they were deemed a good model for studying the effects of MSI1 on ZIKV replication [116, 117, 118, 119, 178]. Initial infection experiments of U251 WT and U251 KO cells were carried out utilising WT ZIKV generated by the reverse genetics system (Figure 3.9A). At 24 hours post infection, a two-fold increase in viral replication was observed in WT cells compared to KO cells (Figure 3.9B).

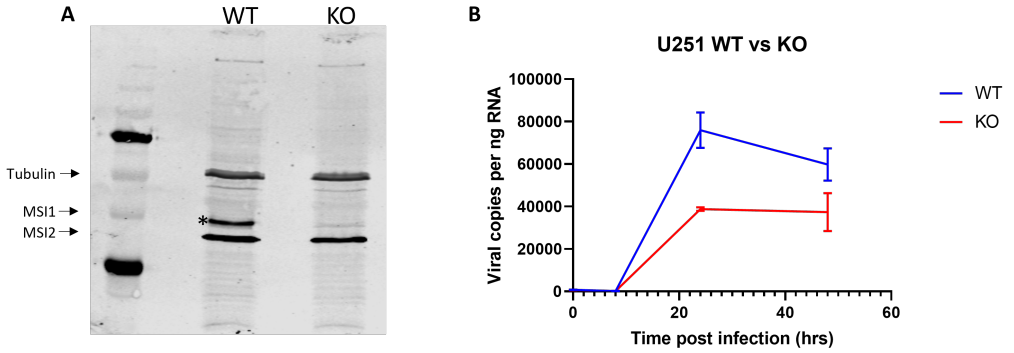

Figure 3.9: Enhancement of ZIKV replication in the presence of MSI1. (A) Probing for MSI1 and tubulin was carried out on U251 WT and U251 MSI1 KO cell lysates. MSI1 is indicted with a black star. MSI2 was also detected as indicated by the black arrow. (B) Following infection of U251 WT and U251 MSI1 KO cells with WT ZIKV at an MOI of 1, total RNA was extracted at 0 hours, 8 hours, 24 hours, and 48 hours post infection and viral genome copies were quantified by RT-qPCR (n=2).

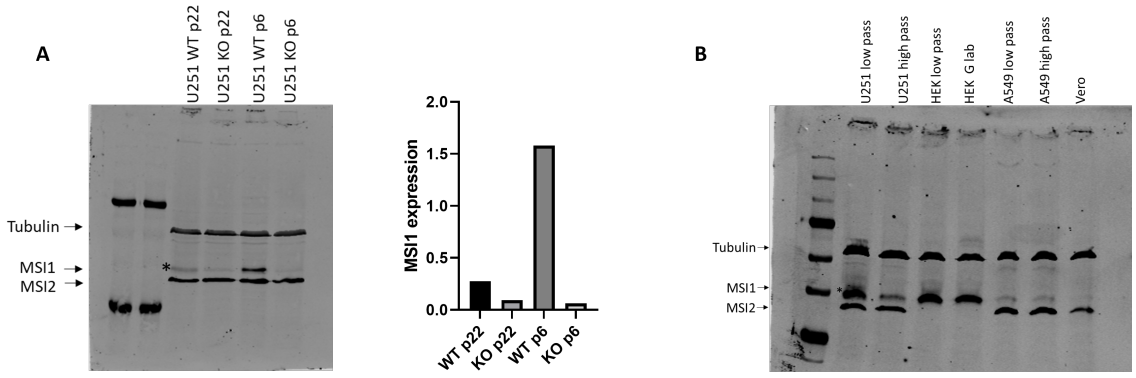

Figure 3.10: MSI1 expression in different cells at different passages. (A) Comparison of MSI1 expression levels in higher vs lower passage U251 cells. U251 WT and MSI1 KO cells were lysed and western blotting carried out to detect tubulin and MSI1 (indicated by *). MSI2 was also detected as shown by the black arrow. MSI1 expression levels were normalised to the tubulin loading control. (B) Comparison of MSI1 levels between different cell types at high and low passage. HEK G cells were low passage HEK cells which were a kind gift from Stephen Graham. High and low passage U251, HEK and A549, as well as Vero cells, were lysed and levels of tubulin and MSI1 detected by western blotting. The additional detection of MSI2 is highlighted by the black arrow.

Over multiple passages the U251 WT cells began to divide at a slower rate that was more comparable to the KO cells. When lysates of older passage U251 WT cells were compared to newer passage cells there was a clear reduction in MSI1 expression

at higher passage (Figure 3.10A). Lysates from other cell types were also tested for MSI1 expression. Again HEK 293 T cells were shown to express MSI1. A549 cells had very low levels of MSI1, and MSI1 levels were almost undetectable in Vero cells (Figure 3.10B).

3.2.3 Investigating the effects of the site mutations on MSI1 driven replication enhancement

As an enhancement in WT ZIKV replication was observed in the presence of MSI1, it was decided that the U251 WT and KO cells would be utilised to investigate whether any of the site mutations disrupted this replication enhancement, and therefore, potentially disrupted MSI1 binding. Low passage stocks of U251 WT cells were generated and used for subsequent experiments to ensure MSI1 levels in U251 WT cells were maintained. Unfortunately, due to cloning difficulties and time constraints, the Site C mutant was not tested, however, it was possible to test the Site C+D mutant.

Infection of U251 WT cells at MOI 1 demonstrated that the Site D and Site C+D mutants replicated approximately two-fold less efficiently than the WT virus at 24 hours post infection (Figure 3.11A). Comparatively, in U251 KO cells, no significant difference in replication was observed (Figure 3.11B). Additionally, the Site A mutant displayed a similar replication profile to the WT virus in both U251 KO and U251 WT cells at MOI 1 (Figure 3.11A/B).

Infection of U251 WT cells at a lower MOI of 0.1 also displayed a significant 5-fold reduction in replication of Site mutants D and C+D compared to WT virus, but at the later time point of 48 hours post infection (Figure 3.11C). Although a trend of reduced replication was observed for these mutants at 24 hours post infection, this was not significant. Similar to what was observed at a higher MOI, at the lower MOI of 0.1, no significant difference in replication was observed for Site mutants D and C+D compared to the WT virus in the U251 KO cells. This indicates that differences in replication efficiencies observed for these mutants compared to WT was dependent on the presence of MSI1 (Figure 3.11D). Additionally, no significant difference was observed between the Site A mutant and WT virus at this lower MOI, although the WT virus displayed an increase in replication in both the WT and KO cells at 48 hours post infection, whilst replication of the Site A virus appeared to plateu (Figure 3.11C/D).

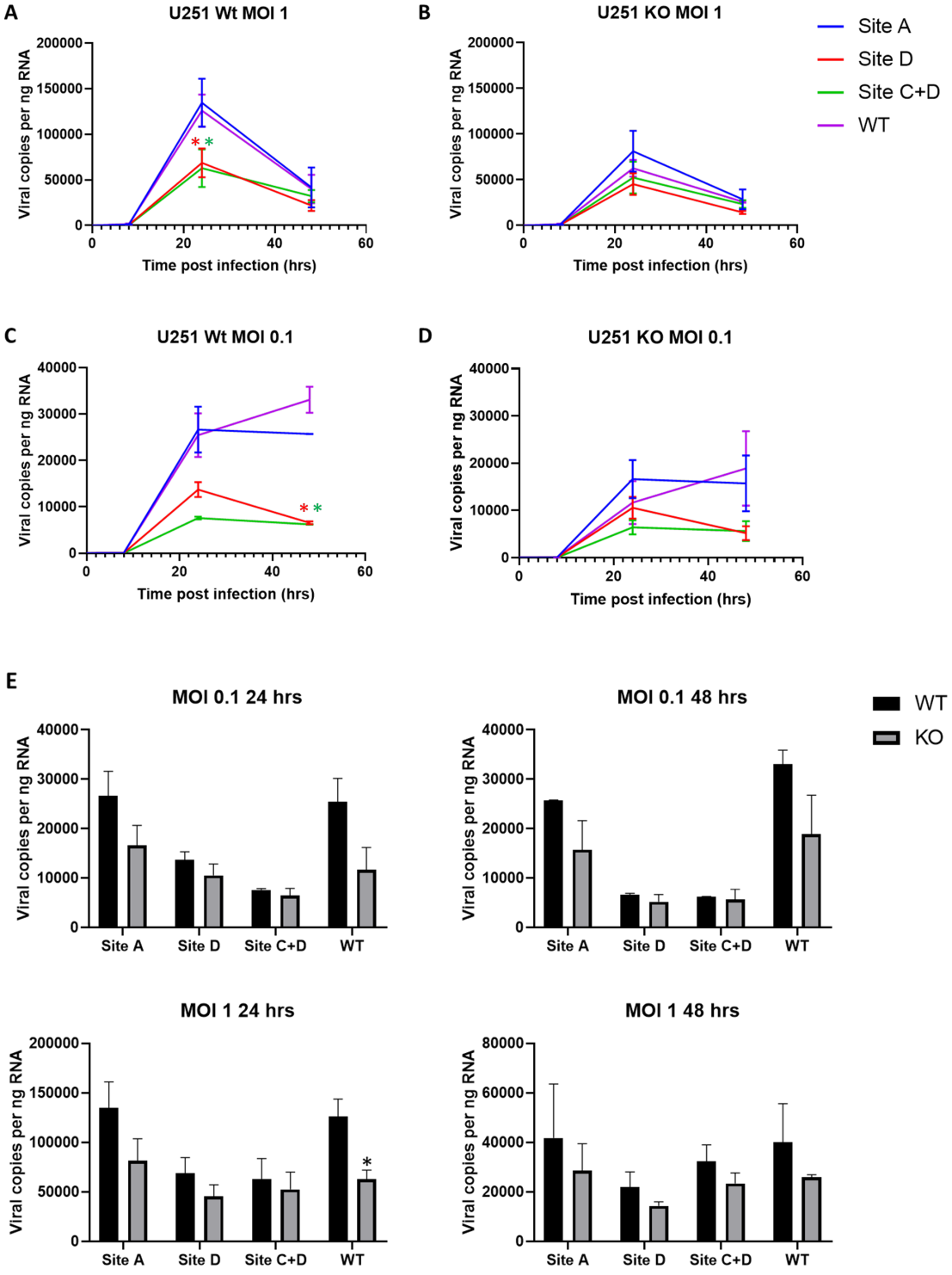

Figure 3.11: Replication of the site mutants in U251 WT vs U251 MSI1 KO cells at high and low MOI. Infection of (A) U251 WT cells or (B) U251 KO cells was carried out with the site mutants or WT ZIKV at MOI 1, n=3. Infections were also carried out at MOI 0.1 in (C) U251 WT or (D) U251 KO cells, n=2. Total RNA was extracted at 0, 8, 24 and 48 hours post infection. Viral genomes were quantified by RT-qPCR and genome copy number normalised by total RNA concentration. (E) Shown is a comparison of viral replication in U251 WT vs U251 MSI1 KO cells at indicated time points for the site mutants and WT virus. *p<0.05, determined by student t test.

No significant increase in replication efficiencies was observed for the site mutants in the presence of MSI1. Only infection with WT virus at MOI 1 showed a significant reduction in replication in U251 KO cells vs U251 WT cells at 24 hours post infection (Figure 3.11E). This indicates that the introduction of these site mutations have disrupted MSI1 dependent replication enhancement.

Cumulatively these results indicate that the mutation of Site D hampers viral replication in a MSI1 dependent manner.

3.3 Discussion

The use of reverse genetics for viral generation is an invaluable tool for studying the effects of different mutations on viral fitness and to further pick apart the interplay between the virus and host. In this study, both a FL ZIKV nanoluc reporter and FL ZIKV construct without a reporter were used, however, the presence of a nanoluc insert had a deleterious effect on viral fitness. It is important to highlight that reporter viruses are extremely useful under some circumstances, streamlining virus detection over standard methods, such as plaque assays or focus forming assays, which can take up to 5 days to produce results. Utilising a reporter virus, it is possible to sample directly from the supernatant for ZIKV and rapidly quantify viral replication, which is useful for drug discovery, particularly for large scale screening of antiviral compounds [196, 197, 198, 199, 200] . This has also proved useful in streamlining neutralisation assays which are important for drug discovery, vaccine development and diagnosis [203, 207]. Additionally, the use of reporter viruses has made it possible to monitor real-time infection in animal models [202, 206]. In this study, the use of FL ZIKV nanoluc reporter constructs were useful for initially screening the mutants for fitness defects, highlighting that the mutation of Site B, D and E reduced nanoluciferase production following the transfection of RNA into Vero cells (Figure 3.2).

Although a highly useful tool, reporter flaviviruses have been shown to have variable stability, although efforts have been made to increase the stability and therefore utility of these viruses. Utilising a small reporter insert, such as nanoluc, produces more stable reporter viruses than the use of larger reporters such as firefly luciferase 2 and red shift luciferase [189]. A common strategy is to insert the reporter between duplicated capsids flanked by the foot and mouth 2A peptide sequence, ensuring that the reporter is separated from the polyprotein. The upstream capsid contains

the cyclisation signals required for viral replication, and the downstream capsid is codon optimised to reduce homology and use of this as a downstream cyclisation site [208, 189, 197]. This strategy was employed in the reverse genetics system utilised in this study. Stability can also be increased by optimising the duplicated capsid length and introducing mutations that will change the reading frame or the charge of the capsid protein if viral recombination takes place [204, 207]. Nevertheless, insertion of a reporter does cause viral attenuation, as has been observed in this study by a reduction in plaque size. This makes these constructs less useful for studying additional mutations that cause viral attenuation and their downstream utility in organoids or animal models [201, 198, 202, 197, 203, 204, 205, 206]. Therefore, for studying the effects of the different site mutations on viral fitness, a FL ZIKV construct without a reporter was deemed more useful.

Despite the first links between microcephaly and ZIKV infection being established following the 2015/2016 epidemic, both African and Asian lineages of ZIKV have been shown to cause microcephaly in mouse models and reduced proliferation and growth of human brain organoids [116, 117, 118, 119]. Interestingly, African strains have been shown to be more neuropathogenic than Asian strains, proving more lethal following the infection of mouse embryos [95, 98, 102]. This is despite no recorded cases of human microcephaly or more severe developmental complications during pregnancy following infection with African lineage viruses, although this may be due to a lack of surveillance.

The link between MSI1 and enhanced ZIKV replication in brain cells provides an interesting hypothesis, linking a host protein to the pathogenesis observed in infants born to mothers infected during pregnancy [178]. However, the work presented here failed to recapitulate the two log enhancement in ZIKV replication previously observed in U251 human glioblastoma cells in the presence of MSI1 [178]. In this study, a 2-fold enhancement in WT ZIKV replication was consistently observed at 24 hours post infection in U251 WT cells compared to U251 KO cells, regardless of whether a higher MOI of 1 was used or a lower MOI of 0.1. Although, a statistically significant difference was only obtained when infections were carried out at the higher MOI of 1 (Figure 3.11E). Indeed, a higher MOI of 3 was utilised in previous work, however, it seems unlikely that this would account for a 2-log vs 2-fold enhancement, as a similar increase in WT ZIKV replication was observed in this study when a low MOI of 0.1 was used (Figure 3.11E). The gap in sampling between the 8 hour and 24 time points may have missed key information about differences in replication, and thus, future work including these earlier time points is also required.

Perhaps MSI1 expression levels in U251 WT cells were much lower in this study compared to previous work, as it was found that the expression of MSI1 was not stable in U251 cells, leading to a reduction in expression levels with increased passage number. Indeed, previous work utilising U251 cells has shown changes in phenotype following passage [209]. Thus, inconsistent expression levels of MSI1 could account for the discrepancy in the extent of replication enhancement in the presence of MSI1, although efforts were made to use low passage cells. In all cell types tested a second lower band was observed below MSI1 which is likely to be MSI2. MSI1 and MSI2 are very similar proteins, sharing 75% amino acid identity and thus perhaps some level of redundancy exists between these proteins [156]. Additionally, MSI2 is highly expressed in neural precursor cells alongside MSI1 [168]. However, although binding of MSI1 to the ZIKV 3′UTR was demonstrated, binding of MSI2 was not detected [178].

Surprisingly, all HEK-293T cells tested, obtained from several different sources at low passage, were found to express MSI1 (Figure 3.10B). It was, therefore, not remarkable that overexpression of MSI1 in HEK-293T cells did not lead to a significant enhancement in ZIKV replication (Figure 3.8B). This is conflicting with previous data that showed MSI1 was absent in HEK-293T cells, which made them useful for studying the effects of MSI1 on ZIKV replication, finding an approximate 5-fold increase in ZIKV replication in the presence of MSI1 [178]. In general, there have been discrepancies between studies in the efficiency of ZIKV infection of HEK-293T cells, with particularly low infection efficiencies found for Asian strains opposed to African strains [52, 210, 211]. Although in this study HEK-293T cells were found to be permissive to ZIKV infection, this variable susceptibility may mean that they are not ideal for studying mutations that affect viral fitness.

Similar to the difference in WT ZIKV replication observed between U251 WT cells and U251 MSI1 KO cells, a 2-fold reduction in replication of the Site D and Site C+D mutant viruses relative to the WT virus was observed at 24 hours post infection in U251 WT cells at MOI 1 (Figure 3.11A). This difference was not observed in U251 KO cells, indicating that the reduction in viral fitness observed for the Site D and Site C+D mutants was linked to MSI1 (Figure 3.11B). Furthermore, minimal differences in replication were observed for the Site D and Site C+D viruses between WT and KO cells, indicating that MSI1 binding was potentially disrupted in these mutants (Figure 3.11E). These MSI1 dependent effects were also observed at lower MOI infection, although at a later time point of 48 hours post infection, with a 5-fold reduction in replication observed for the Site D and Site C+D mutant viruses

(Figure 3.11C). This enhanced difference is exacerbated by the continued increase in replication for the WT virus at 48 hours when a low MOI infection is used, and the reduction in replication observed for the Site D and Site C+D mutants. As the Site C+D mutant displayed similar defects to the Site D mutant, it is likely that the mutation of Site C is not responsible for the replicative defects observed, although further work utilising the Site C mutant is required to confirm this. Site D is a good candidate site due to its presence in both the Asian and African strains of ZIKV [178]. This indicates that if the reduction in replication of the Site D mutant is due to MSI1, then Site D may be the key MSI1 binding site, although pull down analysis is required to confirm this. It is also worthwhile noting that both the Site D and Site C+D viruses displayed fitness defects in Vero cells, including a reduction in plaque size compared to the WT virus, and delayed production of CPE, despite almost undetectable levels of MSI1 in these cells. The quantity of MSI1 required for ZIKV replication enhancement is unknown. Perhaps minimal amounts of MSI1 are sufficient to cause differences in fitness between the site mutants and the WT virus. Alternatively, these mutations may cause changes to RNA structure or disrupt binding of other proteins which could negatively impact viral fitness, this will be discussed in later chapters.

The continued increase in replication at 48 hours when a lower MOI is used compared to the decrease observed at higher MOI may be due to differences in the immune response triggered, allowing the WT virus to continue replicating at later time points following low MOI infection. Indeed, infection of neuronal rat cells at MOI 10 induced much higher levels of the proinflammatory cytokine IL-6 than at MOI 0.1 during early infection, although lower MOI infections of 0.1 and 1 still triggered immune signalling by upregulating IFN-β [212]. The production of IL-6 triggers a signalling cascade mainly via the JAK/STAT3 pathway, promoting an anti-viral response by triggering the transcription of genes, such as those involved in cell signalling and the production of cytokines [213]. IL-6 has been shown to trigger cholesterol 25-hydroxylase (CH25H) which converts cholesterol to 25-hydroxycholesterol and has been demonstrated as having broad antiviral properties, including against ZIKV [214, 215, 216]. Furthermore, there was a positive correlation between MOI and CH25H expression at 24 hours post infection [216]. The activation of TLR3 induced following ZIKV infection leads to IL-6 production, and in cerebral organoids, TLR3 activation has been linked to apoptosis, as use of a TLR3 competitive inhibitor reduced organoid shrinkage [217, 119]. Thus, the elevated levels of IL-6 observed following high MOI infection could explain why at higher MOIs a faster clearance of virus is observed. Testing cellular supernatants following high and low

MOI infection for the secretion of cytokines would confirm this. Similarly, following viral infection, IFN production induces the expression of hundreds of anti-viral genes [67, 149]. However, ZIKV has developed several strategies to overcome this, including NS5 mediated degradation of STAT2, and sfRNA mediated inhibition of IFN-1 responses downstream of the receptors RIG-I and MDA-5 [218, 139]. Thus, although at lower MOI IFN is produced, ZIKV can likely overcome this and continue replicating at later time points.

Higher MOI infections also lead to higher levels of cell death. Previous work utilising high (1) and low (0.001) MOIs showed that ZIKV induced greater cell death in trophectoderm cells at higher MOIs, whereas cells could still survive and differentiate into trophoblasts at the lower MOI infection [219]. Indeed, more floating cells are observed when higher MOI infections are carried out. Furthermore, following a high MOI infection of 3 in U251 cells, it was found that by 48 hours post infection there is a dysregulation of cellular regulator molecules involved in transmembrane signalling, regulating transcription, nuclear signalling, cellular growth, and immune signalling [220]. This was also accompanied by a 50% reduction in cell viability. Therefore, at higher MOI infections, due to the faster progression of infection, it is likely that a combination of the host immune response and reduced cell fitness and viability is leading to a more rapid reduction in viral replication. Additionally, viral stocks are generated by collecting cell supernatants following Vero cell infection, and infection does trigger the production of immune signalling molecules such as cytokines [221]. At higher MOI, the virus supernatants are less diluted and therefore may contain higher levels of these immune signalling molecules that may trigger a more potent immune response. As insect and mammalian cells have different anti-viral immune responses, it may be preferable to generate stocks in insect cells when infections will be carried out in mammalian cells to try and mitigate the introduction of molecules that could trigger immune signalling.

It is well documented that U251 MSI1 KO cells are defective in that they display longer doubling times, altered migration, and delayed cell cycle progression [178, 171, 187]. Indeed, MSI1 upregulates and downregulates many genes involved in cell proliferation, differentiation, and growth [166]. As ZIKV relies on the host machinery to translate its viral proteins and make new progeny virions, any adverse effects on the cell caused by MSI1 KO could also hamper ZIKV replication. An alternative solution is to identify cells that are naturally lacking MSI1, and introduce it, however, overexpression of proteins can still have deleterious effects on the host cell [222]. It would be more biologically relevant to utilise neurospheres or human

brain organoids to study ZIKV replication, particularly for investigating ZIKV induced neuropathology [118]. Additionally, IFN deficient mouse models of infection have been established for ZIKV which display neuropathological effects similar to what is seen in humans [223]. If the disruption of MSI1 binding is confirmed for the Site C mutant this would provide a useful tool to study MSI1 dependent effects in these systems without relying on knockout or overexpression of MSI1.

The Site A virus had similar fitness to the WT virus, displaying similar plaque morphology and replication rates, indicating that the mutation of this site had no effect on viral fitness (Figure 3.4, Figure 3.11). Interestingly, the Site E virus was only rescued following mutation of a nucleotide from C→T upstream of the Site E mutation site and not following Site E reversion (Figure 3.5). Additionally, the Site B mutant was shown to be less fit than WT producing much smaller plaques, whilst it also partially reverted from CC to CG following viral passage (Figure 3.6). Many proteins bind to the flavivirus 3′UTR and thus it is plausible that these site mutations have disrupted the binding of a protein important for the viral life cycle [29]. It is also plausible that these mutations have disrupted the structural elements within the 3′UTR. These possible explanations will be further investigated and discussed in the following chapters.

Chapter 4

Structural mapping of the ZIKV 3′ untranslated region

4.1 Introduction

A combination of in silico and structural mapping methods has generated a structure for the ZIKV 3′UTR, including secondary structure formation, as well as the formation of multiple PK structures (Figure 4.1) [30, 15]. The general architecture of the flavivirus 3′UTR is well conserved between members of the *Flavivirus* genus, highlighting the importance of the structural integrity of the 3′UTR to viral fitness [32, 33, 31, 30]. Indeed, the highly structured flavivirus 3′UTR contains RNA elements that are crucial for viral replication and translation through long range RNA-RNA interactions, as well as binding of host and viral proteins [33, 26, 27, 28, 29, 224]. The structures within the flavivirus 3′UTR RNA are also required for the generation of sfRNAs which are important for viral pathogenesis and immune evasion [45]. This highlights the importance of maintaining the correct structural organisation of the 3′UTR when introducing site mutations.

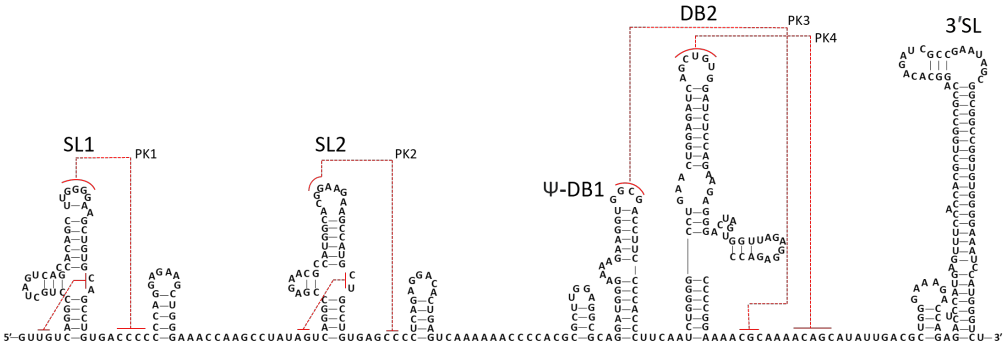

Figure 4.1: Structure of the ZIKV 3′UTR. Shown is the structural architecture of the ZIKV 3′UTR. SL structures, DB structures and the 3′SL are indicated. PK interactions are shown as red lines.

In silico structural mapping is useful for obtaining insights into viral RNA structures and their conservation, and hence potential functionality [33, 225, 226]. For example, the long established RNA folding software Mfold predicts RNA secondary structures by calculating the most thermodynamically stable fold [227]. This is highly useful for picking out potentially important structures for further investigation, however, misses important tertiary structures. Other folding software such as pknotsRG are available to predict tertiary structure formation, however, to refine the *in silico* models, experimental mapping of viral RNA is also required [226]. Methods for the use of different reagents to obtain structural information on RNA molecules are long established [228, 229]. Metal ions, RNASE enzymes and organic molecules have all been utilised to modify RNA, leading to the formation of adducts or cleavage of the RNA which can be detected via a reverse transcription (RT) reaction and analysis of cDNA products [230]. The gold standard method for experimentally mapping RNA structures is selective hydroxyl acylation analysed by primer extension (SHAPE) [230]. Unlike other chemical mapping methods, SHAPE allows quantitative reactivity information to be obtained as it does not display nucleotide selectivity [230, 231]. SHAPE mapping involves modifying RNA with a hydroxyl selective electrophile, such as N-methylisatoic anhydride (NMIA), which can access and therefore modify bases that are not constrained within secondary structures to a greater degree than base paired regions. At these bases, a stable adduct will form, and the site of modification can be detected by carrying out an RT reaction with a labelled primer. The labelled cDNA products produced from termination of the RT reaction at these sites of adduct formation can then be detected by running a sequencing gel if the primer is radioactively labelled, or by separating the cDNA products by capillary electrophoresis if a fluorescently labelled primer was employed. Sequencing reactions are carried out using the same RNA that was utilised in the modification reaction by including a single ddNTP and carrying out an RT reaction. By running the cDNA products generated following modification alongside the sequencing reaction it is possible to identify the exact site of modification in the RNA, and therefore, start to build up a structure of the RNA utilising programmes such as QuSHAPE [231] (Figure 4.2).

As the structure of the 3′UTR is important for viral fitness, it is plausible that the disruption in viral replication observed for some of the site mutants is due to changes in RNA structure. The site mutations were previously predicted to be within single stranded regions of the RNA and, therefore, deemed unlikely to introduce major structural changes to the 3′UTR [178]. To further investigate this, SHAPE mapping was employed. This section aimed to determine if any of the site mutations alter

the structure of the ZIKV 3′UTR, which could account for the changes observed in viral fitness. To do this, optimisation of SHAPE mapping to capture information for the full 3′UTR sequence was required.

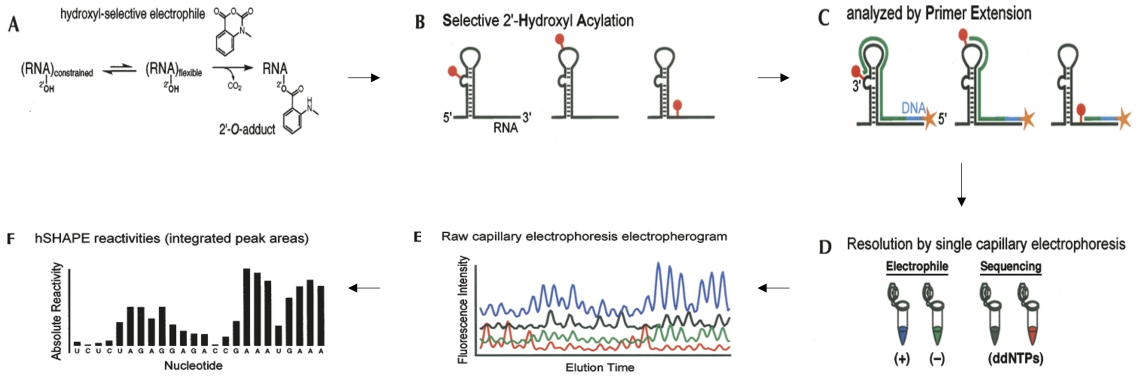

Figure 4.2: Selective hydroxyl acylation analysed by primer extension protocol. Illustrated above is the experimental procedure for carrying out SHAPE analysis. (A) RNA is first modified with a hydroxyl-selective electrophile such as NMIA. (B) Stable adducts form at the site of modification. (C) The site of adduct formation is detected by carrying out a reverse transcription reaction with a labelled primer. The RT enzyme will be halted at sites of modification. (D) A sequencing reaction is carried out in parallel using a different fluorescently labelled primer and ddNTPs. The site of adduct formation in the sequence is determined by running the cDNA products of the RT reaction alongside the sequencing reaction, and separated by capillary electrophoresis. (E) The fluorescent signal is detected, producing a trace for both the samples and sequencing. (F) Using SHAPE data analysis software, such as QuSHAPE, a histogram is obtained of normalised reactivity for each nucleotide in the sequence. Adapted from [231].

4.2 Results

4.2.1 Utilising structured extension cassettes allows SHAPE mapping of the full ZIKV 3′UTR

Previous work has generated a model of the ZIKV 3′UTR structure through a combination of experimental and *in silico* methods [30, 15]. Using traditional SHAPE it is possible to map most of the ZIKV 3′UTR, however, information is lost at the 5′ and 3′ ends of the RNA [231]. Additional sequence can be added to extend the 3′ end creating an RT primer binding site, although this could in itself lead to structural changes within the RNA. Additionally, information is lost at the very 5′ end due to the high intensity full-length signal [231]. To overcome this problem, structured binding cassettes can be added to the 5′ and 3′ ends of the target RNA,

allowing mapping at the very 5′ end, and also creating an RT primer binding site at the 3′ end. As these extension cassettes are highly structured, they should not interact with the target RNA, and therefore, should not affect the overall structure [231, 232].

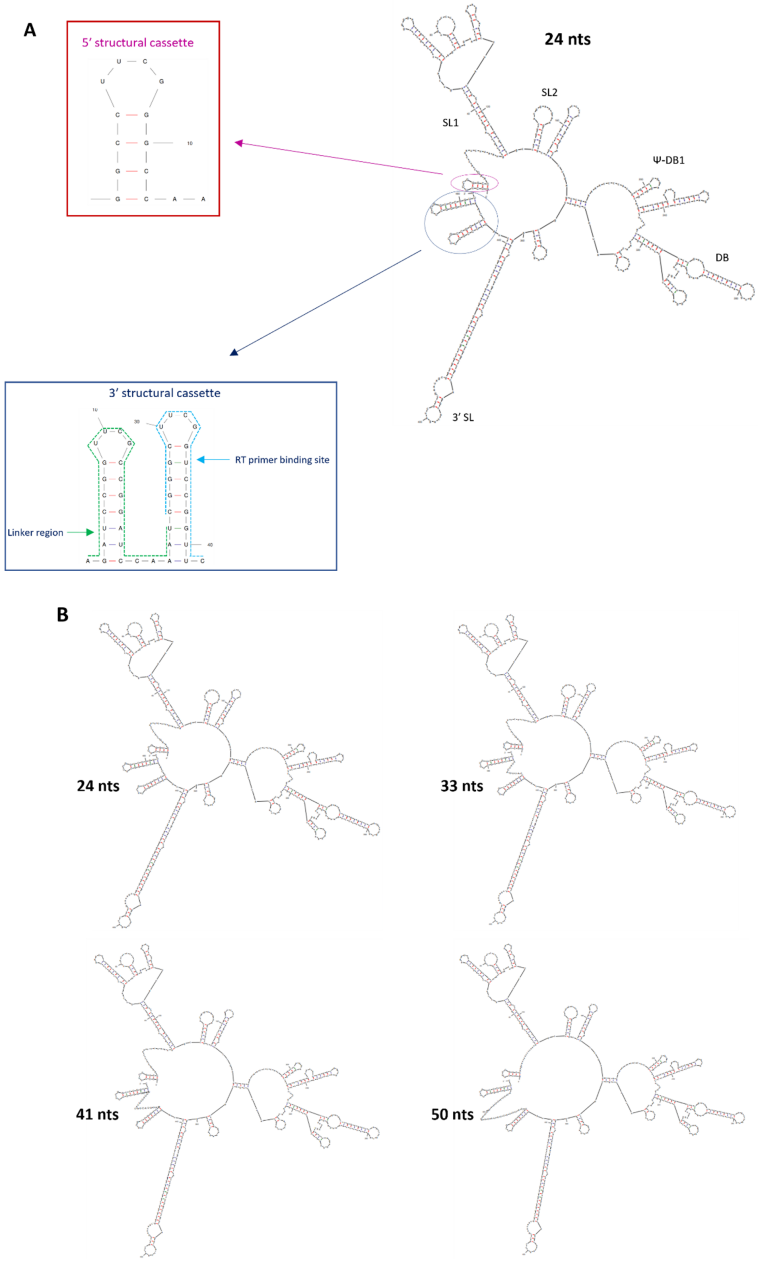

Figure 4.3: Mfold structures of the SHAPE extension cassettes. (A) The mfold structure for the 3′UTR with the 5′ extension cassette and the 3′ extension cassette containing the 24 nucleotide spacer is shown. The mfold structures obtained for the 5′ and 3′ cassette alone are highlighted and their position in relation to the 3′UTR mfold structure. The SL and DB structures are also labelled. (B) Shown are the mfold structures of the 3′UTR plus the 5′ structural cassette, as well as the 3′ structural cassettes containing variable lengths of spacer region. Default parameters were used to run mfold.

Several different 3′ extension cassettes were modelled based on previous work [231, 232]. The extension cassettes were designed to have different length spacer regions between the RT primer binding site and the terminal end of the 3′UTR, with the aim to map the full 3′UTR sequence with a single RT primer. A 5′ extension cassette was also included. The structure of the ZIKV 3′UTR RNA containing the different binding cassettes was tested with the mfold web server using the default parameters. Based on the mfold results, none of the structural cassettes impacted the structure of the ZIKV 3′UTR (Figure 4.3). Consequently, PCR amplification was used to generate a construct containing a T7 promoter site followed by the 5′ extension cassette, the ZIKV 3′UTR, and one of the four different 3′ extension cassettes (Figure 4.4).

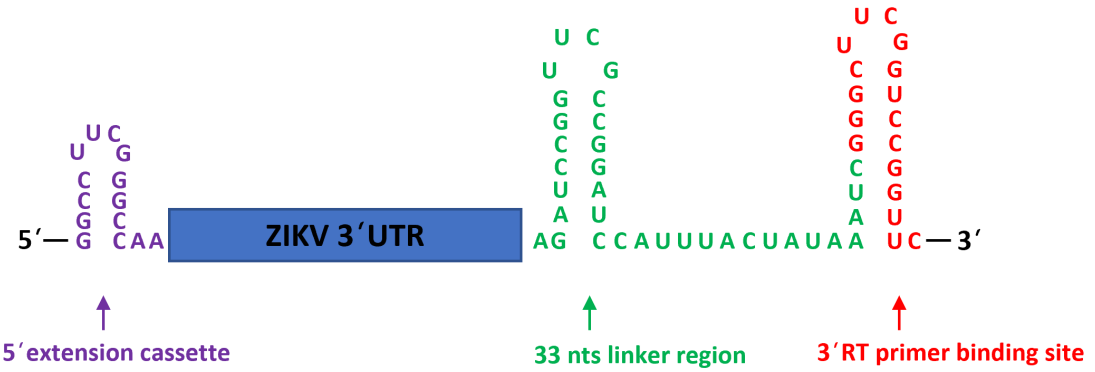

Figure 4.4: SHAPE extension cassette for structural mapping of ZIKV 3′UTR. Depicted is the ZIKV 3′UTR flanked by a 5′ extension cassette coloured in purple, and a 3′ extension cassette, consisting of a spacer region coloured in green and an RT primer binding site shown in red.

As all of the cassettes have the same RT binding site, a single extension cassette primer was required for the RT reaction. Primers were also designed within the 3′ SL region, namely SL1 and SL2. Initially, all primers were labelled with ^{32}P and then an RT reaction was carried out to assess which primer would be optimal for SHAPE probing of the 3′UTR. From this, the SLI primer and the extension cassette primers all produced a good signal, whereas, comparatively, the SL2 primer produced a weak signal. Shown in Figure 4.5 is an abundant RT product, highlighted by a red arrow, which is likely generated due to dissociation of the RT enzyme at the 3′SL structure of the 3′UTR. This product was observed for all the RNA constructs containing the extension cassette, however, the cassette with the 24 nucleotide spacer appeared to have a fainter signal at the 3′SL compared to the cassettes with longer spacer regions. It was therefore concluded that the 24 nt spacer region was not long

enough to obtain high resolution SHAPE mapping data at the very 3′ end of the 3′UTR. As there was no difference in signal intensity between the 33, 41 and 50 nts spacers, it was decided that for future experiments the cassette containing the 33 nts spacer would be utilised. Additionally, for all the cassette structures tested, although high resolution data was obtained for the 3′ end of the RNA, the signal waned towards the full length signal which was very high comparatively. Initially a high RT temperature of 55°C was used to try and promote the RT reaction through the highly structured 3′UTR, although in this case, it seems that the RT enzyme SSIII was too processive at this temperature. To overcome this, all future SHAPE experiments were carried out at a lower RT incubation temperature of 52°C instead of 55°C [233].

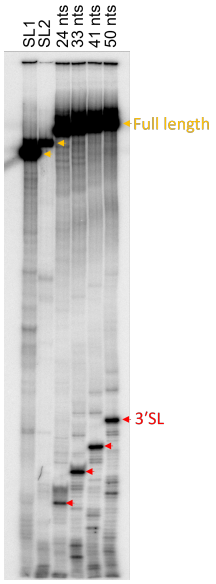

Figure 4.5: Testing reverse transcription primers on the ZIKV 3′UTR RNA. Radiolabelled primers binding to the 3′SL (SL1 or SL2) or primers binding to the extension cassettes with different spacer regions (24, 33, 41 or 50 nts) were tested in an RT reaction using Superscript III at 55°C for 30 mins. Following separation of radiolabeled cDNA products on a sequencing gel, the gel was dried and exposed on a phosphoscreen overnight. Imaging was carried out using the Typhoon phosphoimager. The red arrow highlights the cDNA product generated following stalling at the 3′SL. The yellow arrow highlights the full length signal.

For SHAPE probing, fluorescently labelled primers were employed instead of radiolabelled primers. As fluorescent SHAPE has a greater dynamic range, it was anticipated that a single primer could be used to map the full 3′UTR sequence [234]. Initial tests were carried out on the WT ZIKV 3′UTR RNA containing the 33 nt spacer structural cassette. Briefly, RNA was re-folded and then treated with

NMIA or DMSO prior to RT using a fluorescently labelled primer. A sequencing reaction was also carried out in parallel. Following RT, the samples and sequencing were mixed prior to separation by capillary electrophoresis. A two-capillary approach was employed, allowing the the use of two fluorescently labelled primers [234]. Traditional SHAPE experiments require four flourescently labelled primers, two for the sequencing reactions and two for the NMIA and DMSO reactions. This allows all the samples to be run down a single capillary [235]. Utilising the two capillary approach, the NMIA reaction and sequencing reaction is run down one capillary, and the same sequencing reaction and DMSO reaction is run down a second capillary [234]. Data analysis was carried out in QuSHAPE [234]. QuSHAPE is an automated programme which streamlines the analysis of capillary electrophoresis data, carrying out signal decay correction, alignment of signals within and between capillaries and with the RNA sequencing data, producing histograms depicting reactivity values for each nucleotide (Figure 4.6). This is unlike other data analysis software, such as ShapeFinder, which requires a greater level of user input and experience [234].

The SHAPE reactivities obtained for the WT 3′UTR generally fit well with previous structural modelling data (Figure 4.7) [30]. This includes the PK interactions as indicated by the lack of reactivity at the top and bases of SLI and SLII. At the smaller stem loop structure just downstream from SLI, the SHAPE reactivities from this experiment better fit the model than the previous data, with more of the exposed nucleotides in the bulge region displaying higher reactivities. Additionally, the data obtained for the 3′SL structure fit well with the previously proposed model with high reactivity at the bulge region at the top of the stem loop and unpaired nucleotides in the stem region. Overall, the SHAPE data generated from this study in combination with the likely nucleotide interactions supports the previously generate model for the ZIKV 3′UTR RNA structure. This also highlighted that the addition of the structured extension cassette did not affect the overall structure of the 3′UTR RNA, and therefore, could be used to accurately map the full length of the 3′UTR.

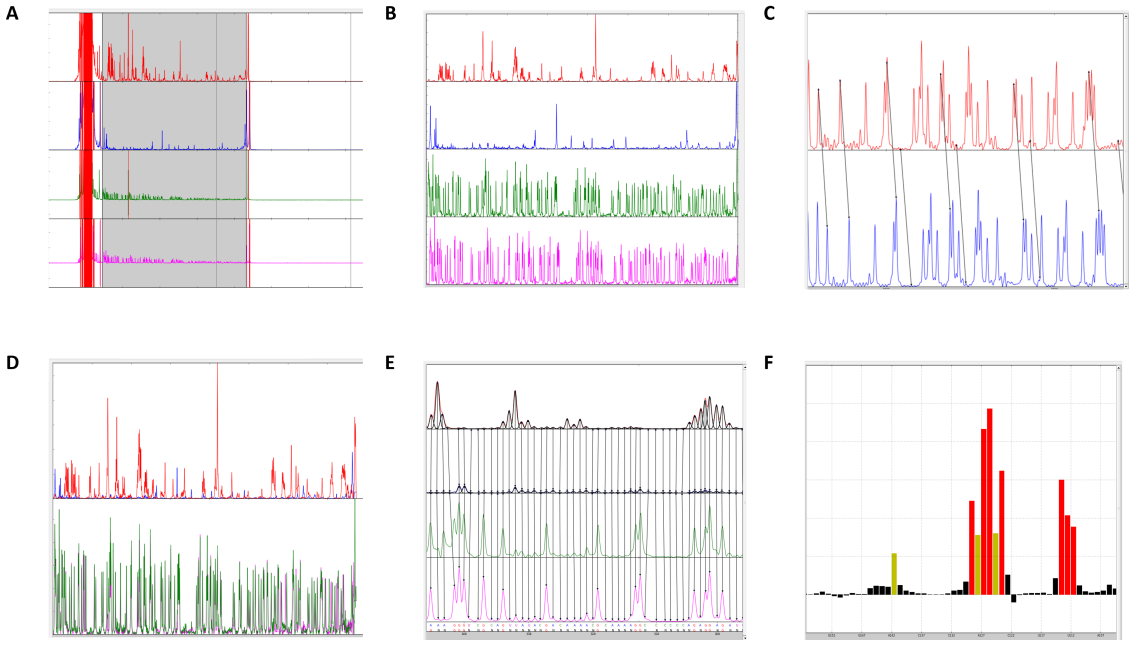

Figure 4.6: QuSHAPE data processing. Shown is the data obtained from a SHAPE experiment carried out on the WT ZIKV 3′UTR with the 33 nucleotide extension cassette. (A) Traces shown display the raw reactivity data for the NMIA treated sample (red), DMSO sample (blue) and sequencing reactions in the NMIA treated sample well (green) and DMSO treated sample well (pink). These signals are obtained by running samples down two separate capillaries, one containing the DMSO treated sample plus the sequencing reaction, and the other containing the NMIA treated sample plus the same sequencing reaction. Highlighted in grey is the region that is selected for further analysis to exclude the full length signal at the 5′ end and the primer signal at the 3′ end, both coloured in red. (B) QuSHAPE performs baseline adjustment to correct for baseline offset, and signal decay correction to correct for the decline in fluorescent signal observed as elution time increases. The resulting trace is shown. (C) Signal alignment is then carried out between the sequencing signals ran down the two separate capillaries shown in blue and red. (D) The top panel shows the resulting alignment of the NMIA treated (red) and DMSO treated (blue) samples. The aligned sequencing trace is also shown in the bottom panel (green + pink). (E) Sequence alignment is then carried out, assigning the positive sequencing signals to the selected ddNTP. In this case ddCTP was used so signals are obtained for G nucleotides. The resulting trace is then matched to the input target sequence to assign bases. (F) The normalization operation subtracts the reactivity value obtained for the DMSO sample from the NMIA sample and normalizes the difference, obtaining a reactivity value for each nucleotide position. Shown is the resulting histogram generated displaying nucleotides with reactivity values of 0-0.4, 0.4-0.85 and >0.85 representing unreactive (black), moderately reactive (yellow), and highly reactive nucleotides (red) respectively.

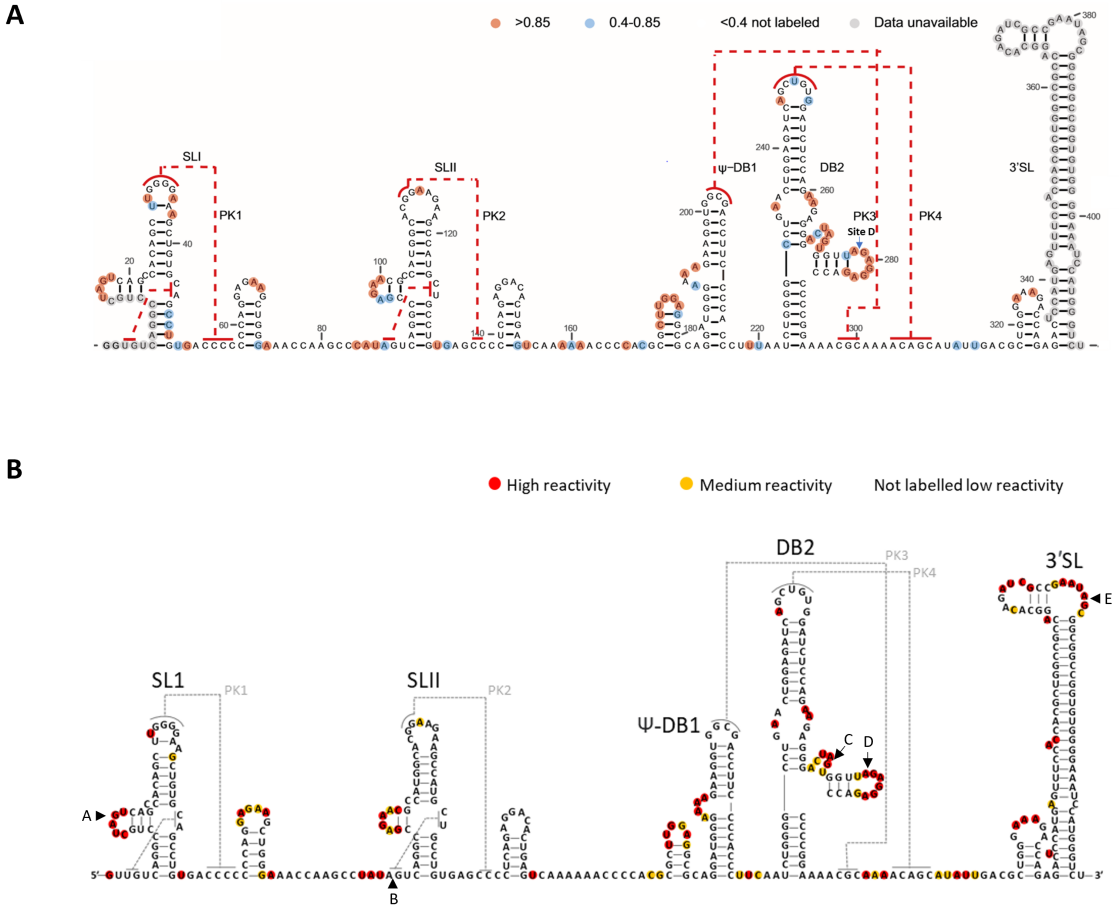

Figure 4.7: The SHAPE reactivity data generated using the extension cassette fits well with the previously generated model of the WT ZIKV 3′UTR. (A) Model of ZIKV 3′UTR with SHAPE data mapped on. As shown by the bases highlighted in grey, data is unavailable for the 3′SL ([30]). (B) Model of ZIKV 3′UTR based on the WT SHAPE reactivities obtained in this study including data for the 3′SL. High reactivity >0.85, medium reactivity 0.4-0.85, and low reactivity 0-0.4. Secondary and tertiary structures are shown, and site mutations are indicated by black arrows.

4.2.2 SHAPE mapping reveals structural changes introduced into the ZIKV 3′UTR following mutation of Sites B and C

Following the successful structural mapping of the WT 3′UTR, fluorescent SHAPE was carried out on the mutant ZIKV 3′UTR RNAs to determine if any of the site mutations impacted the structure of the RNA, and therefore, could explain the loss in viral fitness observed for site mutants B, D, C+D and E. Based on the previous structural mapping, none of the putative MSI1 binding sites identified were

in base-paired regions within the secondary structure, therefore, mutation of these sites was deemed unlikely to affect the RNA structure [178]. Indeed, the SHAPE reactivity data obtained for the Site A, D and E mutant 3′UTRs corresponded to the data obtained for the WT 3′UTR (Figure 4.8A and B). However, Site B is located at the base of SLII at an equivalent site to where an internal PK forms in SL1, and the formation of this internal PK has been shown to be important for supporting complex RNA folding at this site [40]. As SL1 and SLII are likely structural duplications, it seems probable that the Site B mutation could disrupt tertiary structures at SLII [225].

The Site B mutant did indeed display increased reactivities of nucleotides at the top and base of SLII, which would be consistent with the disruption of complex tertiary structures at this site, providing a possible explanation for the reduced viral fitness observed for this mutant (Figure 4.9B). Additionally, the Site C mutation appeared to introduce some changes to the secondary structure. This coincided with a reduction in reactivities of nucleotides located in the bulge regions of the DB structure and increased reactivity of nucleotides in previously base paired regions (Figure 4.9C). This does not appear to affect tertiary structure formation or the structure of the rest of the DB. Cumulatively, this indicates that any changes in viral fitness observed for the Site D or E mutants is unlikely to be due to structural changes introduced into the RNA. For the Site B and Site C+D mutants, structural changes may be responsible for, or at least contribute to, the reduction in viral fitness observed.

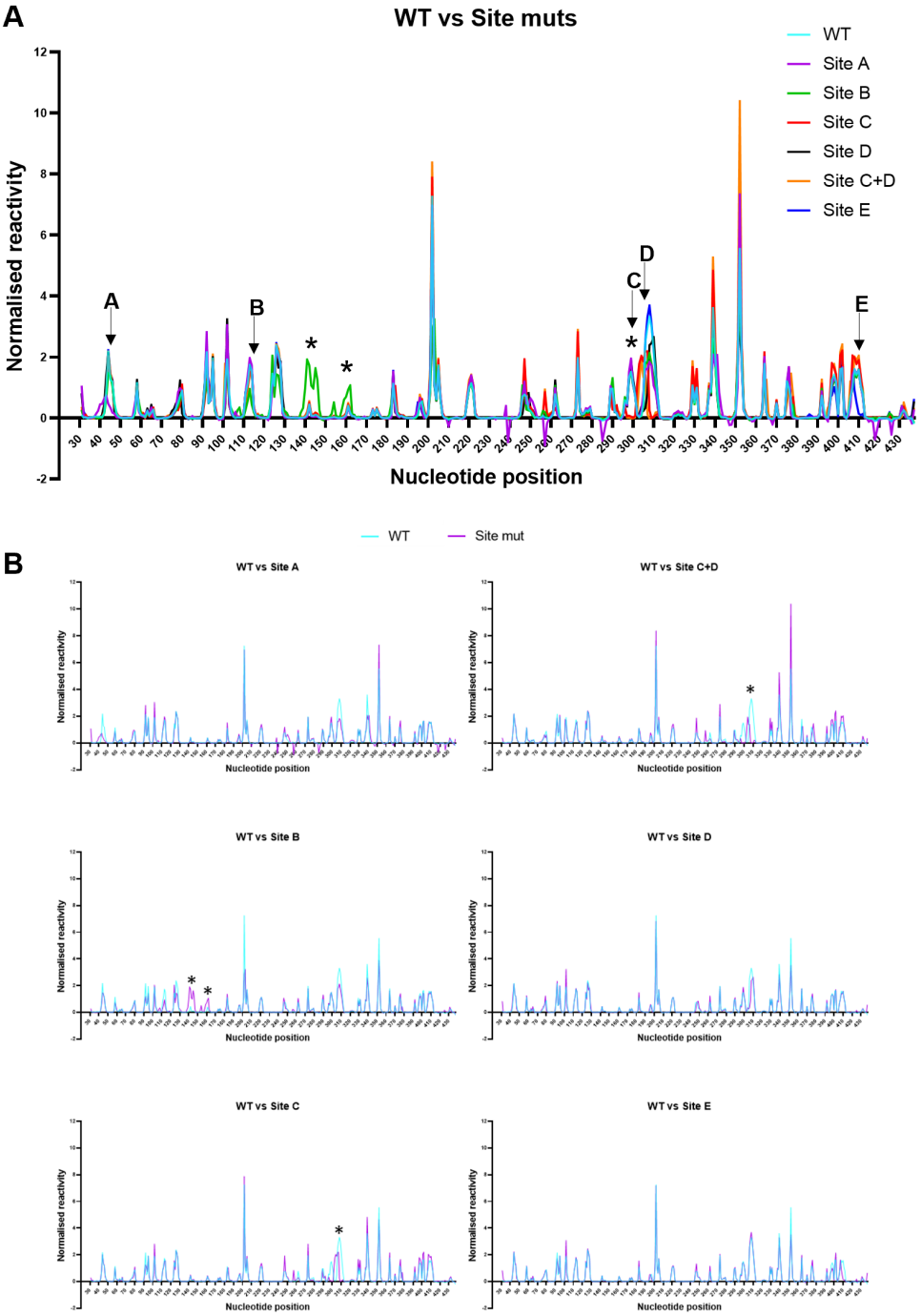

Figure 4.8: Comparing WT and site mutant SHAPE reactivity profiles. (A) Shown are the average reactivity profiles for the site mutants and WT 3′UTR obtained from repeat SHAPE experiments following analysis using QuSHAPE. The asterisks highlight areas where reactivities deviate from the WT profile. The nucleotide positions of each of the site mutations are indicated; Site A (44-45), Site B (115-116), Site C (299-300), Site D (306-307) and Site E (410-411). For WT, Site A, Site B, Site D and Site E, n=3. For Site C and C+D, n=2. (B) The individual reactivity profiles for each mutant are shown alongside WT. The black stars highlight areas where reactivity differs from the WT profile.

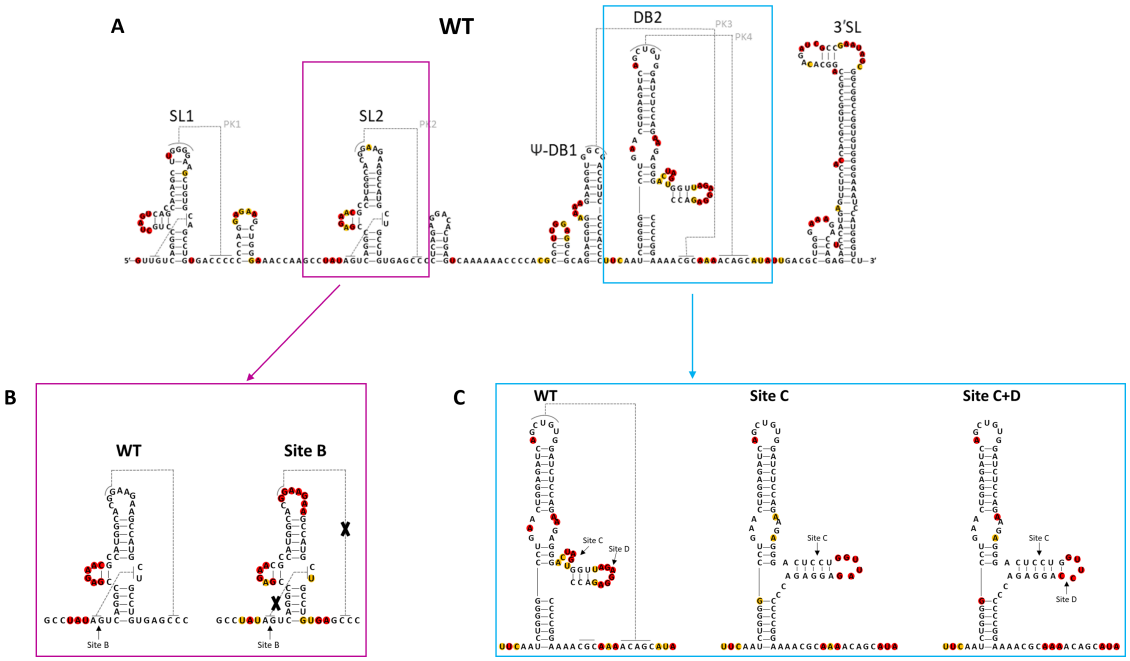

Figure 4.9: Structural disruption within the 3′UTR caused by mutation of Sites B and C. (A) WT ZIKV 3′UTR structure with SHAPE reactivities. Red, orange, and colourless bases depict areas of high, medium, and low reactivity respectively. (B) The structure of SLII is shown for both WT and the Site B mutant. SHAPE reactivities are mapped onto the structure and predicted PK interactions are depicted by the grey lines. The black crosses represent likely disruptions to the PK structure caused by mutation. (C) The second DB structure is shown for the WT, Site C mutant and Site C+D mutant. The grey lines on the WT structures depict where predicted PK interaction sites are located. For the Site C and Site C+D mutants, the structures were constructed based on the changes in SHAPE reactivity observed.

4.3 Discussion

SHAPE analysis is an effective method to gain structural information on RNA, and used in collaboration with *in silico* structural mapping can be used to build more robust models of RNA structure. During a SHAPE experiment it is important that the RNA is representative of the RNA structure *in vivo*. Previous work has found that *in vivo* mapped RNA structures better fit the canonical models previously generated for the ZIKV 3′UTR than *in vitro* mapped RNA structures [15]. However, in this study, the WT 3′UTR structural mapping data fit well with the previously generated model of the ZIKV 3′UTR, indicating that the folding conditions utilised were promoting a 'relevant' conformation, and that the extension cassette was not interfering with RNA structure (Figure 4.7) [15, 30]. Previous studies utilising *in*

vitro SHAPE mapping have failed to capture information at the 3′ end of the 3′UTR, due to utilising primer binding sites within the 3′SL structure [15, 30]. By extending the spacer region in the structural cassette, it was possible to map the end of the 3′UTR, including the 3′SL. Furthermore, by utilising fluorescent SHAPE, only a single primer was required to map the structures within the 3′UTR. This not only reduces costs but is more time efficient, as reactions can be carried out in a 96-well format and QuSHAPE allows rapid data analysis [234]. This also means that once this set up is established it can be employed on different RNA molecules utilising the same primer. The reactivity traces produced for repeat SHAPE experiments on the WT and site mutant RNAs was reproducible, indicating that this is a reliable method for obtaining accurate structural information (Figure 4.8). This provides an efficient high throughput *in vitro* method for obtaining structural information at the 3′ end of the ZIKV 3′UTR.

All the reactivity traces obtained for site mutants A, D and E matched the WT structure, and thus, it seems unlikely that the fitness defects observed for the Site D and E mutants were due to structural changes introduced into the 3′UTR (Figure 4.8). However, it is important to highlight that *in vitro* SHAPE fails to capture dynamic structural conformations that form throughout the course of infection. This includes any different structural conformations that may be introduced following protein binding or long range RNA-RNA interactions [15, 224]. Many long-range RNA-RNA interactions have been identified within the FL ZIKV genome, however, only one long-range interaction has been identified between the 3′UTR and elsewhere in the FL RNA. This is the interaction between the 5′ and 3′ UTRs, promoting genome circularisation and positioning of the RNA dependent RNA polymerase at the 5′ end of the genome so that replication can take place [15, 224, 24]. None of the site mutations are located within the cyclisation sequence and the SHAPE data indicates that there was no effect on secondary structure formation at this site (Figure 4.10).

For the Site E mutant, the reduction in viral fitness observed could be due to disruption in protein binding. Many host and some viral proteins have been identified that bind to the 3′UTR, including many that bind to the 3′SL [29]. Site E itself is located at the top of the 3′SL structure in a bulge region that is highly reactive, and therefore, likely accessible for protein binding. In fact, for JEV and DENV4, it has been shown that La autoantigen binds to the 3′SL, and for JEV binding occurs at a sequence motif ‘AAG’ directly proceeding the equivalent of Site E [236, 237, 238, 239]. Perhaps in the case of ZIKV, La autoantigen binds at Site E which contains the motif of ‘UAG’ instead of the equivalent site to JEV of ‘AAU’

(Figure 4.11). La autoantigen has been identified as important in virion production in JEV, as siRNA knockdown led to a 97% reduction in viral titres [239]. Therefore, the disruption of La autoantigen binding would provide a plausible explanation for why it was not possible to rescue the Site E mutant virus. La autoantigen may contribute to the switch between flavivirus replication and translation through binding to NS3 and NS5, releasing the ends of the UTRs, and allowing genome cyclisation and hence replication to take place [238]. Indeed, La autoantigen has been shown to bind DENV NS3 and NS5 as well as both the 5′ and 3′ UTRs of DENV [238, 237]. To test whether the Site E mutation does disrupt La autoantigen binding, a pull down could be employed utilising the 3′UTR containing the Site E mutation as bait.

Interestingly, the Site E mutant was only recovered once out of the two times reverse genetics was attempted, but with an additional mutation present within the 3′UTR. It is tempting to speculate that this additional mutation restored La autoantigen binding, but perhaps at a secondary site. Certainly, a second La autoantigen binding site was detected in JEV present in a bulge region upstream from the main site of binding [239]. Perhaps in the Site E mutant, the additional mutation present at the top of the 3′SL destabilises the top of the SL allowing La autoantigen binding at an alternative site (Figure 4.11). Again, pull down analysis could be utilised to further investigate this, in addition to SHAPE analysis, to determine if the potential secondary binding site becomes more accessible for protein binding.

Other host proteins have also been identified as binding to the flavivirus 3′SL, including the transcriptional coactivator p100, which binds to the 3′SL of DENV [240]. p100 has been shown to regulate transcription factors involved in cellular signalling pathways, including those involved in cellular growth, differentiation and apoptosis, as well as those involved in immune signalling [241, 242]. For DENV, p100, was shown to be important for viral replication in mammalian cells [240]. The mosquito ortholog of p100, known as Tudor Staphylococcal Nuclease, has also been shown to enhance DENV replication in mosquito cells, however, does not interact with DENV RNA [243]. The mechanism of this replication enhancement still remains unknown [240, 243]. Additionally, the mouse proteosome subunit Mov34, was shown to bind to the 3′SL of JEV, and homologous proteins have been shown to be involved in the regulation of RNA transcription and translation [244, 245]. However, the functionality of Mov34 binding to JEV RNA was not established [244]. For both p100 and Mov34 the exact location of binding was not identified, so it is unclear whether the Site E mutation would disrupt binding of these proteins.

Overall, it seems plausible that the loss in viral fitness observed for the Site E mutant is due to a disruption in La autoantigen binding which can be further investigated by pull down and SHAPE analysis. This opens an interesting avenue for researching the role of La autoantigen in the ZIKV life cycle and provides useful tools for future work on this subject.

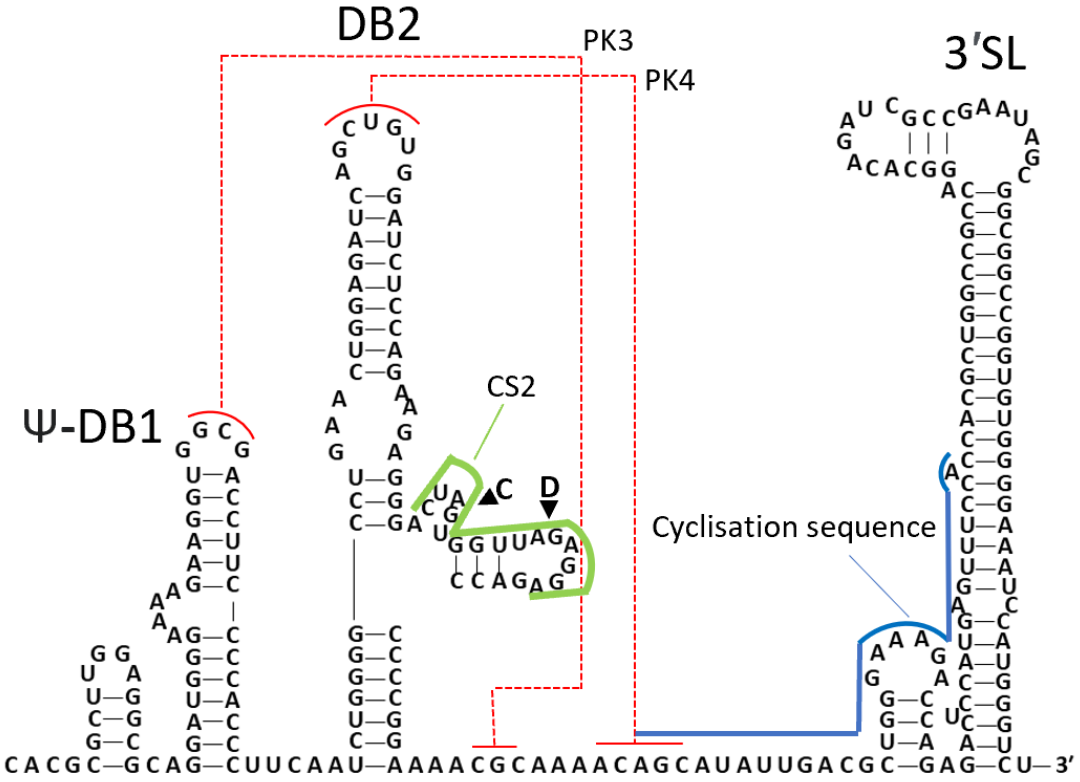

Figure 4.10: Location of CS2 and the cyclisation sequence in the ZIKV 3′UTR. The structures present at the 3′ end of the 3′UTR are shown. Pseudoknot interactions are depicted by the red lines. The green line around the bulge regions of the dumbbell depicts the conserved sequence (CS2) where both the Site C and Site D mutations are indicated with a black arrowhead. The cyclisation sequence is highlighted with a blue line.

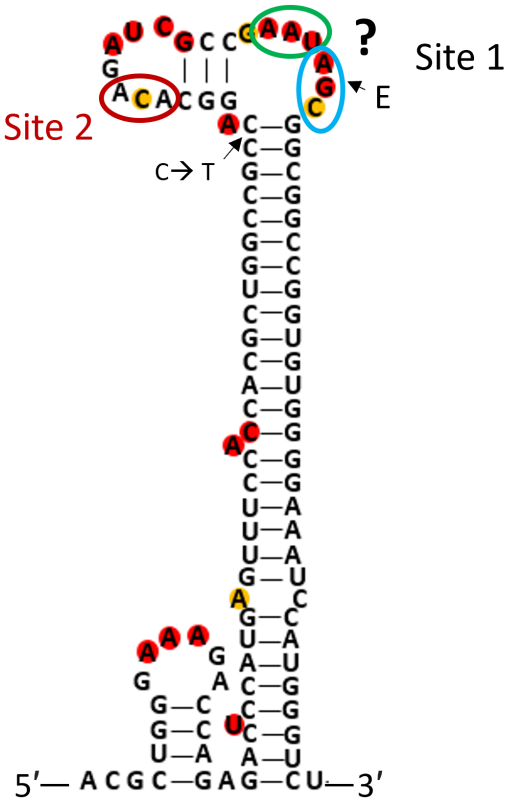

Figure 4.11: Putative binding sites of La autoantigen in the ZIKV 3′SL. Shown is the 3′SL of the ZIKV 3′UTR with SHAPE reactivities mapped on. High reactivity >0.85, medium reactivity 0.4-0.85, and low reactivity 0-0.4. Potential La autoantigen binding sites are circled. The green circle highlights the equivalent site identified in JEV as the main site of La autoantigen binding. Circled in blue is another possible site of binding containing Site E. A secondary site of binding identified in JEV is circled in red. The additional mutation that recovers Site E fitness is also indicated

Interestingly, the Site C mutation altered RNA secondary structure at the bulge region of the DB (Figure 4.9C). Notably, both the Site C and Site D mutations are located within a site that has been identified as highly conserved among mosquito borne flaviviruses, referred to as conserved sequence 2 (CS2) (Figure 4.10) [39]. Recent crystallisation studies of the insect specific flavivirus, Donggang virus, combined with structural modelling, showed that the CS2 forms S3 and P3 helixes which are part of a four-way junction supporting PK formation at the 3′ DB structure [42]. Despite the changes in SHAPE reactivities of CS2 in the Site C mutant, there was no obvious disruption to the PK. Furthermore, the Site C+D mutant showed a non-significant difference in replication compared to the Site D mutant, indicating that the mutation of Site C had a minimal impact on viral fitness. Future

work testing the Site C mutant virus will be conducted to investigate this.

Although no structural changes were introduced by the Site D mutant, changes in sequence alone could still be detrimental to viral fitness. Indeed, the CS2 sequence and not the structure has been deemed more important for viral fitness. Three different mutations within regions of CS2 that should in theory maintain the DB structure led to a ≈50% reduction in translation and a ≈10 fold reduction in replication in a DENV2 replicon [246]. Flaviviruses, such as DENV, WNV and JEV, contain duplicated DB structures, unlike ZIKV, which has a pseudo DB and DB structure [225]. Therefore, these viruses also contain a duplicated CS2 sequence, namely, repeat conserved sequence 2 (RCS2), and it has been suggested that RCS2 and CS2 could act cooperatively in translation and replication [246, 19]. In a DENV2 replicon, the deletion of DBS 1 or 2 containing both RCS2 and CS2 respectively led to a 100X reduction in replication compared to WT, and when both DBS were deleted, replication was completely abolished [18]. Comparatively the Site D mutant only displayed a ≈2 fold reduction in replication compared to WT. It is important to highlight that in the case of these DENV studies, deleting a significant proportion of the 3′UTR could cause other structural disruptions as well as the disruption of protein binding, and thus, adversely affect viral fitness. The 3′ terminal flavivirus PK structure does overlap with the cyclisation sequence, leading to the suggestion that disruption of this PK through binding of proteins to CS2 could allow genome cyclisation and replication to take place [42]. Perhaps disruption of binding of proteins that promote destabilisation of the PK led to the replication defect observed in the Site D mutant. However, if this mutation affected the translation-replication switch, a greater reduction in viral fitness would be expected. It is possible that the mutation just weakened the interaction leading to the slight reduction in replication observed for the Site D mutant.

The high reactivity and single stranded nature of the region containing the CS2 sequence where Site C and Site D are located, identified it as a prime site for MSI1 binding, although this also makes it generally an accessible site for protein binding [188, 178]. Certainly, in the case of DENV, the RNA helicase DDX6 binds to either DB1 or DB2 and the presence of DDX6 was shown to be important for viral replication [247]. This indicates that theoretically DDX6 could bind to ZIKV via its DB structure, however, a yeast three-hybrid screen failed to detect DDX6 binding to ZIKV RNA despite confirming DDX6 binding to DENV RNA [248]. It is also worth considering the possibility that a protein binding site has been introduced via mutation, which is detrimental to viral fitness. It would be interesting to try and

identify differences in protein binding profiles between the Site D mutant and WT 3′UTRs using mass spectrometry.

Clear differences in the structure were observed for the Site B mutant (Figure 4.9B). Although Site B is present in an unpaired region within the secondary structure, it is likely involved in tertiary structure formation at this site [40, 33, 30]. This is supported by the crystal structure for ZIKV SLI, demonstrating that nucleotides present at the equivalent site to Site B in SLII are involved in the formation of an internal PK structure, which supports the formation of a three-way junction [40]. Previous work has shown that mutations disrupting the three-way junction at ZIKV SLI, DENV SLI, WNV SLII, and MVEV SLIV, lead to a reduction in Xrn1 resistance, and hence sfRNA production [40, 134, 41]. In both ZIKV and WNV, the mutation of the three nts proceeding the SL structures, including Site B in ZIKV SLII, has also been shown to disrupt sfRNA production [41, 136]. In MVEV xrRNA2, mutation of the equivalent of the revertant nucleotide in the Site B mutant alone is enough to disrupt Xrn1 resistance, although restoration of base pairing of the internal PK did not rescue Xrn1 resistance [41]. This highlights the difficulty in introducing mutations at this site and highlights the importance of structural mapping following mutation. Utilising the high throughput fluorescent SHAPE mapping set up will allow the rapid screening of different 3′UTR mutants *in vitro*, before the introduction of mutations into the FL virus. This does, however, provide a potential explanation for the loss of viral fitness observed for the Site B mutant, due to the likely role that sfRNA production plays in viral replication as well as immune evasion [136, 148, 45]. In the following Chapter, further investigation of the effects of the Site B mutation on sfRNA production will be conducted.

The results presented in this chapter indicate that the viral defects observed for site mutants C, D and E are not due to structural changes introduced into the 3′UTR. It is possible that these mutants display different protein binding profiles compared to the WT virus, and therefore, future mass spectrometry analysis may reveal interesting hits important for viral fitness. In the case of Site B, it is likely that the disruption to viral fitness is due to disruption of tertiary structure formation at SLII, which may hamper sfRNA production. Further work will be carried out in the following chapter to investigate this. Overall, a reliable high throughput *in vitro* SHAPE method for mapping the full 3′UTR of ZIKV was established and will prove useful for the future screening of 3′UTR mutants.

Chapter 5

Disruption of the three-way junction in SLII of the ZIKV 3′UTR disrupts sfRNA production leading to reduced viral fitness

5.1 Introduction

The general architecture of the 3′UTR is similar between different members of the *Flavivirus* genus, playing important roles in both viral replication and translation [32, 33, 31, 30, 26]. Formation of PK structures and complex folding of the flavivirus 3′UTR structural elements has also been shown to be important for viral pathogenesis [136, 38, 30]. In particular, the formation of a three-way junction is crucial for the production of sfRNAs [136, 134, 40, 41]. ZIKV produces two main sfRNAs during infection, namely sfRNA1 and sfRNA2, as a result of resistance at the SLI and SLII structures to degradation by host enzymes (Figure 5.1). These RNAs are also referred to as xrRNA1 and xrRNA2, owing to their resistance to degradation by the host enzyme Xrn1 [40, 136]. In the case of ZIKV, sfRNA formation was shown to be required for successful viral replication in mammalian cells, as well as for establishing successful infection in mosquitoes, and thus viral transmission [136, 148]. Flaviviral sfRNA has also been linked to the evasion of host immune signalling in both vertebrates and invertebrates [45]. Thus, studying sfRNA production by flaviviruses is important for enhancing our understanding of viral-host interactions. Any mutations that disrupt the structure and lead to viral attenuation also provides useful information for the design of vaccines, of which none are currently licensed for ZIKV.

As shown in previous chapters, it was found that the mutation of two nucleotides at the base of SLII generating the Site B mutant (AG→CC) reduced viral fitness, leading to smaller plaque size and delayed virus production following electropora-

tion of viral RNA into Vero cells. Further investigation utilising SHAPE mapping indicated that this site mutation introduced structural changes to the 3′UTR, likely disrupting PK formation required for the formation of the three-way junction and thus XRN1 resistance and sfRNA production [41, 40]. For simplicity, the nucleotides at Site B (AG) will be referred to as A2 and G3 for comparison with previous studies, referring to the fact that they are the second and third nucleotides of sfRNA2. Reversion of one nucleotide back to the WT sequence (G3) produced the Site B rev virus, indicating that this nucleotide was particularly important for viral fitness. This coincides with previous work whereby mutation of G3 in SLIV of MVEV abolished XRN1 resistance [41]. It is also worthwhile noting that G3 at the base of the SLs of both xrRNA1 and xrRNA2 is well conserved among flaviviruses, highlighting its importance. The A2 residue preceding G3 in the Site B mutation is less well conserved, although it is present at the base of ZIKV SLII, WNV SLI, JEV SLI and both SLs in DENV. Indeed mutation of the equivalent residue in SLI of ZIKV from A to U for crystallization studies had minimal effect on XRN1 resistance, indicating that this nucleotide is not essential (Figure 5.2)[40]. Any disruption to SLII will likely adversely affect viral fitness, as in ZIKV this disrupts sfRNA1 production, as well as sfRNA2 production [136, 148].

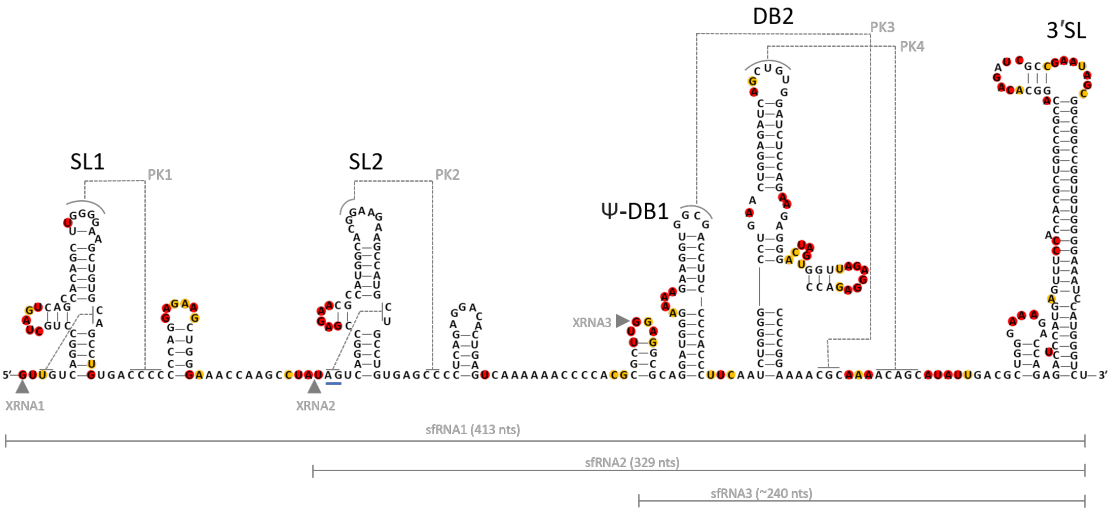

Figure 5.1: ZIKV WT 3′UTR structure. Shown are the secondary and tertiary structural elements that make up the 3′UTR of ZIKV. Bases are coloured to indicate SHAPE reactivity values. Highly reactive, moderately reactive and unreactive bases are red, orange and uncoloured respectively. The corresponding sfRNAs produced from xrRNA1 stalling at structural elements are indicated. The location of the Site B mutation is underlined in blue. This figure was based on previous work from [30].

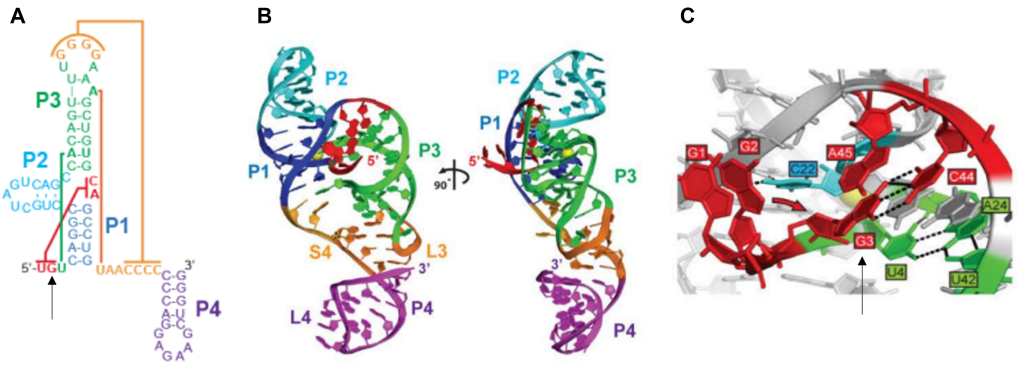

Figure 5.2: Structure of ZIKV xrRNA1. (A) Diagram depicting the internal PK coloured in red, main PK coloured in orange and additional interactions involved in three-way junction formation. As it is predicted that xrRNA2 has a similar structure to xrRNA1, the black arrow depicts the equivalent location of the Site B reversion. (B) Ribbon representation of the crystal structure of xrRNA1 coloured according to Figure A. PDB accession code 5TPY. (C) Shown are the 5′ end interactions of ZIKV xrRNA1. The black arrow is used to highlight the G3 nucleotide which is the site of reversion in xrRNA2 of the Site B mut (Adapted from [40]).

Although the structure of ZIKV xrRNA1 and xrRNA2 are important for sfRNA generation, this specific mutation in SLII has never been investigated. Additionally, few studies have shown that mutation of a single nucleotide within the 3′UTR has such a negative impact on viral fitness in mammalian cells. For ZIKV, previous work has shown that mutation of the three nucleotides proceeding the SL structures negatively impact viral fitness [136]. Furthermore, mutation of a single unpaired C residue in SLI, referred to as C22, disrupts three-way junction formation and abolishes XRN1 resistance in both ZIKV and DENV [134, 40]. Correspondingly this mutation hugely inhibited sfRNA production in the context of ZIKV infection in Vero cells [40]. The equivalent mutation in SLII at position C18, also hampered ZIKV infection in mosquitoes [148]. Similarly, following WNV infection of HEK 293T cells, this mutation was shown to reduce XRN1 resistance in SL1 and abolished resistance in SLII, corresponding to a reduction in sfRNA1 and no sfRNA2 production respectively [134]. However, the effects of these mutations on viral fitness was not further investigated [40, 134]. As the Site B mutant only reverted at one nucleotide, it seems likely that mutation of a single nucleotide in xrRNA2 was sufficient to disrupt this complex fold, and hence production of sfRNA2. This chapter aimed to determine whether the Site B reversion had restored the PK structure, and if this was the case, elucidate the effects on sfRNA production and viral fitness in the context of infection.

5.2 Results

5.2.1 The Site B reversion restores the 3′UTR structure

In the previous chapter, SHAPE mapping demonstrated that the Site B mutation located at the base of SLII introduced a structural change to the 3′UTR, likely disrupting an internal PK structure and thus three-way junction formation. As the flavivirus 3′UTR structure plays an important role in the viral life cycle, this likely explains the reduction in viral fitness observed for the Site B mutant [136, 41, 40, 134, 38, 30]. Following viral passage, the Site B mutant partially reverted to WT sequence from CC to CG. This was accompanied by an increase in plaque size, indicating improved viral fitness. To determine whether the reversion of a single nucleotide back to the WT sequence was enough to restore the PK structure, SHAPE mapping was also carried out on the 3′UTR RNA of the Site B revertant virus using the SHAPE mapping protocol established in Chapter 4. As shown in Figure 5.3, Site B mut again demonstrated a different SHAPE reactivity profile compared to WT, with increased reactivity at the top and base of SLII. The reactivity profile of the Site B revertant was almost identical to the WT 3′UTR, and most importantly, the nucleotides at the top and base of SLII displayed low levels of reactivity. This indicates that a single nucleotide reversion in the Site B mutant was indeed enough to restore the PK structure, accounting for the increased viral fitness observed for Site B rev.

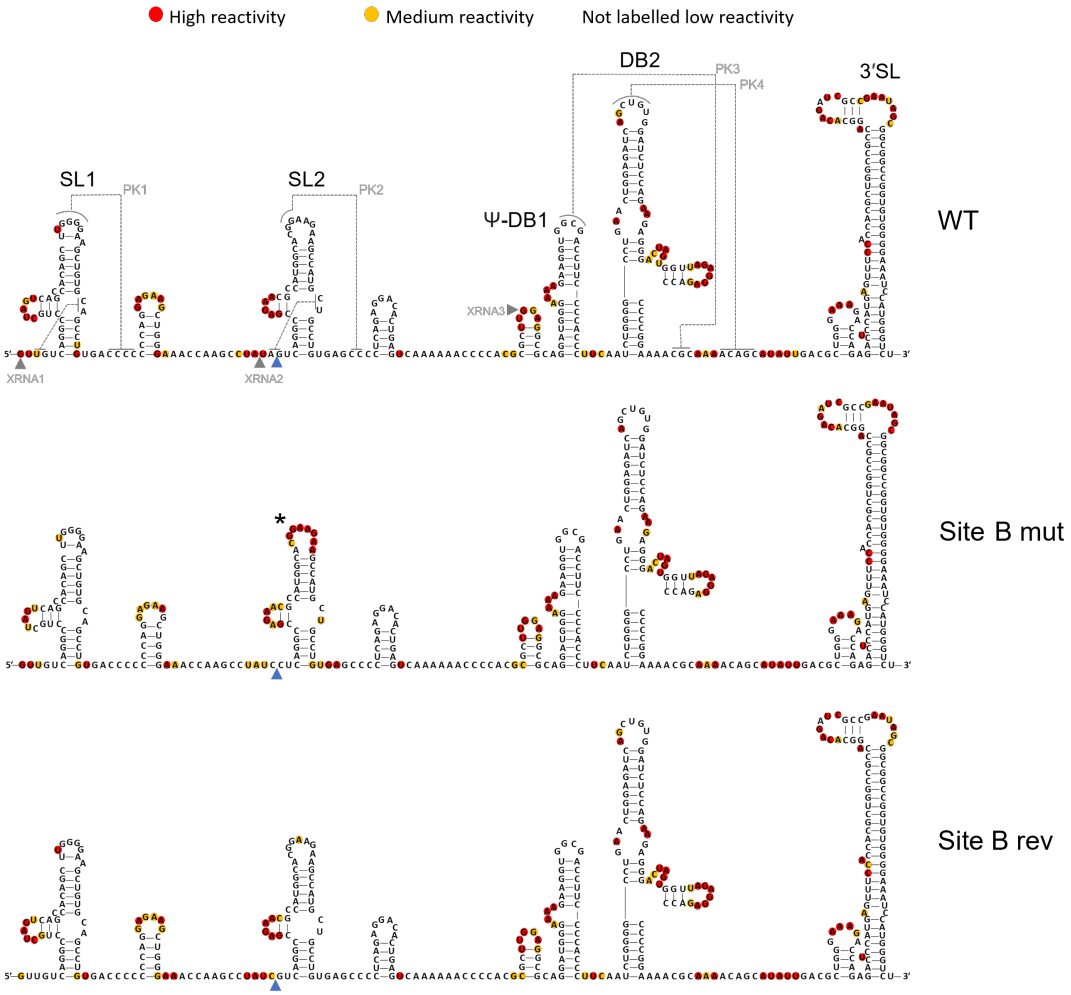

Figure 5.3: SHAPE reactivity profile of Site B mut, WT and Site B rev 3′UTRs. Shown is the structure of the ZIKV 3′UTR with bases coloured according to levels of reactivity. High reactivity (red) >0.85, medium reactivity (orange) 0.4-0.85, and low reactivity (uncoloured) 0-0.4. The blue arrowhead depicts the location of Site B. The star highlights the location of increased reactivity at SL2 in the Site B mut.

5.2.2 The Site B mutant virus is defective in sfRNA production

The structural changes introduced into the 3′UTR of Site B mut were particularly detrimental to viral fitness as there was a rapid reversion to restore the original 3′UTR structure. Furthermore, previous studies have shown that disruption of the three-way junction in xrRNAs can lead to reduced resistance to XRN1 degradation and hence a reduction in sfRNA production [136, 41, 40, 134]. To test this, northern blotting was carried out on total RNA isolated from Vero cells infected with WT, Site B rev and P0 stocks of Site B mut. From this, it was clear that the Site B mutant

produced much less sfRNA than WT and Site B rev. Additionally, reversion of Site B led to the rescue of sfRNA production, although this was still lower than WT levels (Figure 5.4). Cumulatively this linked the disruption of the 3′UTR structure in the Site B mutant to a defect in sfRNA production.

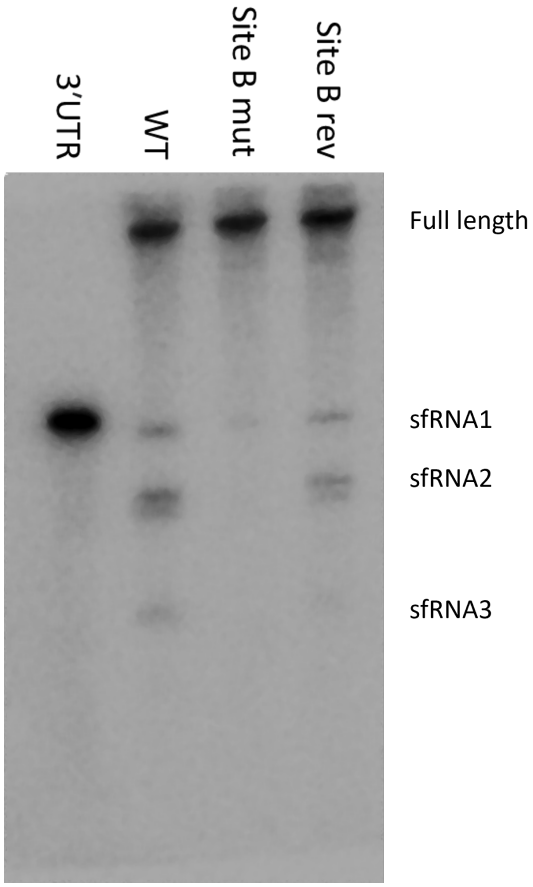

Figure 5.4: The Site B mutant is impaired in sfRNA production. Northern blot on total RNA extracted from Vero cells following infection with WT, Site B mut and Site B rev showing the sfRNA patterns obtained for the respective viruses. The full length signal is also indicated.

5.2.3 The reduction in viral fitness observed for the Site B mutant is not due to impaired viral replication or translation

Flavivirus sfRNA is thought to modulate the host environment to promote viral infection, and it is therefore not surprising that the Site B mutant displays clear fitness defects [45]. The Site B mutation practically abolishes sfRNA production which is important for ZIKV fitness following infection of mammalian cells (Figure 5.4) [136].

To further investigate this, A549 and Vero cells were selected to represent cells that are immunocompetent and immunodeficient respectively. A549 cells were employed instead of U251 cells, as A549 cells are easier to handle and have lower levels of MSI1, and were therefore deemed more comparable to Vero cells. Cells were infected with the Site B virus, Site B rev virus, or WT virus. At 24 hours post-infection, cellular RNA was collected for qPCR and supernatants were collected for viral titration. Cell lysates were also collected following high MOI infection and western blotting for viral E protein was carried out. In both A549 and Vero cells, the Site B virus showed similar levels of viral RNA to both the Site B rev and WT virus, indicating that viral replication was not hampered by the introduction of the Site B mutation (Figure 5.5A). Similarly, the Site B mutation caused no obvious effect on viral translation as shown by western blotting for viral E protein (Figure 5.5C). Interestingly, following infection of A549 cells, the Site B mut virus displayed a slight reduction in viral titre of ≈4X less at MOI 3 and ≈5X less at MOI 0.1 compared to the WT virus, although this was not statistically significant (Figure 5.5A). This trend towards a reduced titre for the Site B mutant was not observed in Vero cells. As A549 cells are IFN competent and Vero cells are IFN deficient, the reduction in titre observed for the Site B mutant may be linked to the immune response. Further repeats are required to confirm these findings. As observed previously, the Site B mut was defective in plaque formation, producing smaller plaques than the WT virus (Figure 5.5B). The Site B rev virus produced larger plaques than Site B mut but still appeared to be attenuated in plaque production compared to WT (Figure 5.5B).

Combined, these results indicate that the single nucleotide mutation of G→C at the base of SLII disrupts proper folding of xrRNA2, hampering the production of sfRNAs and potentially hindering viral immune evasion.

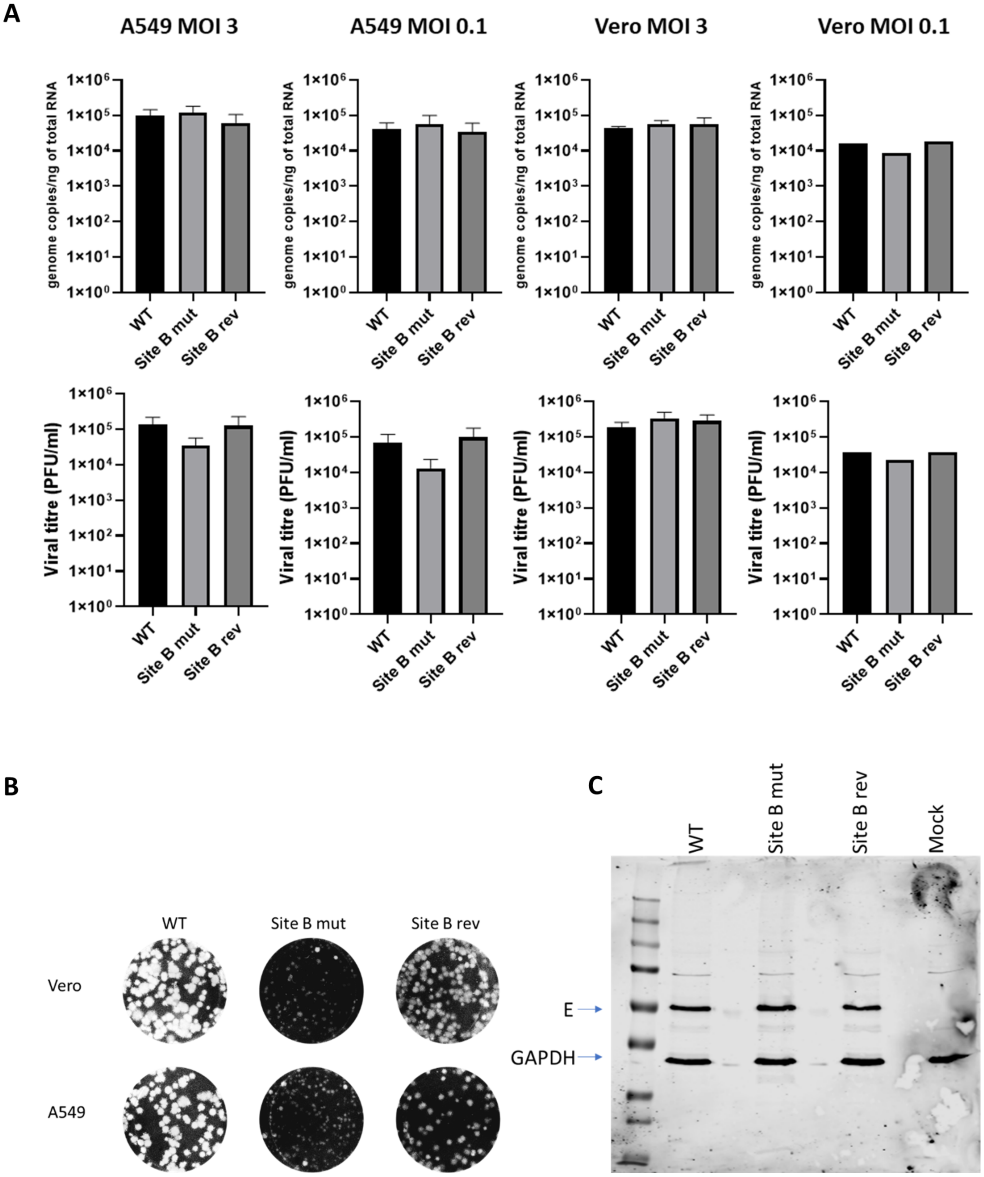

Figure 5.5: Analysis of viral replication, virion production and translation of the Site B mutant, Site B revertant and WT. (A) Replication of WT, Site B mut and Site B rev in A549 and Vero cells. Total RNA was isolated from cells by trizol extraction and viral RNA assessed by RT-qPCR. Viral titres are also shown, determined following titration of supernatants onto Vero cells. Repeat titrations were carried out by Taissa Ricciardi. For A549 MOI 3 n=3, A549 MOI 0.1 n=2, Vero MOI 3 and Vero MOI 0.1 n=1. *$p<0.05$, determined by student t test. (B) Representative plaque assays for Site B rev, Site B mut and WT, highlighting plaque phenotypes. (C) Western blot for viral protein E and loading control GAPDH on viral lysates following infection of A549 cells with WT, Site B mut and Site B rev at MOI 0.1.

5.3 Discussion

The structure of the flavivirus 3′UTR plays an important role in the virus life-cycle, regulating the binding of host and viral proteins and promoting viral replication and translation [26, 27, 28, 29]. Specific structures within the 3′UTR, namely SLI and SLII in ZIKV, form complex structural conformations which have been shown to resist degradation by host enzymes, leading to the production of sfRNAs [40, 136]. The production of sfRNAs is thought to play many different roles in promoting viral infection, and therefore, it is not surprising that changes to the structure of the 3′UTR that subsequently disrupt sfRNA production adversely affect viral fitness [45]. This is the first time that the Site B mutation has been investigated in the context of ZIKV SLII, and thus the first time the specific effects of this mutation on sfRNA production have been investigated.

In the case of the Site B mutant, the fitness defects observed can likely be attributed to disruption of proper folding of xrRNA2 in the 3′UTR structure, and the subsequent detrimental impact on sfRNA production. The Site B mutation itself lies within the internal PK structure formed through an AG-UC interaction. Crystallisation studies of MVEV SLIV and ZIKV SLI have revealed that this internal PK, in conjunction with the second PK structure, supports the formation of the P1-P2-P3 three-way junction which is integral to sfRNA production (Figure 5.2) [40, 41]. In particular, the G-C interaction of the internal PK is essential for the stability of the three-way junction, accordingly, the Site B rev virus only reverted at this particular residue. This restored the 3′UTR to the WT structure, supporting that a single nucleotide mutation was enough to disrupt proper folding (Figure 5.3) [40, 41]. As expected, the Site B mutation disrupted sfRNA production which was partially rescued in the Site B rev virus, although sfRNA levels were still lower than WT (Figure 5.4). This indicates that despite restoration of the WT 3′UTR structure, the single nucleotide reversion is not enough to restore WT levels of sfRNA production. Certainly, the Site B rev virus still contains a mutation of the A2 nucleotide that alongside G3 base pairs within the PK structure [40, 41]. Repeat northern blotting experiments are required, although this is comparable to previous findings for ZIKV SLI, whereby mutation of the residue proceeding G3 marginally reduces XRN1 resistance from 93% for the WT sequence to 80% for the mutant [40]. It is therefore likely that the A-U pairing in SLII has a small stabilizing effect on the internal PK, although the C-G base pairing is central to PK formation. This reaffirms a similar structural organization of ZIKV SLI and SLII despite sequence

differences.

The pattern of sfRNA production for WT ZIKV matched what has been observed previously, whereby mainly sfRNA1 and sfRNA2 are produced and a small amount of sfRNA3, coinciding with stalling of RNA degradation at SL1, SL2 and the pseudo DB structure respectively (Figure 5.4) [136, 148]. Although, more recent work indicates that sfRNA3 production may actually be the result of 3′ degradation of sfRNA [42]. A probe against the DB was able to detect the production of three sfRNAs, whereas a probe against the 3′SL only detected sfRNA1 and sfRNA2, indicating the 3′SL structure was absent from sfRNA3 [42]. In addition to sfRNA3, the production of a fourth sfRNA species has been observed for DENV, although this was not observed for ZIKV [135]. As previously observed in mammalian cells, there is a clear band below sfRNA2 which may be the result of cleavage of a larger RNA species or stalling of host ribonucleases elsewhere [40]. It would be interesting to sequence this additional product and elucidate whether it plays any role in the flaviviral life cycle. As has been previously shown for ZIKV, disruption of xrRNA2 led to complete loss of sfRNA2 and almost complete loss of sfRNA1 production, indicating cooperation between xrRNA1 and 2 in sfRNA generation [136, 148]. This coupling of xrRNA1 and 2 has also been observed in WNV and DENV2, whereby disruption of sfRNA2 led to a reduction in sfRNA1 production [41, 135]. However, SHAPE modelling of the Site B mut showed no effects on formation of the PK at SLI, despite the disruption to PK2.

The production of different sfRNA patterns has been linked to switching between different hosts during infection. Flaviviruses must replicate within both mosquitoes and humans, and thus, need to adapt to very different host environments. For DENV, deletion and accumulation of mutations in xrRNA2 has been linked to adaption to a mosquito host by switching the pattern of sfRNA production [31, 32, 135]. Previous work has shown that the ZIKV and DENV SL structures appear to be inverted in terms of position within the 3′UTR. Additionally, in ZIKV the disruption of xrRNA1 leads to accumulation of sfRNA2. It is therefore tempting to postulate that ZIKV SLI is accumulating mutations/deletions which allows adaption to a new host environment, in a similar manner to DENV SLII [136, 148]. This is further supported by work demonstrating that sfRNA2 was particularly important for ZIKV in the context of mosquito infection. An sfRNA2 deficient virus was defective in crossing the midgut barrier and did not reach the saliva, highlighting the importance of sfRNA2 for viral transmission [136, 148]. However, it has also been suggested that it is deletion of an inhibitory sequence in SLI that leads to the observed enhance-

ment in replication, and not a change in sfRNA pattern [136]. This is supported by the finding that the introduction of mutations to disrupt PK folding at SLI did not enhance replication in mosquito cells but deletion of SLI did [136]. Although, it must be considered, that deletion of the full SLI structure disrupts protein interactions which may also promote viral fitness, particularly if these proteins elicit antiviral effects. Previous work has also linked the production of ZIKV sfRNAs to anti-apoptotic effects in mosquitoes, whereby a mutant defective in sfRNA2 production was shown to stimulate increased levels of the pro-apoptotic enzyme caspase-7 [148]. Furthermore, enhanced expression of caspase-7 and subsequent increase in apoptosis in *Ae. aegypti* mosquitoes has been linked to anti-viral activity against DENV [249]. Therefore, a ZIKV mutant defective in sfRNA2 may trigger a stronger anti-viral response in mosquitoes. It would be interesting to infect mosquito cells with the Site B mutant and Site B revertant to further analyse the effects on viral replication in relation to the sfRNA pattern produced. The mechanism by which ZIKV modulates its sfRNAs and adaption to new host environments is still unknown and requires further investigation.

Interestingly as has been seen before for ZIKV, disruption of xrRNA2 also abrogated sfRNA3 production (Figure 5.4) [136, 40]. This is unlike what has been seen for WNV, whereby infection of HEK-293T cells with a WNV mutant defective in sfRNA2 or sfRNA1/2 increased sfRNA3 [134]. Similarly, for DENV, mutations and deletions in xrRNA2 and subsequent loss of sfRNA2 lead to the production of sfRNA3 and sfRNA4 [135]. As previously discussed, it is still unknown how ZIKV modulates the production of different sfRNA patterns. Furthermore, previous work investigating the higher- order structural organisation of the flavivirus 3′UTR highlighted clear differences as well as similarities. Most notably in relation to sfRNA3, the DBs of ZIKV and WNV have been demonstrated to be compact due to PK3 and PK4 interactions and therefore coupled, whereas the DBs of DENV are extended, indicating that the DENV DBS may function independently from each other [30]. Perhaps in the case of ZIKV, xrRNA2 and xrRNA3 structures are also functionally coupled. This is further evidenced by the fact that disruption of SLI and subsequent increase in sfRNA2 coincides with an increase in sfRNA3 in mosquito cells/mosquitoes [148, 136].

The introduction of mutations designed to disrupt PK formation at the ZIKV DB structure has been shown to hamper ZIKV replication which may be explained by a reduction in sfRNA3 production, or could also be due to a disruption in protein binding [30]. Many different host proteins which are important to the viral life

cycle bind to the flavivirus DB structures. For example, the RNA helicase DDX6 is known to bind to DB1 and DB2 of DENV-2, and knockdown of this protein hampered viral infection, leading to a reduction in viral RNA production and titre [247]. When investigating Site B mut utilising SHAPE, no detection in changes to the structure of the dumbbells was detected, however, it is well known that the flavivirus 3′UTR structure adopts different conformations throughout the course of infection. Long- range interactions occur between the 5′ and 3′UTRs promoting viral replication which could be disrupted if structural changes are introduced into the 3′UTRs [24, 16, 22, 250]. SHAPE on the 3′UTR RNA provides a snapshot of the general conformation of the 3′UTR, but does not capture dynamic conformations, and thus, it cannot be ruled out that other structural conformations important to the ZIKV life cycle have been disrupted. It is also possible to miss structural conformations of the RNA that are induced by protein binding. The importance of sfRNA3 to ZIKV infection remains unclear and hence further work is required, although due to the likely coupling of sfRNA production, this is difficult to study in isolation. It is interesting to note that sfRNA3 appears much less abundant in both mammalian and mosquito cell culture systems compared to mosquito infection [136, 148]. This indicates that it may play a more important role in the context of mosquito infection, coinciding with the fact that mutations leading to disruption of SL2, and thus subsequent disruption of sfRNA3 production, coincides with impaired mosquito infection and hence lower viral transmission [136, 148]. Again, infection of mosquito cells and mosquitoes with the Site B mutant would help to further investigate this hypothesis.

The reduction in fitness of the Site B mutant was not attributed to replication defects, as following infection of A549 and Vero cells, genome copy number was similar between WT, Site B mut and Site B rev (Figure 5.5A). Additionally, no difference in viral E protein levels was observed between WT, Site B and Site B rev, indicating that the fitness defect in the Site B mutant appears to be post-viral replication and translation (Figure 5.5C). The smaller plaque phenotype and the delayed observation of CPE in the Site B mutant may be explained by the potential link between sfRNA production and the induction of apoptosis and cytopathic effects (Figure 5.5B). Contrary to what has been seen in mosquitoes, previous work has shown that the production of sfRNA1 by both DENV and WNV is important for the induction of apoptosis and the ability of these viruses to form plaques, similar to what has been observed for the Site B mutant [153, 38, 148]. Furthermore, complementation of sfRNA1 deficient mutants with a plasmid encoding sfRNA rescued plaque formation [153, 38]. Flavivirus proteins actively induce apoptosis, indicating

that it likely plays some role in promoting viral infection. If this is the case, inhibition of apoptosis could also contribute to the fitness defects observed for the Site B mutant [45].

Interestingly, there was a trend towards a reduction in viral titre for the Site B mutant in A549 cells that was not observed in Vero cells. The lack of statistical significance for this trend may be explained by the fact that the Site B reversion occurred rapidly and was already apparent at passage 2. Although P0 stocks of Site B mut were used to conduct infections, by the time titrations were carried out the virus has already been passaged twice, once during infection, and then again for titration. Accordingly, the appearance of larger plaques was observed for the Site B mutant, indicating that there was some revertant virus present in the viral population. To further investigate the Site B mut and Site B rev viruses, it would be worthwhile to utilise the reverse genetics system and transfect the FL viral RNA into cells, minimising the effects of a mixed viral population on the results. Although this trend was not significant, it supports the findings that the Site B mutatant is defective post replication and translation.

Nevertheless, it is interesting that although no obvious difference between the viruses was observed in IFN deficient Vero cells, a trend towards a higher ratio of genomes compared to productive virus was observed in A549 cells which do mount an IFN response to ZIKV infection [251, 252]. Previous work infecting A549 cells with a ZIKV mutant containing deletions of SLI and SLII indicated that this virus was unable to modulate the host IFN response as well as WT. This mutant virus, despite lower replication levels, induced similar or higher levels of MxA, OAS1 and IRF-7 mRNAs conducive to being unable to inhibit IFN signalling [136]. Further work measuring the immune response to the Site B mutant is required to confirm whether a lack of immune control is contributing to the loss of viral fitness observed for the Site B mutant.

Cumulatively these results indicate that the mutation of a single nucleotide at the base of SLII disrupts proper folding of xrRNA2, leading to impaired sfRNA production and thus reduced viral fitness in mammalian cells. It may be that the defective sfRNA production observed for the Site B mutant leads to an inhibition in apoptosis, as well as a reduced ability of the virus to modulate the host immune response during infection. Further research must provide greater understanding of the link between ZIKV sfRNAs and the modulation of host immune signalling. Additionally, follow up studies in mosquito cells/mosquitoes will further our understanding on the

role of specific ZIKV sfRNAs in switching between mammalian vs mosquito hosts, and the mechanism by which ZIKV induces this switch without hampering viral fitness.

Chapter 6

Conclusions and future work

The main aim of this study was to further elucidate MSI1 enhancement of ZIKV replication, and in doing so investigate the overall importance of the ZIKV 3′UTR to viral fitness. Understanding how the host and virus interact is imperative to understanding the pathology caused by infection. For MSI1, expression in NPCs, as well as its links to enhanced ZIKV replication, indicated that this host protein may be involved in the neural pathology observed in infected neonates [178]. Due to these findings, MSI1 was the initial focus of this thesis.

In Chapter 3, different cells were screened for MSI1 expression to identify cell types useful for studying the effects of MSI1 on ZIKV replication. It was found that MSI1 expression is not stable in U251 human glioblastoma cells, and was unexpectedly expressed in high levels by HEK-293T cells, which were previously thought to be lacking MSI1. It was also demonstrated that A549 cells had very low levels of MSI1 and in Vero cells MSI1 was not detected. This provides useful information on suitable cell types for future studies investigating MSI1.

Reverse genetics was then used to mutate putative MSI1 binding sites in the ZIKV 3′UTR. Utilising U251 cells ± MSI1 highlighted that the mutation of Site D hampered viral replication in a MSI1 dependent manner, with a 2-fold reduction in viral replication observed for the Site D mutant compared to WT. This identifies that Site D is likely important for MSI1 binding, however, future work demonstrating the disruption of MSI1 binding will be carried out by pull down analysis. This mutant, therefore, may provide a highly useful tool for future investigations characterising the effects of MSI1 on ZIKV replication without relying on knockout or knockdown of MSI1. It would be interesting to test more biologically relevant systems, such as brain organoids or mouse models, to further investigate how significant a role MSI1 plays in ZIKV replication.

Mutating sites within the 3′UTR not only provided useful information about the

effects of MSI1 on ZIKV, but also provided useful information on the contribution of the ZIKV 3′UTR to overall viral fitness. MSI1 binding site mutations only consisted of a two nucleotide change, but in some cases drastically affected viral fitness. The 3′UTR provides sites for the binding of host and viral proteins, with specific sequences and RNA structures within the 3′UTR facilitating the switch from replication to translation of the viral genome [26, 27, 28, 29, 24, 224]. It is therefore imperative to screen viruses with 3′UTR mutations for the disruption of binding of off-target proteins as well as structural changes induced by mutation.

The Site E mutant proved to be highly detrimental to viral fitness and was only rescued following the detection of an additional mutation upstream from Site E in the 3′SL of the 3′UTR. Further work is required to characterise the importance of Site E to ZIKV fitness, including the use of reverse genetics to elucidate the role of the additional mutation in viral rescue. The disruption of binding of La autoantigen provides a plausible explanation. Previous work has demonstrated that the binding site of La autoantigen is within the 3′SL in DENV4, and in JEV binding occurs at a site within the 3′SL just proceeding the equivalent to Site E in the ZIKV 3′UTR [236, 237, 238, 239]. Furthermore, knockdown of this protein led to a 97% reduction in viral titres in JEV, which may explain why the Site E mutant virus was not viable [239]. To confirm this, future work will involve pull down analysis for testing protein binding to the ZIKV 3′UTR. This will allow investigation of whether La autoantigen binding has been disrupted by mutation of Site E, and facilitate future studies into the importance of La autoantigen to ZIKV fitness.

In Chapter 4, utilising an adapted structural cassette based on previous work by the Weeks lab, it was possible to SHAPE map the ZIKV 3′UTR [231, 232]. Unlike previous in vitro SHAPE mapping of the ZIKV 3′UTR, this allowed structural information to be obtained for the full 3′UTR structure, including the 3′SL structure. The developed method is reproducible and high throughput, providing a useful tool for the screening of ZIKV 3′UTR mutants. Furthermore, utilising this method not only allowed the visualisation of secondary RNA structures within the 3′UTR but also tertiary PK structures. This was particularly useful for demonstrating the disruption to PK folding caused by mutating Site B, the slight changes in structure caused by mutating Site C, and for demonstrating that no structural changes were introduced by mutating Site A, D or E. As this structural cassette has been shown to have no effect on the 3′UTR structure, it can also be utilised to add additional sequences to the 3′ end of the 3′UTR. Currently, a major restriction in using the ZIKV 3′UTR RNA as bait in a pull down is that modifications such as biotinylation

can affect RNA structure. To overcome this, 3′ end biotinylation can be used, but this is inefficient due to the highly structured 3′SL. Utilising this structural cassette it is possible to enhance biotinylation efficiency by the addition of an unstructured sequence, whilst having a minimal impact on RNA structure (Appendix). This method of enhanced labelling of the ZIKV 3′UTR will be used for future pull down analysis and mass spectrometry to investigate whether any of the site mutations affected the protein binding profile of ZIKV.

In Chapter 3, the Site B mutation was shown to be detrimental to viral fitness, leading to delayed viral rescue and a smaller plaque phenotype. Passage experiments demonstrated that the Site B mutant reverted at a single nucleotide, highlighting that this nucleotide was particularly important for viral fitness. In Chapter 4, SHAPE mapping revealed that the Site B mutation disrupted the three-way junction, which was imperative for PK2 folding and was likely responsible for the observed negative effects on viral fitness. Reversion at one nucleotide not only rescued the PK2 structure, but also viral fitness, and highlighted the importance of maintenance of the structural organisation of the ZIKV 3′UTR (Chapter 5). Indeed, previous work has shown that tertiary structures within the 3′UTR are important for xrRNA resistance to degradation, and thus, sfRNA production [136, 41, 40, 134]. Correspondingly, the Site B mutant was shown to be defective in sfRNA production. Due to the links between sfRNA production and the induction of apoptosis in mammalian cells, this disruption in sfRNA production could explain the smaller plaque type observed for the Site B mutant. The trend of increased genome copy number to virions produced in IFN competent cells also indicated that replication of Site B was not hampered and that disruption was at a later stage in the viral life cycle. As this trend was not observed in Vero cells lacking IFN, it is proposed that the Site B mutant was unable to modulate host immune signalling. This supports previous work showing that ZIKV sfRNA inhibits RIG-I or MDA-5 induction of IFN-beta production, as well as work demonstrating that the replicative defects of an sfRNA deficient WNV mutant compared to WT WNV were only displayed in cells that could mount a type I IFN response [139, 150]. Further work characterising the host immune response to the Site B mut vs the Site B rev and WT virus will further elucidate this. The rapid reversion of the Site B virus, and thus, the presence of WT virions, likely diluted out some of the effects of this mutation. To minimise the effects of a mixed viral population on the results, future work will involve the transfection of the Site B mut and Site B rev FL RNA into cells. Furthermore, studies with sfRNA defective ZIKV mutants in mosquito cells/mosquitoes would also prove interesting and provide insights into the role of specific ZIKV sfRNAs in the switch

between replicating in a mammalian vs mosquito host.

Despite an increased focus on ZIKV research following the 2015/2016 epidemic, and clear links to severe disease, including congenital microcephaly and Guillain Barre syndrome, the mechanisms underpinning these severe pathologies are yet to be fully understood. It is also worthwhile highlighting that ZIKV still poses a huge threat globally, with the potential for worldwide ZIKV spread enhanced by climate change, urbanisation, and international travel. The main methods for ZIKV control are still control of vector populations which have proven difficult to implement due to socio-economic factors. Continued research into viral-host interactions and factors important for viral fitness are imperative for obtaining a better understanding of ZIKV induced pathologies, in addition to the development of antivirals and vaccines to combat ZIKV infection.

Bibliography

[1] P. Simmonds, P. Becher, J. Bukh, E. A. Gould, G. Meyers, T. Monath, S. Muerhoff, A. Pletnev, R. Rico-Hesse, D. B. Smith, and J. T. Stapleton, "ICTV virus taxonomy profile: Flaviviridae," *Journal of General Virology*, vol. 98, no. 1, pp. 2–3, 2017.

[2] ICTV, "ICTV, Virus Taxonomy: 2020 release," 2020. Obtained from the world wide web on 25/09/21: `https://talk.ictvonline.org/ictv-reports/ictv_online_report/positive-sense-rna-viruses/w/flaviviridae/360/genus-flavivirus`.

[3] G. Kuno, G. J. J. Chang, R. Tsuchiya, N. Karabatsos, and B. Cropp, "Phylogeny of the Genus Flavivirus," *Journal of virology*, vol. 72, no. 1, pp. 73–83, 1998.

[4] S. Cook and E. C. Holmes, "A multigene analysis of the phylogenetic relationships among the flaviviruses (Family: Flaviviridae) and the evolution of vector transmission," *Archives of Virology*, vol. 151, no. 2, pp. 309–325, 2006.

[5] B. J. Blitvich and A. E. Firth, "A review of flaviviruses that have no known arthropod vector," *Viruses*, vol. 9, no. 6, pp. 1–25, 2017.

[6] Y. J. S. Huang, S. Higgs, K. M. E. Horne, and D. L. Vanlandingham, "Flavivirus-Mosquito interactions," *Viruses*, vol. 6, no. 11, pp. 4703–4730, 2014.

[7] T. C. Pierson and M. S. Diamond, "The continued threat of emerging flaviviruses," *Nature Microbiology*, vol. 5, no. 6, pp. 796–812, 2020.

[8] S. I. Bhatt, Samir ; W. Gething, Peter ; Brady, Oliver J. ; Messina, Jane P. ; Farlow, Andrew W. ; Moyes, Catherine L. ; Drake, John M. ; Brownstein, John S. ; Hoen, Anne G. ; Sankoh, Osman ; Myers, Monica F. ; George, Dylan B. ; Jaenisch, Thomas ; Wint, G.R. W, "The global distribution and burden of dengue Samir," *Nature*, vol. 496, no. 7446, pp. 504–507, 2013.

[9] WHO, "Dengue and severe dengue," 2022. Obtained from the world wide web on 10/03/22: https://www.who.int/news-room/fact-sheets/detail/dengue-and-severe-dengue.

[10] WHO, "Detection and investigation of serious adverse events following yellow fever vaccination: Guidance from an informal consultation of experts, Geneva, Switzerland, 18-19 November 2008," 2008. Obtained from the world wide web on 10/03/22: https://www.who.int/publications/i/item/detection-and-investigation-of-serious-adverse-events\-following-yellow-fever-vaccination.

[11] N. Irigoyen, A. M. Dinan, L. W. Meredith, I. Goodfellow, I. Brierley, and A. E. Firth, "The translational landscape of Zika virus during infection of mammalian and insect cells," *bioRxiv*, 2017.

[12] C. Polacek, P. Friebe, and E. Harris, "Poly(A)-binding protein binds to the non-polyadenylated 3′ untranslated region of dengue virus and modulates translation efficiency," *Journal of General Virology*, vol. 90, no. 3, pp. 687–692, 2009.

[13] ViralZone, "Zika virus," 2021. Obtained from the world wide web on 25/09/21: https://viralzone.expasy.org/6756?outline=all_by_species.

[14] UniProt, "UbiProtKB Q32ZE1 (POLG ZIKV)," 2021. Obtained from the world wide web on 25/09/21: https://www.uniprot.org/uniprot/Q32ZE1.

[15] P. Li, Y. Wei, M. Mei, L. Tang, L. Sun, W. Huang, J. Zhou, C. Zou, S. Zhang, C. F. Qin, T. Jiang, J. Dai, X. Tan, and Q. C. Zhang, "Integrative Analysis of Zika Virus Genome RNA Structure Reveals Critical Determinants of Viral Infectivity," *Cell Host and Microbe*, vol. 24, no. 6, pp. 875–886.e5, 2018.

[16] C. V. Filomatori, M. F. Lodeiro, D. E. Alvarez, M. M. Samsa, L. Pietrasanta, and A. V. Gamarnik, "A 5′ RNA element promotes dengue virus RNA synthesis on a circular genome," *Genes and Development*, vol. 20, no. 16, pp. 2238–2249, 2006.

[17] H. Dong, D. Ray, S. Ren, B. Zhang, F. Puig-Basagoiti, Y. Takagi, C. K. Ho, H. Li, and P.-Y. Shi, "Distinct RNA Elements Confer Specificity to Flavivirus RNA Cap Methylation Events," *Journal of Virology*, vol. 81, no. 9, pp. 4412–4421, 2007.

[18] D. E. Alvarez, A. L. De Lella Ezcurra, S. Fucito, and A. V. Gamarnik, "Role of RNA structures present at the 3′UTR of dengue virus on translation, RNA synthesis, and viral replication," *Virology*, vol. 339, no. 2, pp. 200–212, 2005.

[19] D. E. Alvarez, M. F. Lodeiro, S. J. Ludueña, L. I. Pietrasanta, and A. V. Gamarnik, "Long-Range RNA-RNA Interactions Circularize the Dengue Virus Genome," *Journal of Virology*, vol. 79, no. 11, pp. 6631–6643, 2005.

[20] A. A. Khromykh, H. Meka, K. J. Guyatt, and E. G. Westaway, "Essential Role of Cyclization Sequences in Flavivirus RNA Replication," *Journal of Virology*, vol. 75, no. 14, pp. 6719–6728, 2001.

[21] P. Friebe and E. Harris, "Interplay of RNA Elements in the Dengue Virus 5′ and 3′ Ends Required for Viral RNA Replication," *Journal of Virology*, vol. 84, no. 12, pp. 6103–6118, 2010.

[22] C. V. Filomatori, N. G. Iglesias, S. M. Villordo, D. E. Alvarez, and A. V. Gamarnik, "RNA sequences and structures required for the recruitment and activity of the dengue virus polymerase," *Journal of Biological Chemistry*, vol. 286, no. 9, pp. 6929–6939, 2011.

[23] B. Zhang, H. Dong, D. A. Stein, P. L. Iversen, and P. Y. Shi, "West Nile virus genome cyclization and RNA replication require two pairs of long-distance RNA interactions," *Virology*, vol. 373, no. 1, pp. 1–13, 2008.

[24] T. J. Sanford, H. V. Mears, T. Fajardo, N. Locker, and T. R. Sweeney, "Circularization of flavivirus genomic RNA inhibits de novo translation initiation," *Nucleic acids research*, vol. 47, no. 18, pp. 9789–9802, 2019.

[25] X.-D. Li, C.-L. Deng, Z.-M. Yuan, H.-Q. Ye, and B. Zhang, "Different Degrees of 5′-to-3′ DAR Interactions Modulate Zika Virus Genome Cyclization and Host-Specific Replication," *Journal of Virology*, vol. 94, no. 5, 2020.

[26] W. Ng, S. Bradrick, R. Soto-Acosta, E. Ooi, and M. Garcia-Blanco, "The 5′ and 3′ Untranslated Regions of the Flaviviral Genome," *Viruses*, vol. 9, no. 6, p. 137, 2017.

[27] A. Fernandez-Sanles, P. Rios-Marco, C. Romero-Lopez, and A. Berzal-Herranz, "Functional information stored in the conserved structural RNA domains of flavivirus genomes," *Frontiers in Microbiology*, vol. 8, pp. 1–16, 2017.

[28] M. A. Brinton and M. Basu, "Functions of the 3′ and 5′ genome RNA regions of members of the genus Flavivirus," *Virus Research*, vol. 206, pp. 108–119, 2015.

[29] J. A. Roby, G. P. Pijlman, J. Wilusz, and A. A. Khromykh, "Noncoding subgenomic flavivirus RNA: Multiple functions in West Nile virus pathogenesis and modulation of host responses," *Viruses*, vol. 6, no. 2, pp. 404–427, 2014.

[30] Y. Zhang, Y. Zhang, Z.-Y. Liu, M.-L. Cheng, J. Ma, Y. Wang, C.-F. Qin, and X. Fang, "Long non-coding subgenomic flavivirus RNAs have extended 3D structures and are flexible in solution," *EMBO reports*, vol. 20, no. 11, pp. 1–20, 2019.

[31] S. M. Villordo, C. V. Filomatori, I. Sanchez-Vargas, C. D. Blair, and A. V. Gamarnik, "Dengue Virus RNA Structure Specialization Facilitates Host Adaptation," *PLoS Pathogens*, vol. 11, no. 1, pp. 1–22, 2015.

[32] J. S. Kieft, J. L. Rabe, and E. G. Chapman, "RNA : Conservation , folding , and host adaptation," *RNA Biology*, vol. 12, no. 11, pp. 1169–1177, 2015.

[33] G. P. Göertz, S. R. Abbo, J. J. Fros, and G. P. Pijlman, "Functional RNA during Zika virus infection," *Virus Research*, vol. 254, no. July 2017, pp. 41–53, 2018.

[34] A. A. Khromykh, N. Kondratieva, J.-Y. Sgro, A. Palmenberg, and E. G. Westaway, "Significance in Replication of the Terminal Nucleotides of the Flavivirus Genome," *Journal of Virology*, vol. 77, no. 19, pp. 10623–10629, 2003.

[35] S. Elghonemy, W. G. Davis, and M. A. Brinton, "The majority of the nucleotides in the top loop of the genomic 3′ terminal stem loop structure are cis-acting in a West Nile virus infectious clone," *Virology*, vol. 331, no. 2, pp. 238–246, 2005.

[36] P. A. Silva, R. Molenkamp, T. J. Dalebout, N. Charlier, J. H. Neyts, W. J. Spaan, and P. J. Bredenbeek, "Conservation of the pentanucleotide motif at the top of the yellow fever virus 17D 3′ stem-loop structure is not required for replication," *Journal of General Virology*, vol. 88, no. 6, pp. 1738–1747, 2007.

[37] M. Tilgner, T. S. Deas, and P. Y. Shi, "The flavivirus-conserved pentanucleotide in the 3′ stem-loop of the West Nile virus genome requires a specific sequence and structure for RNA synthesis, but not for viral translation," *Virology*, vol. 331, no. 2, pp. 375–386, 2005.

[38] G. P. Pijlman, A. Funk, N. Kondratieva, J. Leung, S. Torres, L. van der Aa, W. J. Liu, A. C. Palmenberg, P. Y. Shi, R. A. Hall, and A. A. Khromykh, "A Highly Structured, Nuclease-Resistant, Noncoding RNA Produced by Flaviviruses Is Required for Pathogenicity," *Cell Host and Microbe*, vol. 4, no. 6, pp. 579–591, 2008.

[39] R. C. Olsthoorn and J. F. Bol, "Sequence comparison and secondary structure analysis of the 3′ noncoding region of flavivirus genomes reveals multiple pseudoknots," *Rna*, vol. 7, no. 10, pp. 1370–1377, 2001.

[40] B. M. Akiyama, H. M. Laurence, A. R. Massey, D. A. Costantino, X. Xie, Y. Yang, P. Y. Shi, J. C. Nix, J. D. Beckham, and J. S. Kieft, "Zika virus produces noncoding RNAs using a multi-pseudoknot structure that confounds a cellular exonuclease," *Science*, vol. 354, no. 6316, pp. 1148–1152, 2016.

[41] E. G. Chapman, D. A. Costantino, J. L. Rabe, S. L. Moon, J. Wilusz, J. C. Nix, and J. S. Kieft, "The structural basis of pathogenic subgenomic flavivirus RNA (sfRNA) production," *Science*, vol. 344, no. 6181, pp. 307–310, 2014.

[42] B. M. Akiyama, M. E. Graham, Z. O′donoghue, J. D. Beckham, and J. S. Kieft, "Three-dimensional structure of a flavivirus dumbbell RNA reveals molecular details of an RNA regulator of replication," *Nucleic Acids Research*, vol. 49, no. 12, pp. 7122–7138, 2021.

[43] I. Brierley, S. Pennell, and R. J. Gilbert, "Viral RNA pseudoknots: Versatile motifs in gene expression and replication," *Nature Reviews Microbiology*, vol. 5, no. 8, pp. 598–610, 2007.

[44] E. B. Melian, E. Hinzman, T. Nagasaki, A. E. Firth, N. M. Wills, A. S. Nouwens, B. J. Blitvich, J. Leung, A. Funk, J. F. Atkins, R. Hall, and A. A. Khromykh, "NS1′ of Flaviviruses in the Japanese Encephalitis Virus Serogroup Is a Product of Ribosomal Frameshifting and Plays a Role in Viral Neuroinvasiveness," *Journal of Virology*, vol. 84, no. 3, pp. 1641–1647, 2010.

[45] A. Slonchak and A. A. Khromykh, "Subgenomic flaviviral RNAs: What do we know after the first decade of research," *Antiviral Research*, vol. 159, no. September, pp. 13–25, 2018.

[46] J. J. H. Chu and M. L. Ng, "Interaction of West Nile virus with $\alpha v\beta 3$ integrin mediates virus entry into cells," *Journal of Biological Chemistry*, vol. 279, no. 52, pp. 54533–54541, 2004.

[47] C. W. Davis, H.-Y. Nguyen, S. L. Hanna, M. D. Sanchez, R. W. Doms, and T. C. Pierson, "West Nile Virus Discriminates between DC-SIGN and DC-SIGNR for Cellular Attachment and Infection," *Journal of Virology*, vol. 80, no. 3, pp. 1290–1301, 2006.

[48] S. T. Chen, R. S. Liu, M. F. Wu, Y. L. Lin, S. Y. Chen, D. T. W. Tan, T. Y. Chou, I. S. Tsai, L. Li, and S. L. Hsieh, "CLEC5A regulates Japanese encephalitis virus-induced neuroinflammation and lethality," *PLoS Pathogens*, vol. 8, no. 4, 2012.

[49] L. Meertens, X. Carnec, M. P. Lecoin, F. Guivel-benhassine, E. Lew, G. Lemke, O. Schwartz, and A. Amara, "The TIM and TAM Families of Phosphatidylserine Receptors," *Cell host & microbe*, vol. 12, no. 4, pp. 544–557, 2012.

[50] A. S. Richard, B. S. Shim, Y. C. Kwon, R. Zhang, Y. Otsuka, K. Schmitt, F. Berri, M. S. Diamond, and H. Choe, "AXL-dependent infection of human fetal endothelial cells distinguishes Zika virus from other pathogenic flaviviruses," *Proceedings of the National Academy of Sciences of the United States of America*, vol. 114, no. 8, pp. 2024–2029, 2017.

[51] J. Chen, Y. F. Yang, Y. Yang, P. Zou, J. Chen, Y. He, S. L. Shui, Y. R. Cui, R. Bai, Y. J. Liang, Y. Hu, B. Jiang, L. Lu, X. Zhang, J. Liu, and J. Xu, "AXL promotes Zika virus infection in astrocytes by antagonizing type i interferon signalling," *Nature Microbiology*, vol. 3, no. 3, pp. 302–309, 2018.

[52] R. Hamel, O. Dejarnac, S. Wichit, P. Ekchariyawat, A. Neyret, N. Luplertlop, M. Perera-Lecoin, P. Surasombatpattana, L. Talignani, F. Thomas, V.-M. Cao-Lormeau, V. Choumet, L. Briant, P. Desprès, A. Amara, H. Yssel, and D. Misse, "Biology of Zika Virus Infection in Human Skin Cells," *Journal of Virology*, vol. 89, no. 17, pp. 8880–8896, 2015.

[53] M. F. Wells, M. R. Salick, O. Wiskow, D. J. Ho, K. A. Worringer, R. J. Ihry, S. Kommineni, B. Bilican, J. R. Klim, E. J. Hill, L. T. Kane, C. Ye, A. Kaykas, and K. Eggan, "Genetic Ablation of AXL Does Not Protect Human Neural Progenitor Cells and Cerebral Organoids from Zika Virus Infection," *Cell Stem Cell*, vol. 19, no. 6, pp. 703–708, 2016.

[54] D. P. Strange, B. Jiyarom, N. P. Zarandi, X. Xie, C. Baker, H. Sadri-Ardekani, P.-Y. Shi, and S. Verma, "Axl Promotes Zika Virus Entry and Modulates the Antiviral," *American Society for Microbiology*, vol. 10, no. 4, pp. 1–16, 2019.

[55] A. K. Hastings, L. J. Yockey, B. W. Jagger, J. Hwang, R. Uraki, H. F. Gaitsch, L. A. Parnell, B. Cao, I. U. Mysorekar, C. V. Rothlin, E. Fikrig, M. S. Diamond, and A. Iwasaki, "TAM Receptors Are Not Required for Zika Virus Infection in Mice," *Cell Reports*, vol. 19, no. 3, pp. 558–568, 2017.

[56] D. Sirohi and R. J. Kuhn, "Zika Virus Structure, Maturation, and Receptors," *Journal of Infectious Diseases*, vol. 216, no. S10, pp. S935–S944, 2017.

[57] H. M. Van Der Schaar, M. J. Rust, Chen, H. Van Der Ende-Metselaar, J. Wilschut, X. Zhuang, and J. M. Smit, "Dissecting the cell entry pathway of dengue virus by single-particle tracking in living cells," *PLoS Pathogens*, vol. 4, no. 12, 2008.

[58] J. J. H. Chu and M. L. Ng, "Infectious Entry of West Nile Virus Occurs through a Clathrin-Mediated Endocytic Pathway," *Journal of Virology*, vol. 78, no. 19, pp. 10543–10555, 2004.

[59] Y. Modis, S. Ogata, D. Clements, and S. C. Harrison, "Structure of the dengue virus envelope protein after membrane fusion," *Nature*, vol. 427, no. 6972, pp. 313–319, 2004.

[60] S. Mukhopadhyay, R. J. Kuhn, and M. G. Rossmann, "A structural perspective of the Flavivirus life cycle," *Nature Reviews Microbiology*, vol. 3, no. 1, pp. 13–22, 2005.

[61] S. S. Bradrick, "Causes and consequences of flavivirus RNA methylation," *Frontiers in Microbiology*, vol. 8, no. DEC, pp. 1–6, 2017.

[62] Y. Zhou, D. Ray, Y. Zhao, H. Dong, S. Ren, Z. Li, Y. Guo, K. A. Bernard, P.-Y. Shi, and H. Li, "Structure and Function of Flavivirus NS5 Methyltransferase," *Journal of Virology*, vol. 81, no. 8, pp. 3891–3903, 2007.

[63] H. Dong, D. C. Chang, X. Xie, Y. X. Toh, K. Y. Chung, G. Zou, J. Lescar, S. P. Lim, and P. Y. Shi, "Biochemical and genetic characterization of dengue virus methyltransferase," *Virology*, vol. 405, no. 2, pp. 568–578, 2010.

[64] A. Niedzwiecka, J. Marcotrigiano, J. Stepinski, M. Jankowska-Anyszka, A. Wyslouch-Cieszynska, M. Dadlez, A. C. Gingras, P. Mak, E. Darzynkiewicz, N. Sonenberg, S. K. Burley, and R. Stolarski, "Biophysical studies of eIF4E cap-binding protein: Recognition of mRNA 5′ cap structure and synthetic fragments of eIF4G and 4E-BP1 proteins," *Journal of Molecular Biology*, vol. 319, no. 3, pp. 615–635, 2002.

[65] M. A. Garcia-Blanco, S. G. Vasudevan, S. S. Bradrick, and C. Nicchitta, "Flavivirus RNA transactions from viral entry to genome replication," *Antiviral Research*, vol. 134, pp. 244–249, 2016.

[66] S. Daffis, K. J. Szretter, J. Schriewer, J. Li, S. Youn, J. Errett, T. Y. Lin, S. Schneller, R. Zust, H. Dong, V. Thiel, G. C. Sen, V. Fensterl, W. B. Klimstra, T. C. Pierson, R. M. Buller, M. Gale Jr, P. Y. Shi, and M. S. Diamond, "2′-O methylation of the viral mRNA cap evades host restriction by IFIT family members," *Nature*, vol. 468, no. 7322, pp. 452–456, 2010.

[67] S. L. Cumberworth, J. J. Clark, A. Kohl, and C. L. Donald, "Inhibition of type I interferon induction and signalling by mosquito-borne flaviviruses," *Cellular Microbiology*, vol. 19, no. 5, 2017.

[68] H. Roth, V. Magg, F. Uch, P. Mutz, P. Klein, K. Haneke, V. Lohmann, R. Bartenschlager, O. T. Fackler, N. Locker, G. Stoecklin, and A. Ruggieri, "Flavivirus infection uncouples translation suppression from cellular stress responses," *mBio*, vol. 8, no. 1, pp. 1–18, 2017.

[69] D. Edgil, C. Polacek, and E. Harris, "Dengue Virus Utilizes a Novel Strategy for Translation Initiation When Cap-Dependent Translation Is Inhibited," *Journal of Virology*, vol. 80, no. 6, pp. 2976–2986, 2006.

[70] Y. Song, J. Mugavero, and C. B. Stauft, "Dengue and Zika Virus 5′ Untranslated Regions Harbor Internal Ribosomal Entry Site Functions," *mBio*, vol. 10, no. 2, pp. 1–16, 2019.

[71] Z. A. Jaafar and J. S. Kieft, "Viral RNA structure-based strategies to manipulate translation," *Nature Reviews Microbiology*, vol. 17, no. 2, pp. 110–123, 2019.

[72] Y. Arhab, A. G. Bulakhov, T. V. Pestova, and C. U. Hellen, "Dissemination of internal ribosomal entry sites (IRES) between viruses by horizontal gene transfer," *Viruses*, vol. 12, no. 6, pp. 1–29, 2020.

[73] P. Kumar, T. R. Sweeney, M. A. Skabkin, O. V. Skabkina, C. U. Hellen, and T. V. Pestova, "Inhibition of translation by IFIT family members is determined by their ability to interact selectively with the 5′-terminal regions of cap0-, cap1- and 5′ppp- mRNAs," *Nucleic Acids Research*, vol. 42, no. 5, pp. 3228–3245, 2014.

[74] Y. Ci and L. Shi, "Compartmentalized replication organelle of flavivirus at the ER and the factors involved," *Cellular and Molecular Life Sciences*, vol. 78, no. 11, pp. 4939–4954, 2021.

[75] F. Weber, V. Wagner, S. B. Rasmussen, R. Hartmann, and S. R. Paludan, "Double-Stranded RNA Is Produced by Positive-Strand RNA Viruses and DNA Viruses but Not in Detectable Amounts by Negative-Strand RNA Viruses," *Journal of Virology*, vol. 80, no. 10, pp. 5059–5064, 2006.

[76] M. Issur, B. J. Geiss, I. Bougie, F. Picard-Jean, S. Despins, J. Mayette, S. E. Hobdey, and M. Bisaillon, "The flavivirus NS5 protein is a true RNA guanylyltransferase that catalyzes a two-step reaction to form the RNA cap structure," *Rna*, vol. 15, no. 12, pp. 2340–2350, 2009.

[77] G. Bartelma and R. Padmanabhan, "Expression, purification, and characterization of the RNA 5′-triphosphatase activity of dengue virus type 2 nonstructural protein 3," *Virology*, vol. 299, no. 1, pp. 122–132, 2002.

[78] M. P. Egloff, D. Benarroch, B. Selisko, J. L. Romette, and B. Canard, "An RNA cap (nucleoside-2′-O-)-methyltransferase in the flavivirus RNA polymerase NS5: Crystal structure and functional characterization," *EMBO Journal*, vol. 21, no. 11, pp. 2757–2768, 2002.

[79] J. Junjhon, J. G. Pennington, T. J. Edwards, R. Perera, J. Lanman, and R. J. Kuhn, "Ultrastructural Characterization and Three-Dimensional Architecture of Replication Sites in Dengue Virus-Infected Mosquito Cells," *Journal of Virology*, vol. 88, no. 9, pp. 4687–4697, 2014.

[80] S. Welsch, S. Miller, I. Romero-Brey, A. Merz, C. K. Bleck, P. Walther, S. D. Fuller, C. Antony, J. Krijnse-Locker, and R. Bartenschlager, "Composition and Three-Dimensional Architecture of the Dengue Virus Replication and Assembly Sites," *Cell Host and Microbe*, vol. 5, no. 4, pp. 365–375, 2009.

[81] I. M. Yu, W. Zhang, H. A. Holdaway, L. Li, V. A. Kostyuchenko, P. R. Chipman, R. J. Kuhn, M. G. Rossmann, and J. Chen, "Structure of the immature dengue virus at low pH primes proteolytic maturation," *Science*, vol. 319, no. 5871, pp. 1834–1837, 2008.

[82] F. X. Heinz and K. Stiasny, "The Antigenic Structure of Zika Virus and Its Relation to Other Flaviviruses: Implications for Infection and Immunoprophylaxis," *Microbiology and Molecular Biology Reviews*, vol. 81, no. 1, pp. 1–27, 2017.

[83] D. Sirohi, Z. Chen, L. Sun, T. Klose, T. C. Pierson, M. G. Rossmann, and R. J. Kuhn, "The 3.8Å resolution cryo-EM structure of Zika Virus," *Science*, vol. 352, no. 6282, pp. 467–470, 2016.

[84] V. A. Kostyuchenko, E. X. Lim, S. Zhang, G. Fibriansah, T. S. Ng, J. S. Ooi, J. Shi, and S. M. Lok, "Structure of the thermally stable Zika virus," *Nature*, vol. 533, no. 7603, pp. 425–428, 2016.

[85] T. Y. Tan, G. Fibriansah, V. A. Kostyuchenko, T. S. Ng, X. X. Lim, S. Zhang, X. N. Lim, J. Wang, J. Shi, M. C. Morais, D. Corti, and S. M. Lok, "Capsid protein structure in Zika virus reveals the flavivirus assembly process," *Nature Communications*, vol. 11, no. 1, pp. 1–13, 2020.

[86] B. H. Song, S. I. Yun, M. Woolley, and Y. M. Lee, "Zika virus: History, epidemiology, transmission, and clinical presentation," *Journal of Neuroimmunology*, vol. 308, pp. 50–64, 2017.

[87] D. J. Gubler, N. Vasilakis, and D. Musso, "History and Emergence of Zika Virus," *Journal of Infectious Diseases*, vol. 216, no. Suppl 10, pp. S860–S867, 2017.

[88] A. Enfissi, J. Codrington, J. Roosblad, M. Kazanji, and D. Rousset, "Zika virus genome from the Americas," *The Lancet*, vol. 387, no. 10015, pp. 227–228, 2016.

[89] T. Wongsurawat, P. Jenjaroenpun, N. Athipanyasilp, B. Kaewnapan, N. Leelahakorn, N. Angkasekwinai, W. Kantakamalakul, R. Sutthent, D. W. Ussery, N. Horthongkham, and I. Nookaew, "Genome Sequences of Zika Virus Strains Recovered from Amniotic Fluid, Placenta, and Fetal Brain of a Microcephaly Patient in Thailand, 2017," *Microbiology Resource Announcements*, vol. 7, no. 11, 2018.

[90] P. T. Lan, L. C. Quang, V. T. Q. Huong, N. V. Thuong, P. C. Hung, T. T. L. N. Huong, H. P. Thao, N. T. T. Thao, A. W. Mounts, and L. D. Nolen, "Fetal Zika Virus Infection in Vietnam," *PLoS Currents*, no. July 2016, pp. 17–19, 2017.

[91] P. D. Yadav, B. Malhotra, G. Sapkal, D. A. Nyayanit, G. Deshpande, N. Gupta, U. T. Padinjaremattathil, H. Sharma, R. R. Sahay, P. Sharma, and D. T. Mourya, "Zika virus outbreak in Rajasthan, India in 2018 was caused by a virus endemic to Asia," *Infection, Genetics and Evolution*, vol. 69, no. January, pp. 199–202, 2019.

[92] WHO, "ZIKV EPIDEMIOLOGY UPDATE," 2019. Obtained from the world wide web on 30/09/21: `zika-epidemiology-update-july-2019.pdf(who.int)`.

[93] F. Anfasa, J. Siegers, M. van der Kroeg, N. Mumtaz, V. Stalin Raj, F. de Vrij, W. Widagdo, G. Gabriel, S. Salinas, Y. Simonin, C. Reusken, S. Kushner, M. Koopmans, B. Haagmans, B. Martina, and D. van Riel, "Phenotypic Differences between Asian and African Lineage Zika Viruses in Human Neural Progenitor Cells," *mSphere*, vol. 2, no. 4, pp. 1–10, 2017.

[94] E. Gabriel, A. Ramani, U. Karow, M. Gottardo, K. Natarajan, L. M. Gooi, G. Goranci-Buzhala, O. Krut, F. Peters, M. Nikolic, S. Kuivanen, E. Korhonen, T. Smura, O. Vapalahti, A. Papantonis, J. Schmidt-Chanasit, M. Riparbelli, G. Callaini, M. Krönke, O. Utermöhlen, and J. Gopalakrishnan, "Recent Zika Virus Isolates Induce Premature Differentiation of Neural Progenitors in Human Brain Organoids," *Cell Stem Cell*, vol. 20, no. 3, pp. 397–406.e5, 2017.

[95] Y. Simonin, F. Loustalot, C. Desmetz, V. Foulongne, O. Constant, C. Fournier-Wirth, F. Leon, J. P. Molès, A. Goubaud, J. M. Lemaitre, M. Maquart, I. Leparc-Goffart, L. Briant, N. Nagot, P. Van de Perre, and S. Salinas, "Zika Virus Strains Potentially Display Different Infectious Profiles in Human Neural Cells," *EBioMedicine*, vol. 12, pp. 161–169, 2016.

[96] F. T. Goodfellow, K. A. Willard, S. L. Stice, M. A. Brindley, X. Wu, and S. Scoville, "Strain-dependent consequences of zika virus infection and differential impact on neural development," *Viruses*, vol. 10, no. 10, 2018.

[97] D. R. Smith, T. R. Sprague, B. S. Hollidge, S. M. Valdez, S. L. Padilla, S. A. Bellanca, J. W. Golden, S. R. Coyne, D. A. Kulesh, L. J. Miller, A. D. Haddow, J. W. Koehler, G. D. Gromowski, R. G. Jarman, M. T. P. Alera, I. K. Yoon, R. Buathong, R. G. Lowen, C. D. Kane, T. D. Minogue, S. Bavari, R. B. Tesh, S. C. Weaver, K. J. Linthicum, M. L. Pitt, and F. Nasar, "African and asian zika virus isolates display phenotypic differences both in vitro and in vivo," *American Journal of Tropical Medicine and Hygiene*, vol. 98, no. 2, pp. 432–444, 2018.

[98] S. Tripathi, V. R. Balasubramaniam, J. A. Brown, I. Mena, A. Grant, S. V. Bardina, K. Maringer, M. C. Schwarz, A. M. Maestre, M. Sourisseau, R. A. Albrecht, F. Krammer, M. J. Evans, A. Fernandez-Sesma, J. K. Lim, and

A. Garcia-Sastre, "A novel Zika virus mouse model reveals strain specific differences in virus pathogenesis and host inflammatory immune responses," *PLoS Pathogens*, vol. 13, no. 3, pp. 1–19, 2017.

[99] A. S. Jaeger, R. A. Murrieta, L. R. Goren, C. M. Crooks, R. V. Moriarty, A. M. Weiler, S. Rybarczyk, M. R. Semler, C. Huffman, A. Mejia, H. A. Simmons, M. Fritsch, J. E. Osorio, J. C. Eickhoff, S. L. O′Connor, G. D. Ebel, T. C. Friedrich, and M. T. Aliota, "Zika viruses of African and Asian lineages cause fetal harm in a mouse model of vertical transmission," *PLoS Neglected Tropical Diseases*, vol. 13, no. 4, pp. 1–18, 2019.

[100] N. K. Duggal, J. M. Ritter, E. M. McDonald, H. Romo, F. Guirakhoo, B. S. Davis, G. J. J. Chang, and A. C. Brault, "Differential neurovirulence of African and Asian genotype Zika virus isolates in outbred immunocompetent mice," *American Journal of Tropical Medicine and Hygiene*, vol. 97, no. 5, pp. 1410–1417, 2017.

[101] Q. Shao, S. Herrlinger, Y.-N. Zhu, M. Yang, F. Goodfellow, S. L. Stice, X.-P. Qi, M. A. Brindley, and J.-F. Chen, "The African Zika virus MR-766 is more virulent and causes more severe brain damage than current Asian lineage and dengue virus," *Development (Cambridge, England)*, vol. 144, pp. 4114–4124, nov 2017.

[102] F. Aubry, S. Jacobs, M. Darmuzey, S. Lequime, L. Delang, A. Fontaine, N. Jupatanakul, E. F. Miot, S. Dabo, C. Manet, X. Montagutelli, A. Baidaliuk, F. Gambaro, E. Simon-Lorière, M. Gilsoul, C. M. Romero-Vivas, V. M. Cao-Lormeau, R. G. Jarman, C. T. Diagne, O. Faye, O. Faye, A. A. Sall, J. Neyts, L. Nguyen, S. J. Kaptein, and L. Lambrechts, "Recent African strains of Zika virus display higher transmissibility and fetal pathogenicity than Asian strains," *Nature Communications*, vol. 12, no. 1, pp. 1–14, 2021.

[103] M. A. Sheridan, V. Balaraman, D. J. Schust, T. Ezashi, R. Michael Roberts, and A. W. Franz, "African and Asian strains of Zika virus differ in their ability to infect and lyse primitive human placental trophoblast," *PLoS ONE*, vol. 13, no. 7, pp. 1–18, 2018.

[104] Z. Y. Liu, W. F. Shi, and C. F. Qin, "The evolution of Zika virus from Asia to the Americas," *Nature Reviews Microbiology*, vol. 17, no. 3, pp. 131–139, 2019.

[105] ECDC, "Aedes aegypti-Factsheet for experts," 2016a. Obtained from the world wide web on 30/09/21: https://www.ecdc.europa.eu/en/disease-vectors/facts/mosquito-factsheets/aedes-aegypti.

[106] ECDC, "Aedes albopictus- Factsheet for experts," 2016b. Obtained from the world wide web on 30/09/21: https://www.ecdc.europa.eu/en/disease-vectors/facts/mosquito-factsheets/aedes-albopictus.

[107] T. Chouin-Carneiro, A. Vega-Rua, M. Vazeille, A. Yebakima, R. Girod, D. Goindin, M. Dupont-Rouzeyrol, R. Lourenço-de Oliveira, and A. B. Failloux, "Differential Susceptibilities of Aedes aegypti and Aedes albopictus from the Americas to Zika Virus," *PLoS Neglected Tropical Diseases*, vol. 10, no. 3, pp. 1–11, 2016.

[108] L. R. Petersen, D. J. Jamieson, A. M. Powers, and M. A. Honein, "Zika Virus," *New England Journal of Medicine*, vol. 374, no. 16, pp. 1552–1563, 2016.

[109] E. B. Kauffman and L. D. Kramer, "Zika Virus Mosquito Vectors: Competence, Biology, and Vector Control," *Journal of Infectious Diseases*, vol. 216, no. Suppl 10, pp. S976–S990, 2017.

[110] A. A. Hoffmann, I. Iturbe-Ormaetxe, A. G. Callahan, B. L. Phillips, K. Billington, J. K. Axford, B. Montgomery, A. P. Turley, and S. L. O'Neill, "Stability of the wMel Wolbachia Infection following Invasion into Aedes aegypti Populations," *PLoS Neglected Tropical Diseases*, vol. 8, no. 9, 2014.

[111] C. H. Tan, P. S. J. Wong, M. I. Li, H. T. Yang, L. C. Ng, and S. L. O'Neill, "wMel limits zika and chikungunya virus infection in a Singapore Wolbachia-introgressed Ae. aegypti strain, wMel-Sg," *PLoS Neglected Tropical Diseases*, vol. 11, no. 5, pp. 1–10, 2017.

[112] CDC, "Microcephaly and Other Birth Defects," 2019. Obtained from the world wide web on 30/09/21: https://www.cdc.gov/zika/healtheffects/birth_defects.html.

[113] F. J. Carod-Artal, O. Wichmann, J. Farrar, and J. Gascon, "Neurological complications of dengue virus infection," *The Lancet Neurology*, vol. 12, no. 9, pp. 906–919, 2013.

[114] European Centre for Disease Prevention and Control, "Rapid risk assessment: Zika virus epidemic in the Americas: potential association with microcephaly and Guillain-Barré syndrome," Tech. Rep. December, 2015.

[115] J. Mlakar, M. Korva, N. Tul, M. Popovic, M. Poljšak-Prijatelj, J. Mraz, M. Kolenc, K. Resman Rus, T. Vesnaver Vipotnik, V. Fabjan Vodušek, A. Vizjak, J. Pizem, M. Petrovec, and T. Avsivc Zupanc, "Zika Virus Associated with Microcephaly," *New England Journal of Medicine*, vol. 374, no. 10, pp. 951–958, 2016.

[116] F. R. Cugola, I. R. Fernandes, F. B. Russo, B. C. Freitas, J. L. Dias, K. P. Guimaraes, C. Benazzato, N. Almeida, G. C. Pignatari, S. Romero, C. M. Polonio, C. Isabela, C. L. Freitas, W. N. Brandao, C. Rossato, D. G. Andrade, D. P. Faria, A. T. Garcez, C. A. Buchpigel, C. T. Braconi, E. Mendes, S. A. Amadou, P. M. de A.Zanotto, J. P. S. Peron, A. R. Muotri, and P. C. Beltrao-Braga, "The Brazilian Zika virus strain causes birth defects in experimental models," *Nature*, vol. 534, no. 7606, pp. 267–271, 2016.

[117] X. Qian, H. N. Nguyen, M. M. Song, C. Hadiono, S. C. Ogden, C. Hammack, B. Yao, G. R. Hamersky, F. Jacob, C. Zhong, K. J. Yoon, W. Jeang, L. Lin, Y. Li, J. Thakor, D. A. Berg, C. Zhang, E. Kang, M. Chickering, D. Nauen, C. Y. Ho, Z. Wen, K. M. Christian, P. Y. Shi, B. J. Maher, H. Wu, P. Jin, H. Tang, H. Song, and G. L. Ming, "Brain-Region-Specific Organoids Using Mini-bioreactors for Modeling ZIKV Exposure," *Cell*, vol. 165, no. 5, pp. 1238–1254, 2016.

[118] P. P. Garcez, E. C. Loiola, R. M. Da Costa, L. M. Higa, P. Trindade, R. Delvecchio, J. M. Nascimento, R. Brindeiro, A. Tanuri, and S. K. Rehen, "Zika virus: Zika virus impairs growth in human neurospheres and brain organoids," *Science*, vol. 352, no. 6287, pp. 816–818, 2016.

[119] J. Dang, S. K. Tiwari, G. Lichinchi, Y. Qin, V. S. Patil, A. M. Eroshkin, and T. M. Rana, "Zika Virus Depletes Neural Progenitors in Human Cerebral Organoids through Activation of the Innate Immune Receptor TLR3," *Cell Stem Cell*, vol. 19, no. 2, pp. 258–265, 2016.

[120] C. Li, D. Xu, Q. Ye, S. Hong, Y. Jiang, X. Liu, N. Zhang, L. Shi, C. Qin, and X. Zhiheng, "Zika Virus Disrupts Neural Progenitor Development and Leads to Microcephaly in Mice," *Cell Stem Cell*, vol. 19, no. 1, pp. 120–126, 2016.

[121] Q. Shao, S. Herrlinger, S. L. Yang, F. Lai, J. M. Moore, M. A. Brindley, and J. F. Chen, "Zika virus infection disrupts neurovascular development and results in postnatal microcephaly with brain damage," *Development (Cambridge)*, vol. 143, no. 22, pp. 4127–4136, 2016.

[122] H. Tang, C. Hammack, S. C. Ogden, Z. Wen, and X. Qian, "Zika Virus Infects Human Cortical Neural Precursors and Attenuates their Growth," *Cell Stem Cell*, vol. 18, no. 5, pp. 587–590, 2016.

[123] J. O. Rayner, R. Kalkeri, S. Goebel, Z. Cai, B. Green, S. Lin, B. Snyder, K. Hagelin, K. B. Walters, and F. Koide, "Comparative pathogenesis of Asian and African-lineage Zika virus in Indian rhesus macaque's and development of a non-human primate model suitable for the evaluation of new drugs and vaccines," *Viruses*, vol. 10, no. 5, 2018.

[124] F. Koide, S. Goebel, B. Snyder, K. B. Walters, A. Gast, K. Hagelin, R. Kalkeri, and J. Rayner, "Development of a zika virus infection model in cynomolgus macaques," *Frontiers in Microbiology*, vol. 7, no. DEC, pp. 1–8, 2016.

[125] Y. Simonin, D. van Riel, P. Van de Perre, B. Rockx, and S. Salinas, "Differential virulence between Asian and African lineages of Zika virus," *PLoS Neglected Tropical Diseases*, vol. 11, no. 9, pp. 1–8, 2017.

[126] N. Berthet, E. Nakouné, B. Kamgang, B. Selekon, S. Descorps-Declère, A. Gessain, J. C. Manuguerra, and M. Kazanji, "Molecular characterization of three zika flaviviruses obtained from sylvatic mosquitoes in the Central African Republic," *Vector-Borne and Zoonotic Diseases*, vol. 14, no. 12, pp. 862–865, 2014.

[127] O. Faye, C. C. Freire, A. Iamarino, O. Faye, J. V. C. de Oliveira, M. Diallo, P. M. Zanotto, and A. A. Sall, "Molecular Evolution of Zika Virus during Its Emergence in the 20th Century," *PLoS Neglected Tropical Diseases*, vol. 8, no. 1, 2014.

[128] D. Musso and D. J. Gubler, "City of New Orleans Zika Virus Plan," *Nature*, vol. 11, no. 1, pp. 10–20, 2016.

[129] A. D. Haddow, A. J. Schuh, C. Y. Yasuda, M. R. Kasper, V. Heang, R. Huy, H. Guzman, R. B. Tesh, and S. C. Weaver, "Genetic characterization of zika virus strains: Geographic expansion of the asian lineage," *PLoS Neglected Tropical Diseases*, vol. 6, no. 2, 2012.

[130] D. L. Carbaugh, R. S. Baric, and H. M. Lazear, "Envelope Protein Glycosylation Mediates Zika Virus Pathogenesis," *Journal of Virology*, vol. 93, no. 12, pp. 1–16, 2019.

[131] V. K. Nagarajan, C. I. Jones, S. F. Newbury, and P. J. Green, "XRN 5′ → 3′ exoribonucleases: Structure, mechanisms and functions," *Biochimica et Biophysica Acta*, vol. 1829, pp. 590–603, 2013.

[132] P. A. G. C. Silva, C. F. Pereira, T. J. Dalebout, W. J. M. Spaan, and P. J. Bredenbeek, "An RNA Pseudoknot Is Required for Production of Yellow Fever Virus Subgenomic RNA by the Host Nuclease XRN1," *Journal of Virology*, vol. 84, no. 21, pp. 11395–11406, 2010.

[133] A. Funk, K. Truong, T. Nagasaki, S. Torres, N. Floden, E. Balmori Melian, J. Edmonds, H. Dong, P.-Y. Shi, and A. A. Khromykh, "RNA Structures Required for Production of Subgenomic Flavivirus RNA," *Journal of Virology*, vol. 84, no. 21, pp. 11407–11417, 2010.

[134] E. G. Chapman, S. L. Moon, J. Wilusz, and J. S. Kieft, "RNA structures that resist degradation by Xrn1 produce a pathogenic dengue virus RNA," *eLife*, vol. 2014, no. 3, pp. 1–25, 2014.

[135] C. V. Filomatori, J. M. Carballeda, S. M. Villordo, S. Aguirre, H. M. Pallares, A. M. Maestre, I. Sanchez-Vargas, C. D. Blair, C. Fabri, M. A. Morales, A. Fernandez-Sesma, and A. V. Gamarnik, "Dengue virus genomic variation associated with mosquito adaptation defines the pattern of viral non-coding RNAs and fitness in human cells," *PLoS Pathogens*, vol. 13, no. 3, pp. 1–23, 2017.

[136] H. M. Pallares, G. S. Costa Navarro, S. M. Villordo, F. Merwaiss, L. de Borba, M. M. Gonzalez Lopez Ledesma, D. S. Ojeda, A. Henrion-Lacritick, M. A. Morales, C. Fabri, M. C. Saleh, and A. V. Gamarnik, "Zika Virus Subgenomic Flavivirus RNA Generation Requires Cooperativity between Duplicated RNA Structures That Are Essential for Productive Infection in Human Cells," *Journal of Virology*, vol. 94, no. 18, pp. 1–20, 2020.

[137] A. MacFadden, Z. Òdonoghue, P. A. Silva, E. G. Chapman, R. C. Olsthoorn, M. G. Sterken, G. P. Pijlman, P. J. Bredenbeek, and J. S. Kieft, "Mechanism and structural diversity of exoribonuclease-resistant RNA structures in flaviviral RNAs," *Nature Communications*, vol. 9, no. 1, pp. 1–11, 2018.

[138] R. Y. Chang, T. W. Hsu, Y. L. Chen, S. F. Liu, Y. J. Tsai, Y. T. Lin, Y. S. Chen, and Y. H. Fan, "Japanese encephalitis virus non-coding RNA inhibits activation of interferon by blocking nuclear translocation of interferon

regulatory factor 3," *Veterinary Microbiology*, vol. 166, no. 1-2, pp. 11–21, 2013.

[139] C. L. Donald, B. Brennan, S. L. Cumberworth, V. V. Rezelj, J. J. Clark, M. T. Cordeiro, R. Freitas de Oliveira Francca, L. J. Pena, G. S. Wilkie, A. Da Silva Filipe, C. Davis, J. Hughes, M. Varjak, M. Selinger, L. Zuvanov, A. M. Owsianka, A. H. Patel, J. McLauchlan, B. D. Lindenbach, G. Fall, A. A. Sall, R. Biek, J. Rehwinkel, E. Schnettler, and A. Kohl, "Full Genome Sequence and sfRNA Interferon Antagonist Activity of Zika Virus from Recife, Brazil," *PLoS Neglected Tropical Diseases*, vol. 10, no. 10, pp. 1–20, 2016.

[140] E. Schnettler, H. Tykalova, M. Watson, M. Sharma, M. G. Sterken, D. J. Obbard, S. H. Lewis, M. McFarlane, L. Bell-Sakyi, G. Barry, S. Weisheit, S. M. Best, R. J. Kuhn, G. P. Pijlman, M. E. Chase-Topping, E. A. Gould, L. Grubhoffer, J. K. Fazakerley, and A. Kohl, "Induction and suppression of tick cell antiviral RNAi responses by tick-borne flaviviruses," *Nucleic Acids Research*, vol. 42, no. 14, pp. 9436–9446, 2014.

[141] S. L. Moon, J. R. Anderson, Y. Kumagai, C. J. Wilusz, S. Akira, A. A. Khromykh, and J. Wilusz, "A noncoding RNA produced by arthropod-borne flaviviruses inhibits the cellular exoribonuclease XRN1 and alters host mRNA stability," *Rna*, vol. 18, no. 11, pp. 2029–2040, 2012.

[142] C. D. Blair, "Mosquito RNAi is the major innate immune pathway controlling arbovirus infection and transmission," *Future Microbiology*, vol. 6, no. 3, pp. 265–277, 2011.

[143] E. Schnettler, M. G. Sterken, J. Y. Leung, S. W. Metz, C. Geertsema, R. W. Goldbach, J. M. Vlak, A. Kohl, A. A. Khromykh, and G. P. Pijlman, "Noncoding Flavivirus RNA Displays RNA Interference Suppressor Activity in Insect and Mammalian Cells," *Journal of Virology*, vol. 86, no. 24, pp. 13486–13500, 2012.

[144] S. L. Moon, B. J. Dodd, D. E. Brackney, C. J. Wilusz, G. D. Ebel, and J. Wilusz, "Flavivirus sfRNA suppresses antiviral RNA interference in cultured cells and mosquitoes and directly interacts with the RNAi machinery," *Virology*, vol. 485, pp. 322–329, 2015.

[145] G. P. Göertz, J. W. van Bree, A. Hiralal, B. M. Fernhout, C. Steffens, S. Boeren, T. M. Visser, C. B. Vogels, S. R. Abbo, J. J. Fros, C. J. Koenraadt, M. M. van Oers, and G. P. Pijlman, "Subgenomic flavivirus RNA binds the

mosquito DEAD/H-box helicase ME31B and determines Zika virus transmission by Aedes aegypti," *Proceedings of the National Academy of Sciences of the United States of America*, vol. 116, no. 38, pp. 19136–19144, 2019.

[146] G. P. Göertz, J. J. Fros, P. Miesen, C. B. F. Vogels, M. L. van der Bent, C. Geertsema, C. J. M. Koenraadt, R. P. van Rij, M. M. van Oers, and G. P. Pijlman, "Noncoding Subgenomic Flavivirus RNA Is Processed by the Mosquito RNA Interference Machinery and Determines West Nile Virus Transmission by Culex pipiens Mosquitoes," *Journal of Virology*, vol. 90, no. 22, pp. 10145–10159, 2016.

[147] S. Wu, L. He, Y. Li, T. Wang, L. Feng, L. Jiang, P. Zhang, and X. Huang, "MiR-146a facilitates replication of dengue virus by dampening interferon induction by targeting TRAF6," *Journal of Infection*, vol. 67, no. 4, pp. 329–341, 2013.

[148] A. Slonchak, L. E. Hugo, M. E. Freney, S. Hall-Mendelin, A. A. Amarilla, F. J. Torres, Y. X. Setoh, N. Y. Peng, J. D. Sng, R. A. Hall, A. F. van den Hurk, G. J. Devine, and A. A. Khromykh, "Zika virus noncoding RNA suppresses apoptosis and is required for virus transmission by mosquitoes," *Nature Communications*, vol. 11, no. 1, pp. 1–14, 2020.

[149] R. E. Randall and S. Goodbourn, "Interferons and viruses: An interplay between induction, signalling, antiviral responses and virus countermeasures," *Journal of General Virology*, vol. 89, no. 1, pp. 1–47, 2008.

[150] A. Schuessler, A. Funk, H. M. Lazear, D. A. Cooper, S. Torres, S. Daffis, B. K. Jha, Y. Kumagai, O. Takeuchi, P. Hertzog, R. Silverman, S. Akira, D. J. Barton, M. S. Diamond, and A. A. Khromykh, "West Nile Virus Noncoding Subgenomic RNA Contributes to Viral Evasion of the Type I Interferon-Mediated Antiviral Response," *Journal of Virology*, vol. 86, no. 10, pp. 5708–5718, 2012.

[151] G. Manokaran, E. Finol, C. Wang, J. Gunaratne, J. Bahl, E. Z. Ong, H. C. Tan, O. M. Sessions, and A. M. Ward, "Dengue subgenomic RNA binds TRIM25 to inhibit interferon expression for epidemiological fitness," *Science*, vol. 350, no. 6257, pp. 217–221, 2015.

[152] K. Bidet, D. Dadlani, and M. A. Garcia-Blanco, "G3BP1, G3BP2 and CAPRIN1 Are Required for Translation of Interferon Stimulated mRNAs and Are Targeted by a Dengue Virus Non-coding RNA," *PLoS Pathogens*, vol. 10, no. 7, 2014.

[153] Y. Liu, H. Liu, J. Zou, B. Zhang, and Z. Yuan, "Dengue virus subgenomic RNA induces apoptosis through the Bcl-2-mediated PI3k/Akt signaling pathway," *Virology*, vol. 448, pp. 15–25, 2014.

[154] Y. Pan, A. Cheng, M. Wang, Z. Yin, and R. Jia, "The Dual Regulation of Apoptosis by Flavivirus," *Frontiers in Microbiology*, vol. 12, no. March, pp. 1–17, 2021.

[155] H. Sparks, B. Monogue, B. Akiyama, J. Kieft, and J. D. Beckham, "Disruption of Zika Virus xrRNA1-Dependent sfRNA1 Production Results in Tissue-Specific Attenuated Viral Replication," *Viruses*, vol. 12, 2020.

[156] M. Nakamura, H. Okano, J. A. Blendy, and C. Montell, "Musashi, a neural RNA-binding protein required for drosophila adult external sensory organ development," *Neuron*, vol. 13, no. 1, pp. 67–81, 1994.

[157] H. Okano, T. Imai, and M. Okabe, "Musashi: A translational regulator of cell fate," *Journal of Cell Science*, vol. 115, no. 7, pp. 1355–1359, 2002.

[158] S. I. Sakakibara, Y. Nakamura, H. Satoh, and H. Okano, "RNA-binding protein Musashi2: Developmentally regulated expression in neural precursor cells and subpopulations of neurons in mammalian CNS," *Journal of Neuroscience*, vol. 21, no. 20, pp. 8091–8107, 2001.

[159] N. Ruth Zearfoss, L. M. Deveau, C. C. Clingman, E. Schmidt, E. S. Johnson, F. Massi, and S. P. Ryder, "A conserved three-nucleotide core motif defines musashi RNA binding specificity," *Journal of Biological Chemistry*, vol. 289, no. 51, pp. 35530–35541, 2014.

[160] T. Nagata, R. Kanno, Y. Kurihara, S. Uesugi, T. Imai, S. ichi Sakakibara, H. Okano, and M. Katahira, "Structure, backbone dynamics and interactions with RNA of the C-terminal RNA-binding domain of a mouse neural RNA-binding protein, Musashi1," *Journal of Molecular Biology*, vol. 287, no. 2, pp. 315–330, 1999.

[161] Y. Miyanoiri, H. Kobayashi, T. Imai, M. Watanabe, T. Nagata, S. Uesugi, H. Okano, and M. Katahira, "Origin of Higher Affinity to RNA of the N-terminal RNA-binding Domain than That of the C-terminal One of a Mouse Neural Protein, Musashi1, as Revealed by Comparison of Their Structures, Modes of Interaction, Surface Electrostatic Potentials, and Backbone ," *Journal of Biological Chemistry*, vol. 278, no. 42, pp. 41309–41315, 2003.

[162] H. Kawahara, Y. Okada, T. Imai, A. Iwanami, P. S. Mischel, and H. Okano, "Musashi1 cooperates in abnormal cell lineage protein 28 (Lin28)-mediated let-7 family microRNA biogenesis in early neural differentiation," *Journal of Biological Chemistry*, vol. 286, no. 18, pp. 16121–16130, 2011.

[163] H. Kawahara, T. Imai, H. Imataka, M. Tsujimoto, K. Matsumoto, and H. Okano, "Neural RNA-binding protein Musashi1 inhibits translation initiation by competing with eIF4G for PABP," *Journal of Cell Biology*, vol. 181, no. 4, pp. 639–653, 2008.

[164] H. Y. Kwon, J. Bajaj, T. Ito, A. Blevins, J. Weeks, N. K. Lytle, C. S. Koechlein, D. Rizzieri, V. G. Oehler, R. Sasik, G. Hardiman, and T. Reya, "Tetraspanin 3 is Required for the Development and Propagation of Acute Myelogenous Leukemia Hyog," *Cell Stem Cell*, vol. 17, no. 2, pp. 152–164, 2016.

[165] S. M. Park, R. P. Deering, Y. Lu, P. Tivnan, S. Lianoglou, F. Al-Shahrour, B. L. Ebert, N. Hacohen, C. Leslie, G. Q. Daley, C. J. Lengner, and M. G. Kharas, "Musashi-2 controls cell fate, lineage bias, and TGF-β signaling in HSCs," *Journal of Experimental Medicine*, vol. 211, no. 1, pp. 71–87, 2014.

[166] R. de Sousa Abreu, P. C. Sanchez-Diaz, C. Vogel, S. C. Burns, D. Ko, T. L. Burton, D. T. Vo, S. Chennasamudaram, S. Y. Le, B. A. Shapiro, and L. O. Penalva, "Genomic analyses of Musashi1 downstream targets show a strong association with cancer-related processes," *Journal of Biological Chemistry*, vol. 284, no. 18, pp. 12125–12135, 2009.

[167] S. I. Sakakibara, T. Imai, K. Hamaguchi, M. Okabe, J. Aruga, K. Nakajima, D. Yasutomi, T. Nagata, Y. Kurihara, S. Uesugi, T. Miyata, M. Ogawa, K. Mikoshiba, and H. Okano, "Mouse-Musashi-1, a neural RNA-Binding protein highly enriched in the mammalian CNS stem cell," *Developmental Biology*, vol. 176, no. 2, pp. 230–242, 1996.

[168] S. ichi Sakakibara, Y. Nakamura, T. Yoshida, S. Shibata, M. Koike, H. Takano, S. Ueda, Y. Uchiyama, T. Noda, and H. Okano, "RNA-binding protein Musashi family: Roles for CNS stem cells and a subpopulation of ependymal cells revealed by targeted disruption and antisense ablation," *Proceedings of the National Academy of Sciences of the United States of America*, vol. 99, no. 23, pp. 15194–15199, 2002.

[169] T. Imai, A. Tokunaga, T. Yoshida, M. Hashimoto, K. Mikoshiba, G. Weinmaster, M. Nakafuku, and H. Okano, "The Neural RNA-Binding Protein Musashi1

Translationally Regulates Mammalian," *Society*, vol. 21, no. 12, pp. 3888–3900, 2001.

[170] E. P. Spana and C. Q. Doe, "Numb antagonizes Notch signaling to specify sibling neuron cell fates," *Neuron*, vol. 17, no. 1, pp. 21–26, 1996.

[171] C. Battelli, G. N. Nikopoulos, J. G. Mitchell, and J. M. Verdi, "The RNA-binding protein Musashi-1 regulates neural development through the translational repression of p21WAF-1," *Molecular and Cellular Neuroscience*, vol. 31, no. 1, pp. 85–96, 2006.

[172] D. T. Vo, D. Subramaniam, M. Remke, T. L. Burton, P. J. Uren, J. A. Gelfond, R. De Sousa Abreu, S. C. Burns, M. Qiao, U. Suresh, A. Korshunov, A. M. Dubuc, P. A. Northcott, A. D. Smith, S. M. Pfister, M. D. Taylor, S. C. Janga, S. Anant, C. Vogel, and L. O. Penalva, "The RNA-binding protein musashi1 affects medulloblastoma growth via a network of cancer-related genes and is an indicator of poor prognosis," *American Journal of Pathology*, vol. 181, no. 5, pp. 1762–1772, 2012.

[173] R. J. Byers, T. Currie, E. Tholouli, S. J. Rodig, and J. L. Kutok, "MSI2 protein expression predicts unfavorable outcome in acute myeloid leukemia," *Blood*, vol. 118, no. 10, pp. 2857–2867, 2011.

[174] T. Ito, H. Y. Kwon, B. Zimdahl, K. L. Congdon, J. Blum, W. E. Lento, C. Zhao, A. Lagoo, G. Gerrard, L. Foroni, H. Goh, S.-h. Kim, D.-w. Kim, C. Chuah, G. Vivian, J. P. Radich, C. T. Jordan, and T. Reya, "Regulation of myeloid leukemia by the cell fate determinant Musashi," *Nature*, vol. 466, no. 7307, pp. 765–768, 2010.

[175] A. Kahvejian, Y. V. Svitkin, R. Sukarieh, M. N. M'Boutchou, and N. Sonenberg, "Mammalian poly(A)-binding protein is a eukaryotic translation initiation factor, which acts via multiple mechanisms," *Genes and Development*, vol. 19, no. 1, pp. 104–113, 2005.

[176] C. Cragle and A. M. MacNicol, "Musashi protein-directed translational activation of target mRNAs is mediated by the poly(A) polymerase, germ line development defective-2," *Journal of Biological Chemistry*, vol. 289, no. 20, pp. 14239–14251, 2014.

[177] R. G. Fox, F. D. Park, C. S. Koechlein, M. Kritzik, and T. Reya, "Musashi Signaling in Stem Cells and Cancer," *Annual Review of Cell and Developmental Biology*, vol. 31, no. 1, pp. 249–267, 2015.

[178] P. L. Chavali, L. Stojic, L. W. Meredith, N. Joseph, M. S. Nahorski, T. J. Sanford, T. R. Sweeney, B. A. Krishna, M. Hosmillo, A. E. Firth, R. Bayliss, C. L. Marcelis, S. Lindsay, I. Goodfellow, C. G. Woods, and F. Gergely, "Neurodevelopmental protein Musashi-1 interacts with the Zika genome and promotes viral replication," *Science*, vol. 357, no. 6346, pp. 83–88, 2017.

[179] S. Shibata, M. Umei, H. Kawahara, M. Yano, S. Makino, and H. Okano, "Characterization of the RNA-binding protein Musashi1 in zebrafish," *Brain Research*, vol. 1462, pp. 162–173, 2012.

[180] J. R. de Oliveira Dias, C. V. Ventura, B. de Paula Freitas, J. Prazeres, L. O. Ventura, V. Bravo-Filho, T. Aleman, A. I. Ko, A. Zin, R. Belfort, and M. Maia, "Zika and the Eye: Pieces of a Puzzle," *Progress in Retinal and Eye Research*, vol. 66, no. November 2017, pp. 85–106, 2018.

[181] G. F. Franzco Oliver, J. M. Carr, and J. R. Franzco Smith, "Emerging infectious uveitis: Chikungunya, dengue, Zika and Ebola: A review," *Clinical and Experimental Ophthalmology*, vol. 47, no. 3, pp. 372–380, 2018.

[182] W. Ma, S. Li, S. Ma, L. Jia, F. Zhang, Y. Zhang, J. Zhang, G. Wong, S. Zhang, X. Lu, M. Liu, J. Yan, W. Li, C. Qin, D. Han, C. Qin, N. Wang, X. Li, and G. F. Gao, "Zika Virus Causes Testis Damage and Leads to Male Infertility in Mice," *Cell*, vol. 167, no. 6, pp. 1511–1524, 2016.

[183] S. Salinas, N. Erkilic, K. Damodar, J.-P. Moles, C. Fournier-Wirth, P. Van de Perre, V. Kalatzis, and Y. Simonin, "Zika Virus Efficiently Replicates in Human Retinal Epithelium and Disturbs Its Permeability," *Journal of Virology*, vol. 91, no. 3, pp. 1–4, 2017.

[184] H. M. Lazear, J. Govero, A. M. Smith, D. J. Platt, E. Fernandez, J. J. Miner, and M. S. Diamond, "A Mouse Model of Zika Virus Pathogenesis HHS Public Access," *Cell Host Microbe*, vol. 19, no. 5, pp. 720–730, 2016.

[185] K. Susaki, J. Kaneko, Y. Yamano, K. Nakamura, W. Inami, T. Yoshikawa, Y. Ozawa, S. Shibata, O. Matsuzaki, H. Okano, and C. Chiba, "Musashi-1, an RNA-binding protein, is indispensable for survival of photoreceptors," *Experimental Eye Research*, vol. 88, no. 3, pp. 347–355, 2009.

[186] S. Erlin, W. Wenjie, W. Lining, L. Bingxin, L. Mingde, S. Yan, and H. Ruifa, "Musashi-1 maintains blood-testis barrier structure during spermatogenesis and regulates stress granule formation upon heat stress," *Molecular Biology of the Cell*, vol. 26, no. 10, pp. 1947–1956, 2015.

[187] P. J. Uren, D. T. Vo, P. R. de Araujo, R. Pötschke, S. C. Burns, E. Bahrami-Samani, M. Qiao, R. de Sousa Abreu, H. I. Nakaya, B. R. Correa, C. Kühnöl, J. Ule, J. L. Martindale, K. Abdelmohsen, M. Gorospe, A. D. Smith, and L. O. F. Penalva, "RNA-Binding Protein Musashi1 Is a Central Regulator of Adhesion Pathways in Glioblastoma," *Molecular and Cellular Biology*, vol. 35, no. 17, pp. 2965–2978, 2015.

[188] A. d. B. Schneider and M. T. Wolfinger, "Musashi binding elements in Zika and related Flavivirus 3′UTRs: A comparative study in silico," *Scientific Reports*, vol. 9, no. 1, 2019.

[189] M. Mutso, S. Saul, K. Rausalu, O. Susova, E. Žusinaite, S. Mahalingam, and A. Merits, "Reverse genetic system, genetically stable reporter viruses and packaged subgenomic replicon based on a Brazilian zika virus isolate," *Journal of General Virology*, vol. 98, no. 11, pp. 2712–2724, 2017.

[190] U. K. Laemmli, "Cleavage of Structural Proteins during the Assembly of the Head of Bacteriophage T4," *Nature*, vol. 227, pp. 680–685, 1970.

[191] M. Trimborn, S. M. Bell, C. Felix, Y. Rashid, H. Jafri, P. D. Griffiths, L. M. Neumann, A. Krebs, A. Reis, K. Sperling, H. Neitzel, and A. P. Jackson, "Mutations in microcephalin cause aberrant regulation of chromosome condensation," *American Journal of Human Genetics*, vol. 75, no. 2, pp. 261–266, 2004.

[192] A. P. Jackson, H. Eastwood, S. M. Bell, J. Adu, C. Toomes, I. M. Carr, E. Roberts, D. J. Hampshire, Y. J. Crow, A. J. Mighell, G. Karbani, H. Jafri, Y. Rashid, R. F. Mueller, A. F. Markham, and C. G. Woods, "Identification of microcephalin, a protein implicated in determining the size of the human brain," *American Journal of Human Genetics*, vol. 71, no. 1, pp. 136–142, 2002.

[193] M. Xu, E. M. Lee, Z. Wen, Y. Cheng, W. K. Huang, X. Qian, J. Tcw, J. Kouznetsova, S. C. Ogden, C. Hammack, F. Jacob, H. N. Nguyen, M. Itkin, C. Hanna, P. Shinn, C. Allen, S. G. Michael, A. Simeonov, W. Huang, K. M. Christian, A. Goate, K. J. Brennand, R. Huang, M. Xia, G. L. Ming, W. Zheng, H. Song, and H. Tang, "Identification of small-molecule inhibitors of Zika virus infection and induced neural cell death via a drug repurposing screen," *Nature Medicine*, vol. 22, no. 10, pp. 1101–1107, 2016.

[194] F. M. Cambuli, B. R. Correa, A. Rezza, S. C. Burns, M. Qiao, P. J. Uren, E. Kress, A. Boussouar, P. A. Galante, L. O. Penalva, and M. Plateroti, "A Mouse Model of Targeted Musashi1 Expression in Whole Intestinal Epithelium Suggests Regulatory Roles in Cell Cycle and Stemness," *Stem Cells*, vol. 33, no. 12, pp. 3621–3634, 2015.

[195] Y. Oh, F. Zhang, Y. Wang, E. M. Lee, I. Y. Choi, H. Lim, F. Mirakhori, R. Li, L. Huang, T. Xu, H. Wu, C. Li, F. Qin, Z. Wen, Q.-f. Wu, H. Tang, Z. Xu, H. Song, G.-l. Ming, and G. Lee, "Zika virus directly infects peripheral neurons and induces cell death," *Nature neuroscience*, vol. 20, no. 9, pp. 1209–1212, 2017.

[196] F. Puig-Basagoiti, T. S. Deas, P. Ren, M. Tilgner, D. M. Ferguson, and P. Y. Shi, "High-throughput assays using a luciferase-expressing replicon, virus-like particles, and full-length virus for West Nile virus drug discovery," *Antimicrobial Agents and Chemotherapy*, vol. 49, no. 12, pp. 4980–4988, 2005.

[197] C. Shan, X. Xie, A. Muruato, S. L. Rossi, C. M. Roundy, S. R. Azar, Y. Yang, R. B. Tesh, N. Bourne, A. D. Barrett, N. Vasilakis, S. C. Weaver, and P.-Y. Shi, "An Infectious cDNA Clone of Zika Virus to Study Viral Virulence, Mosquito Transmission, and Antiviral Inhibitors," *Cell Host Microbe*, vol. 19, no. 6, pp. 891–900, 2016.

[198] G. Zou, H. Y. Xu, M. Qing, Q. Y. Wang, and P. Y. Shi, "Development and characterization of a stable luciferase dengue virus for high-throughput screening," *Antiviral Research*, vol. 91, no. 1, pp. 11–19, 2011.

[199] S. J. Kaptein, T. De Burghgraeve, M. Froeyen, B. Pastorino, M. M. Alen, J. A. Mondotte, P. Herdewijn, M. Jacobs, X. De Lamballerie, D. Schols, A. V. Gamarnik, F. Sztaricskai, and J. Neyts, "A derivate of the antibiotic doxorubicin is a selective inhibitor of dengue and yellow fever virus replication in vitro," *Antimicrobial Agents and Chemotherapy*, vol. 54, no. 12, pp. 5269–5280, 2010.

[200] T. S. Deas, I. Binduga-Gajewska, M. Tilgner, P. Ren, D. A. Stein, H. M. Moulton, P. L. Iversen, E. B. Kauffman, L. D. Kramer, and P.-Y. Shi, "Inhibition of Flavivirus Infections by Antisense Oligomers Specifically Suppressing Viral Translation and RNA Replication," *Journal of Virology*, vol. 79, no. 8, pp. 4599–4609, 2005.

[201] M. M. Samsa, J. A. Mondotte, J. J. Caramelo, and A. V. Gamarnik, "Uncoupling cis-Acting RNA Elements from Coding Sequences Revealed a Requirement

of the N-Terminal Region of Dengue Virus Capsid Protein in Virus Particle Formation," *Journal of Virology*, vol. 86, no. 2, pp. 1046–1058, 2012.

[202] J. W. Schoggins, M. Dorner, M. Feulner, N. Imanaka, M. Y. Murphy, A. Ploss, and C. M. Rice, "Dengue reporter viruses reveal viral dynamics in interferon receptor-deficient mice and sensitivity to interferon effectors in vitro," *Proceedings of the National Academy of Sciences of the United States of America*, vol. 109, no. 36, pp. 14610–14615, 2012.

[203] P. T. Zhang, C. Shan, X. D. Li, S. Q. Liu, C. L. Deng, H. Q. Ye, B. D. Shang, P. Y. Shi, M. Lv, B. F. Shen, C. F. Qin, and B. Zhang, "Generation of a recombinant West Nile virus stably expressing the Gaussia luciferase for neutralization assay," *Virus Research*, vol. 211, pp. 17–24, 2016.

[204] E. Volkova, K. A. Tsetsarkin, E. Sippert, F. Assis, G. Liu, M. Rios, and A. G. Pletnev, "Novel approach for insertion of heterologous sequences into full-length ZIKV genome results in superior level of gene expression and insert stability," *Viruses*, vol. 12, no. 1, 2020.

[205] G. Gadea, S. Bos, P. Krejbich-Trotot, E. Clain, W. Viranaicken, C. El-Kalamouni, P. Mavingui, and P. Desprès, "A robust method for the rapid generation of recombinant Zika virus expressing the GFP reporter gene," *Virology*, vol. 497, pp. 157–162, 2016.

[206] X. F. Li, X. D. Li, C. L. Deng, H. L. Dong, Q. Y. Zhang, Q. Ye, H. Q. Ye, X. Y. Huang, Y. Q. Deng, B. Zhang, and C. F. Qin, "Visualization of a neurotropic flavivirus infection in mouse reveals unique viscerotropism controlled by host type I interferon signaling," *Theranostics*, vol. 7, no. 4, pp. 912–925, 2017.

[207] C. Baker, Y. Liu, J. Zou, A. Muruato, X. Xie, and P. Y. Shi, "Identifying optimal capsid duplication length for the stability of reporter flaviviruses," *Emerging Microbes and Infections*, vol. 9, no. 1, pp. 2256–2265, 2020.

[208] A. V. Shustov, P. W. Mason, and I. Frolov, "Production of Pseudoinfectious Yellow Fever Virus with a Two-Component Genome," *Journal of Virology*, vol. 81, no. 21, pp. 11737–11748, 2007.

[209] A. Torsvik, D. Stieber, P. O. Enger, A. Golebiewska, A. Molven, A. Svendsen, B. Westermark, S. P. Niclou, T. K. Olsen, M. Chekenya Enger, and R. Bjerkvig, "U-251 revisited: Genetic drift and phenotypic consequences of long-term cultures of glioblastoma cells," *Cancer Medicine*, vol. 3, no. 4, pp. 812–824, 2014.

[210] W. Hou, N. Armstrong, L. A. Obwolo, M. Thomas, X. Pang, K. S. Jones, and Q. Tang, "Determination of the Cell Permissiveness Spectrum, Mode of RNA Replication, and RNA-Protein Interaction of Zika Virus," *BMC Infectious Diseases*, vol. 17, no. 1, pp. 1–12, 2017.

[211] S. Ramos da Silva, F. Cheng, I. C. Huang, J. U. Jung, and S. J. Gao, "Efficiencies and kinetics of infection in different cell types/lines by African and Asian strains of Zika virus," *Journal of Medical Virology*, vol. 91, no. 2, pp. 179–189, 2018.

[212] J. H. Lawrence, M. L. Sherer, P. Tavlarides-Hontz, M. S. Parcells, and J. M. Schwarz, "An investigation into the immune response of cultured neural rat cells following Zika virus infection," *Journal of Neuroimmunology*, vol. 332, pp. 73–77, 2019.

[213] L. Velazquez-Salinas, A. Verdugo-Rodriguez, L. L. Rodriguez, and M. V. Borca, "The role of interleukin 6 during viral infections," *Frontiers in Microbiology*, vol. 10, no. MAY, pp. 6–11, 2019.

[214] T. Magoro, A. Dandekar, L. T. Jennelle, R. Bajaj, G. Lipkowitz, A. R. Angelucci, P. O. Bessong, and Y. S. Hahn, "IL-1β/TNF-α/IL-6 inflammatory cytokines promote STAT1-dependent induction of CH25H in Zika virus-infected human macrophages," *Journal of Biological Chemistry*, vol. 294, no. 40, pp. 14591–14602, 2019.

[215] M. Blanc, W. Y. Hsieh, K. A. Robertson, K. A. Kropp, T. Forster, G. Shui, P. Lacaze, S. Watterson, S. J. Griffiths, N. J. Spann, A. Meljon, S. Talbot, K. Krishnan, D. F. Covey, M. R. Wenk, M. Craigon, Z. Ruzsics, J. Haas, A. Angulo, W. J. Griffiths, C. K. Glass, Y. Wang, and P. Ghazal, "The Transcription Factor STAT-1 Couples Macrophage Synthesis of 25-Hydroxycholesterol to the Interferon Antiviral Response," *Immunity*, vol. 38, no. 1, pp. 106–118, 2013.

[216] C. Li, Y. Q. Deng, S. Wang, F. Ma, R. Aliyari, X. Y. Huang, N. N. Zhang, M. Watanabe, H. L. Dong, P. Liu, X. F. Li, Q. Ye, M. Tian, S. Hong, J. Fan, H. Zhao, L. Li, N. Vishlaghi, J. E. Buth, C. Au, Y. Liu, N. Lu, P. Du, F. X. F. Qin, B. Zhang, D. Gong, X. Dai, R. Sun, B. G. Novitch, Z. Xu, C. F. Qin, and G. Cheng, "25-Hydroxycholesterol Protects Host against Zika Virus Infection and Its Associated Microcephaly in a Mouse Model," *Immunity*, vol. 46, no. 3, pp. 446–456, 2017.

[217] A. Plociennikowska, J. Frankish, T. Moraes, D. Del Prete, F. Kahnt, C. Acuna, M. Slezak, M. Binder, and R. Bartenschlager, "TLR3 Activation by Zika Virus Stimulates Inflammatory Cytokine Production Which Dampens the Antiviral Response Induced by RIG-I-Like Receptors," *Journal of Virology*, vol. 95, no. 10, 2021.

[218] A. Grant, S. S. Ponia, S. Tripathi, V. Balasubramaniam, L. Miorin, M. Sourisseau, M. C. Schwarz, M. P. Sanchez-Seco, M. J. Evans, S. M. Best, and A. Garcia-Sastre, "Zika Virus Targets Human STAT2 to Inhibit Type i Interferon Signaling," *Cell Host and Microbe*, vol. 19, no. 6, pp. 882–890, 2016.

[219] L. Tan, L. A. Lacko, T. Zhou, D. Tomoiaga, R. Hurtado, T. Zhang, A. Sevilla, A. Zhong, C. E. Mason, S. Noggle, T. Evans, H. Stuhlmann, R. E. Schwartz, and S. Chen, "Pre- and peri-implantation Zika virus infection impairs fetal development by targeting trophectoderm cells," *Nature Communications*, vol. 10, no. 1, pp. 1–12, 2019.

[220] A. A. Sher, K. K. Glover, and K. M. Coombs, "Zika virus infection disrupts astrocytic proteins involved in synapse control and axon guidance," *Frontiers in Microbiology*, vol. 10, no. MAR, pp. 1–20, 2019.

[221] K. K. Glover, A. Gao, A. Zahedi-Amiri, and K. M. Coombs, "Vero Cell Proteomic Changes Induced by Zika Virus Infection," *Proteomics*, vol. 19, no. 4, 2019.

[222] G. Prelich, "Gene overexpression: Uses, mechanisms, and interpretation," *Genetics*, vol. 190, no. 3, pp. 841–854, 2012.

[223] T. E. Morrison and M. S. Diamond, "Animal Models of Zika Virus Infection, Pathogenesis, and Immunity," *Journal of virology*, vol. 91, no. 8, 2017.

[224] R. G. Huber, X. N. Lim, W. C. Ng, A. Y. Sim, H. X. Poh, Y. Shen, S. Y. Lim, K. B. Sundstrom, X. Sun, J. G. Aw, H. K. Too, P. H. Boey, A. Wilm, T. Chawla, M. M. Choy, L. Jiang, P. F. de Sessions, X. J. Loh, S. Alonso, M. Hibberd, N. Nagarajan, E. E. Ooi, P. J. Bond, O. M. Sessions, and Y. Wan, "Structure mapping of dengue and Zika viruses reveals functional long-range interactions," *Nature Communications*, vol. 10, no. 1, 2019.

[225] S. M. Villordo, J. M. Carballeda, C. V. Filomatori, and A. V. Gamarnik, "RNA STRUCTURE DUPLICATIONS AND FLAVIVIRUS HOST ADAPTION," *Trends Microbiology*, vol. 24, no. 4, pp. 270–283, 2016.

[226] D. H. Mathews and D. H. Turner, "Prediction of RNA secondary structure by free energy minimization," *Current Opinion in Structural Biology*, vol. 16, no. 3, pp. 270–278, 2006.

[227] M. Zuker, "Mfold web server for nucleic acid folding and hybridization prediction," *Nucleic Acids Research*, vol. 31, no. 13, pp. 3406–3415, 2003.

[228] S. Stern, D. Moazed, and H. Noller, "Structural Analysis of RNA Using Chemical and Enzymatic Probing Monitored by Primer Extension," in *Methods in Enzymology*, vol. 164, ch. Structural, Academic Press, Inc., 1988.

[229] C. Ehresmann, F. Baudin, M. Mougel, P. Romby, J. P. Ebel, and B. Ehresmann, "Probing the structure of RNAs in solution," *Nucleic Acids Research*, vol. 15, no. 22, pp. 9109–9128, 1987.

[230] K. M. Weeks, "Advances in RNA secondary and tertiary structure analysis by chemical probing," *Current Opinion in Structural Biology*, vol. 20, no. 3, pp. 295–304, 2010.

[231] K. A. Wilkinson, E. J. Merino, and K. M. Weeks, "Selective 2′-hydroxyl acylation analyzed by primer extension (SHAPE): Quantitative RNA structure analysis at single nucleotide resolution," *Nature Protocols*, vol. 1, no. 3, pp. 1610–1616, 2006.

[232] E. J. Merino, K. A. Wilkinson, J. L. Coughlan, and K. M. Weeks, "RNA Structure Analysis at Single Nucleotide Resolution by Selective 2′-Hydroxyl Acylation and Primer Extension (SHAPE)," *Journal of the American Chemical Society*, vol. 127, pp. 4223–4231, 2005.

[233] Thermofisher, "Superscript III Reverse Transcriptase (Invitrogen)," 2004. Obtained from the world wide web on 20/09/21: `https://www.thermofisher.com/document-connect/document-connect.html?url=https%3A%2F%2Fassets.thermofisher.com%2FTFS-Assets%2FLSG%2Fmanuals%2FsuperscriptIII_man.pdf`.

[234] F. Karabiber, J. L. McGinnis, O. V. Favorov, and K. M. Weeks, "QuShape: Rapid, accurate, and best-practices quantification of nucleic acid probing information, resolved by capillary electrophoresis," *Rna*, vol. 19, no. 1, pp. 63–73, 2013.

[235] S. M. Vasa, N. Guex, K. A. Wilkinson, K. M. Weeks, and M. C. Giddings, "ShapeFinder: A software system for high-throughput quantitative analysis

of nucleic acid reactivity information resolved by capillary electrophoresis," *Bioinformatics*, vol. 14, pp. 1979–1990, 2008.

[236] M. De Nova-Ocampo, N. Villegas-Sepúlveda, and R. M. Del Angel, "Translation elongation factor-1α, La, and PTB interact with the 3′ untranslated region of dengue 4 virus RNA," *Virology*, vol. 295, no. 2, pp. 337–347, 2002.

[237] B. M. García-Montalvo, F. Medina, and R. M. Del Angel, "La protein binds to NS5 and NS3 and to the 5′ and 3′ ends of Dengue 4 virus RNA," *Virus Research*, vol. 102, no. 2, pp. 141–150, 2004.

[238] M. Monroy-Yocupicio, R. Padmanabhan, F. Medina, and R. M. Del Angel, "Mosquito La protein binds to the 3′ untranslated region of the positive and negative polarity dengue virus RNAs and relocates to the cytoplasm of infected cells," *Virology*, vol. 357, pp. 29–40, 2007.

[239] S. Vashist, M. Anantpadma, H. Sharma, and S. Vrati, "La protein binds the predicted loop structures in the 3′ non-coding region of Japanese encephalitis virus genome: Role in virus replication," *Journal of General Virology*, vol. 90, no. 6, pp. 1343–1352, 2009.

[240] Y. Lei, Y. Huang, H. Zhang, L. Yu, M. Zhang, and A. Dayton, "Functional interaction between cellular p100 and the dengue virus 3′ UTR," *Journal of General Virology*, vol. 92, no. 4, pp. 796–806, 2011.

[241] J. D. Leverson, P. J. Koskinen, F. C. Orrico, E. M. Rainio, K. J. Jalkanen, A. B. Dash, R. N. Eisenman, and S. A. Ness, "Pim-1 kinase and p100 cooperate to enhance c-Myb activity," *Molecular Cell*, vol. 2, no. 4, pp. 417–425, 1998.

[242] T. Välineva, J. Yang, R. Palovuori, and O. Silvennoinen, "The transcriptional co-activator protein p100 recruits histone acetyltransferase activity to STAT6 and mediates interaction between the CREB-binding protein and STAT6," *Journal of Biological Chemistry*, vol. 280, no. 15, pp. 14989–14996, 2005.

[243] S. H. Merkling, V. Raquin, S. Dabo, A. Henrion-Lacritick, H. Blanc, I. Moltini-Conclois, L. Frangeul, H. Varet, M. C. Saleh, and L. Lambrechts, "Tudor-SN Promotes Early Replication of Dengue Virus in the Aedes aegypti Midgut," *iScience*, vol. 23, no. 2, 2020.

[244] M. Ta and S. Vrati, "Mov34 Protein from Mouse Brain Interacts with the 3′ Noncoding Region of Japanese Encephalitis Virus," *Journal of Virology*, vol. 74, no. 11, pp. 5108–5115, 2000.

[245] L. Aravind and C. P. Ponting, "Homologues of 26S proteasome subunits are regulators of transcription and translation," *Protein Science*, vol. 7, no. 5, pp. 1250–1254, 1998.

[246] M. Manzano, E. D. Reichert, S. Polo, B. Falgout, W. Kasprzak, B. A. Shapiro, and R. Padmanabhan, "Identification of cis-acting elements in the 3′-untranslated region of the dengue virus type 2 RNA that modulate translation and replication," *Journal of Biological Chemistry*, vol. 286, no. 25, pp. 22521–22534, 2011.

[247] A. M. Ward, K. Bidet, A. Yinglin, S. G. Ler, K. Hogue, W. Blackstock, J. Gunaratne, and M. A. Garcia-Blanco, "Quantitative mass spectrometry of DENV-2 RNA-interacting proteins reveals that the DEAD-box RNA helicase DDX6 binds the DB1 and DB2 3′ UTR structures," *RNA Biology*, vol. 8, no. 6, pp. 1173–1186, 2011.

[248] S. Jansen, E. Smlatic, D. Copmans, S. Debaveye, F. Tangy, P. O. Vidalain, J. Neyts, and K. Dallmeier, "Identification of host factors binding to dengue and Zika virus subgenomic RNA by efficient yeast three-hybrid screens of the human ORFeome," *RNA Biology*, vol. 18, no. 5, pp. 732–744, 2021.

[249] K. O′Neill, N. Huang, D. Unis, and R. J. Clem, "Rapid selection against arbovirus-induced apoptosis during infection of a mosquito vector," *Proceedings of the National Academy of Sciences of the United States of America*, vol. 112, no. 10, pp. E1152–E1161, 2015.

[250] Z. Y. Liu, X. F. Li, T. Jiang, Y. Q. Deng, Q. Ye, H. Zhao, J. Y. Yu, and C. F. Qin, "Viral RNA switch mediates the dynamic control of flavivirus replicase recruitment by genome cyclization," *eLife*, vol. 5, pp. 1–27, 2016.

[251] E. Frumence, M. Roche, P. Krejbich-Trotot, C. El-Kalamouni, B. Nativel, P. Rondeau, D. Missé, G. Gadea, W. Viranaicken, and P. Desprès, "The South Pacific epidemic strain of Zika virus replicates efficiently in human epithelial A549 cells leading to IFN-β production and apoptosis induction," *Virology*, vol. 493, pp. 217–226, 2016.

[252] J. M. Emeny and M. J. Morgan, "Regulation of the interferon system: Evidence that vero cells have a genetic defect in interferon production," *Journal of General Virology*, vol. 43, no. 1, pp. 247–252, 1979.

Chapter 7

Appendix

7.1 Intro

Previous work by Chavali *et al.*, 2017 utilised in vitro biotinylation to label ZIKV 3′UTR RNA, and used it as bait in a pull down to display MSI1 binding. However, as this thesis has shown, maintenance of the RNA structure is vital for the functionality of the RNA, including the binding of host and viral proteins. As shown below, initial attempts to recapitulate the pull down carried out by Chavali *et al.*, 2017, failed to demonstrate MSI1 binding (Figure 7.1). In vitro biotinylations randomly incorporate Biotin-16-UTP into the RNA, and therefore, depending on where these random incorporations occur, could affect the formation of RNA structures. To minimise the effects on RNA structure, end labelling is preferred. 3′ end labelling kits are available, however, due to the highly stable 3′ SL structure at the terminal of the ZIKV 3′UTR, 3′ end labelling of this RNA is highly inefficient. As previously shown in Chapter 4, the use of a specifically designed structural cassette to add additional sequence onto the end of the ZIKV 3′UTR had no effect on the ZIKV 3′UTR RNA structure. The methods and work detailed below show that utilising the structured cassette allows the addition of extra unstructured sequence onto the end of the ZIKV 3′UTR to enhance biotinylation efficiency. Although this work is incomplete, it may provide useful information for future investigations utilising ZIKV 3′UTR RNA as bait for protein pull downs.

7.2 Methods

7.2.1 Pull down

ZIKV 3′UTR DNA was generated using the F primer (TAATACGACTCACTATAG CACCAATCTTAATGTTGTCAGGCCTG), adding a T7 promoter to the 5′ end of the 3′UTR, and the reverse primer (AGACCCATGGATTTCCCCACACCGGC) which anneals to the end of the ZIKV 3′UTR. PCR amplification was carried out with the reaction conditions as follows; 1X Buffer for KOD Hot start DNA Polymerase, 1 mM MgSO4, 0.2 mM of each dNTP, 0.3 μM forward and reverse primers, 0.02 U/μL KOD Hot Start DNA polymerase (Novagen) and 40 ng FL WT plasmid template. Cycling conditions were an initial denaturation of 95°C followed by 28X (95°C for 30 seconds, 60°C for 30 seconds, 70°C for 30 seconds) and a final extension of 70°C for 5 minutes. Following PCR amplification, DNA was ethanol precipitated and purified by gel extraction.

1 μg of ZIKV 3′UTR DNA was used in an in vitro transcription reaction containing recombinant T7 polymerase (50 ng/μL), 40 mM Hepes pH 7.5, 32 mM MgoAc, 40 mM DTT, 2 mM spermidine, 5 mM each of ATP, GTP, CTP, 1.3 mM UTP, 0.7 mM Biotin-16-UTP (Invitrogen) and 1.6U/μL RNaseOUT (Invitrogen). Reactions were incubated at 37°C for 2 hours prior to DNASE (NEB) treatment for 1 hour at 37°C and purification by phenol chloroform extraction and ethanol precipitation. Following resuspension in water, RNA was purified by passing down two Illustra MicroSpin G-50 columns (GE Healthcare). RNA was quantified using the Qubit RNA Broad Range Assay kit (Invitrogen).

RNA was refolded by heating at 60°C for 10 minutes and then slowly cooled down to 40°C by lowering the temperature by 5°C every 5 minutes. The temperature was then lowered to 37°C for 3 minutes, MgCl2 added, and incubation at 37°C continued for 7 minutes. The temperature was then reduced to 22°C for 5 minutes and the RNA held at 4°C. Washing and preparation of Dynabeads MyOne Streptavidin T1 for RNA binding was carried out following the manufacturer's instructions (Invitrogen). 1 mg of U251 lysates in lysis buffer (25 mM Tris HCl pH 7.5, 150 mM KCl, 5 mM EDTA, 5 mM MgCL2, 1% NP40, 0.5 mM DTT, protease inhibitor cocktail (Roche), 100 U/mL RNASE OUT) was pre-cleared with 40 μL beads for 30 minutes on a rotator at 4°C. Pre-cleared lysates were diluted 1:2 in lysis buffer and 0.1 μg/μL tRNA added prior to incubation with 10 pmol of refolded biotinylated RNA at 4°C

with gentle rotation. Following a 2 hour incubation, 40 μL of beads was added and the samples incubated at 4°C for another hour. Beads were then washed three times with protein lysis buffer containing 300 mM KCl and then resuspended in 5X protein sample buffer (10% SDS, 50% glycerol, 25% 2-mercaptoethanol, 0.0125% w/v bromophenol blue, 0.3125 M Tris HCl pH 6.8). Beads were spun down and boiled at 95°C for 5 minutes and the supernatants collected and stored at -80°C.

Samples were boiled again before western blotting with a monoclonal antibody raised against MSI1 EP1302 (1:500, ab52865, abcam) and rat anti-beta tubulin (1:10) grown from a hybridoma kindly provided by Stephen Graham. Goat anti-rabbit IgG H&L IRDye 800CW antibody (1:10,000, ab216773, abcam) and Goat anti-rat IgG H&L Alexa Fluor 680 (1:10,000, ab175778, abcam) were used for detection using an Odyssey CLx Imaging System (Li-Cor).

7.2.2 3′ end biotinylation

ZIKV 3′UTR RNA was generated by PCR amplification as described in Section 7.2.1. ZIKV 3′UTR DNA containing a 3′ structured extension cassette and poly(C) tail was generated by PCR using KOD polymerase and the reaction conditions described in Section 7.2.1. The forward primer (TAATACGACTCACTATAGGCCTTCGGGCCAAGCACCAATCTTAATGTTGTCAGG) encoding a T7 promoter and 5′ structured extension cassette, and the reverse primer (GGGGGGGGGAACCGGACCGAAGCCCGATTTATAGTAAATGGATCCGGCGAACCGGATCTAGACCCATGGATTTCCCCAC) encoding the 3′ structured extension cassette and a poly(C) tail were used to amplify the 3′UTR. The following cycling conditions were used; 95°C for 2 minutes followed by 28X (95°C for 30 seconds, 57°C for 30 seconds, 70°C for 30 seconds) and a final extension of 70°C for 5 minutes. Samples were ethanol precipitated into a smaller volume and purified by gel extraction.

1 μg of DNA was then added to a transcription reaction containing recombinant T7 polymerase (50 ng/μL), 40 mM Hepes pH 7.5, 32 mM MgoAc, 40 mM DTT, 2 mM spermidine, 10 mM each of ATP, GTP, CTP, UTP. Reactions were incubated at 37°C for 2 hours prior to DNASE (NEB) treatment for 1 hour. RNA was then purified by phenol chloroform extraction and ethanol precipitation and resuspended in water.

T4 RNA ligase was used to ligate biotinylated cytidine Bis(phosphate) to the 3′ end

of the ZIKV 3′UTR RNA using the Pierce RNA 3′ End Biotinylation kit (Thermo Scientific). RNA was heated to 85°C for 5 minutes and snap cooled on ice. Reactions contained 3 μL 10X RNA ligase buffer, 1 μL RNASE inhibitor (40 U/μL), 50 pmol RNA, 1 μL biotinylated cytidine (Bis)phosphate (1mM), 2 μL T4 RNA ligase (20 U/μL), 15 μL 30% PEG in a total reaction volume of 30 μL. Reactions were incubated at 16°C overnight and RNA purified by phenol chloroform extraction and ethanol precipitation. Following resuspension in water, RNA was quantified using the Qubit RNA broad range Assay kit.

To assess the efficacy of 3′ end biotinylation, 20 ng of RNA was incubated with 0.5 μg of streptavidin (Acro Biosystems) at 37°C for 10 minutes. Samples were then resuspended in RNA loading dye (0.05% bromophenol blue, 0.05% xylene cyanol, 20 mM EDTA pH 8 and 91% formamide) and heated to 85°C for 2 minutes. Samples were resolved in a 6% polyacrylamide gel containing 7M urea. The gel was pre-run for 30 minutes at 300V in 1X Tris-Borate-EDTA (TBE) prior to loading of samples and running at 300V for 30 minutes. The gel was stained with 1 μg/mL ethidium bromide in 0.5X TBE for 30 minutes prior to visualisation in a UV transilluminator.

7.3 MSI1 pull down with in vitro biotinylated ZIKV 3′UTR RNA

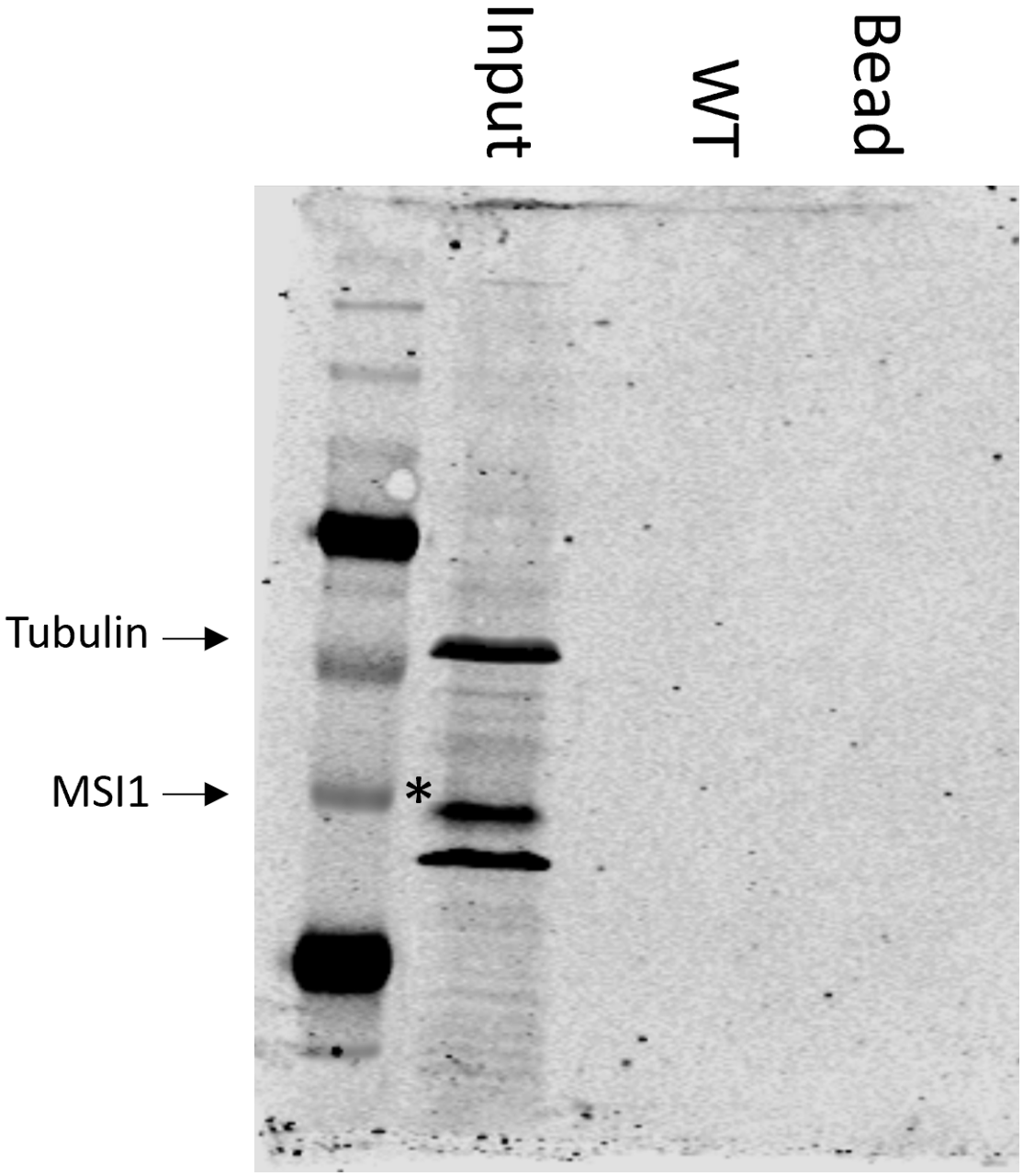

Figure 7.1: MSI1 pull down. Shown is the result of a MSI pull down using U251 cell lysates and in vitro biotinylated 3′UTR RNA, utilising the method developed by Chavali *et al.*, 2017. No protein binding was detected.

7.4 Enhancing 3′ end biotinylation of the ZIKV 3′UTR using the 3′ structural cassette

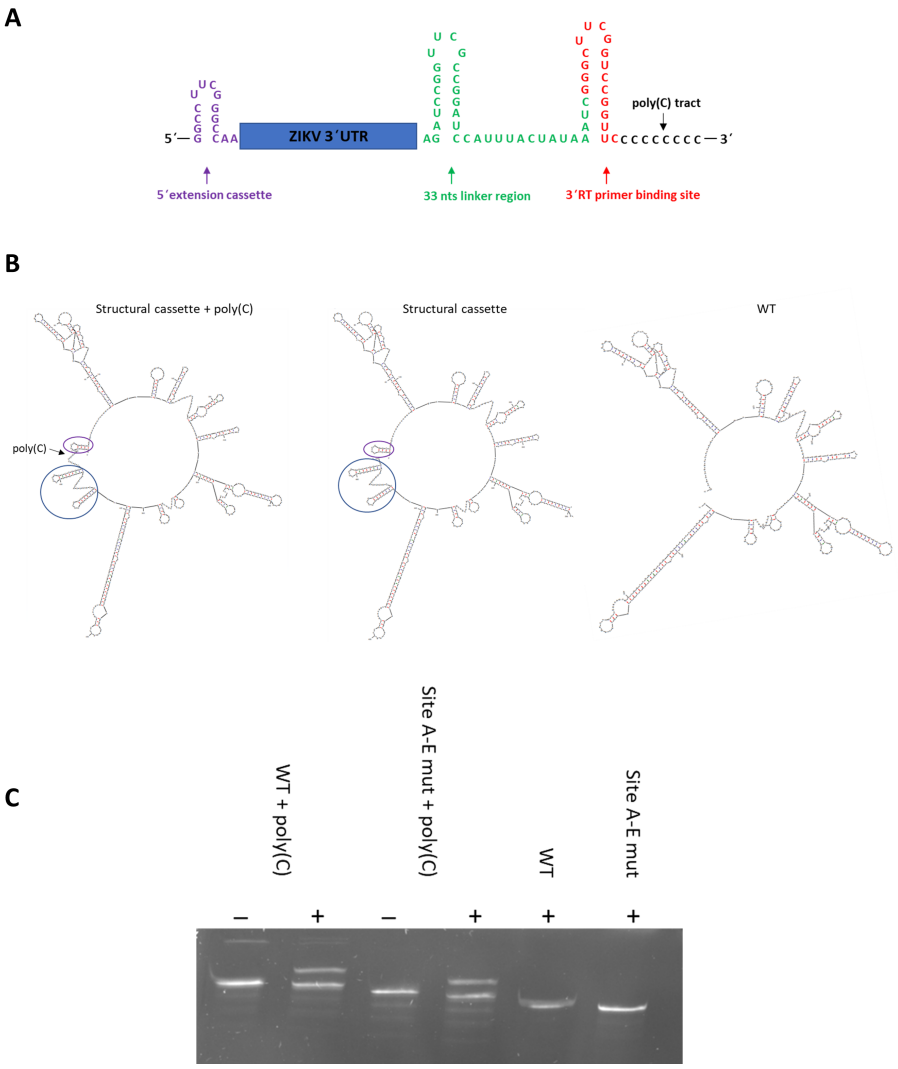

Figure 7.2: (A) Shown is the structured extension cassette with a poly(C) tract added to enhance the efficiency of 3′end biotinylation of the ZIKV 3′UTR RNA. The presence of the 3′RT primer site allows for SHAPE structural mapping of the ZIKV 3′UTR to ensure any modifications do not affect RNA structure. (B) Mfold structures show that addition of the poly(C) tract likely has no effect on overall 3′UTR structure. (C) Shown is a UREA denaturing gel used to detect streptavidin binding to the ZIKV 3′UTR. WT 3′UTR RNA containing the structured binding cassette plus a poly(C) tail (WT + Poly(C)) or without the cassette (WT) were generated. 3′UTR RNA with mutations at Site A, B, C, D and E with the structured cassette (Site A-E mut + Poly(C)) or without the cassette (Site A-E mut) were also generated. RNA was incubated with streptavidin (+) or with water (-), mixed with RNA loading dye and heated prior to running.